



**Politecnico
di Torino**

Politecnico di Torino

Corso di Laurea Magistrale in
Petroleum Engineering
A.Y. 2021/2022

Physicochemical Properties and CO₂ Absorption Capacity of Bio-Based Ionic Liquid Solutions: High-Pressure PVT Measurements

Graduation Session March 2025

Relatori:

Prof. Sergio Bocchini
Prof. Dario Viberti
Dr. Eloisa Salina Borello
Dr. Silvia Mazzotta
Anna Vittoria De Napoli

Candidato:

Ali Shakeri Kondori S301572

Acknowledgment

I would like to express my sincere gratitude to all those who have supported me throughout the course of this research and the writing of this thesis.

First and foremost, I am deeply grateful to my advisors, *Prof. Sergio Bocchini* (DISAT) and *Prof. Dario Viberti* (DIATI), for their continuous guidance, insightful suggestions, and unwavering support. Their expertise and encouragement have been invaluable in shaping the direction and depth of this work.

I would also like to thank the faculty and staff of the IIT at Environment Park, Torino for providing an excellent academic environment and the necessary resources to carry out this research. Special thanks go to my supervisors *Silvia Mazzotta* and *Anna Vittoria De Napoli*, who deserve special recognition for their insightful conversations and invaluable support during the experimental work which contributed massively to finishing this project.

I am also indebted to Energy Center LAB and colleagues *Eloisa Salina Borello* and *Marialuna Loffredo* whose academic and technical support made this study possible. Their commitment to PVT experiments has been a constant source of motivation.

Lastly, I would want to express my sincere gratitude to my family and club-mates for their support, love, and tolerance throughout the difficult parts of this journey, cheering me up whenever I was in need despite being many kilometers away. Their compassion has been essential to both my academic and personal development. Special thanks to *Hamid* who supported me in these last months with his wisdom and guidance.

Thank you all for helping me bring this thesis to completion.

Abstract

Mitigating climate change needs creative approaches to cutting CO₂ emissions. Choline proline ([Cho][Pro]) and dimethyl pyrrolidinium proline ([DMP][Pro]) are two biobased ionic liquids (ILs) that are being studied in this thesis as potential substitutes for post-combustion CO₂ capture. Although ionic liquids have adjustable characteristics, low volatility, and excellent thermal stability, their intrinsic high viscosity may restrict the efficiency of mass transfer and CO₂ absorption. To get around this, the study investigates how diluting the ionic liquids with dimethyl sulfoxide (DMSO) can best balance chemical reactivity and physical mass transfer while keeping the characteristics of biobased ILs.

The ionic liquids were synthesized through controlled reactions with bioavailable precursors, and they were then characterized using a variety of methods, such as differential scanning calorimetry (DSC), density and viscosity measurements, ATR-IR spectroscopy, and thermogravimetric analysis-infrared (TGA-IR). Gravimetric analysis and Pressure–Volume–Temperature (PVT) experiments were used to assess CO₂ absorption performance under various pressure and temperature situations. According to the results, DMSO dilution considerably lowers viscosity, which improves CO₂ uptake and guarantees better absorption kinetics.

These results demonstrate the potential of biobased ionic liquids as more ecologically friendly and effective solvents for CO₂ collection, providing a sustainable substitute for traditional amine-based systems.

Nomenclature

AA Amino Acid

AAILs Amino Acid-based Ionic Liquids

AEEA Aminoethylethanolamine

ATR-IR Attenuated Total Reflection Infrared

APIs Active Pharmaceutical Ingredients

BBILs Bio-based Ionic Liquids

BF₄⁻ Boron tetrafluoride

[bmim][PF₆] 1-Butyl-3-methylimidazolium hexafluorophosphate

[Cho][Pro] Choline Proline

ChILs Cholinium based Ionic Liquids

ChAAIL Choline-Amino Acid based Ionic Liquids

[CnMIM]⁺ 1-alkyl-3-methylimidazolium

[Cnpy]⁺ N-alkyl pyridinium

DES Deep-Eutectic Solvent

DMC Dimethyl Carbonate

DMP Dimethyl Pyrrolidinium: 1,1-dimethylpyrrolidinium

[DMP][CH₃OCOO] 1,1-dimethylpyrrolidinium methyl carbonate

[DMP][Pro] 1,1-dimethylpyrrolidinium Proline

DMSO Dimethyl Sulfoxide

EcL Energy Center Lab

FT-IR Fourier-Transform Infrared Spectroscopy

GHG Greenhouse Gases

IIT Italian Institute of Technology

IL Ionic Liquid

IoM Institute of Medicine

IR Infrared

LIG laser-induced graphene

MMEA Methyl Monoethanolamine

MEA Monoethanolamine

PF₆⁻ Hexafluorophosphate

PIL Protic ionic liquid

PVT Pressure-Volume-Temperature

PT Proton Transfer

Pyri₄-DCA butylpyridinium dicyanamide

[PYR₁₄][TFSI] *1-butyl-1-methylpyrrolidinium bis(trifluoromethanesulfonyl)imide*

RTIL Room-Temperature Ionic Liquid

SC Standard Condition

Tf₂N Bistriflimide

TSIL Task-Specific Ionic Liquid

Summary

Summary	5
1. Introduction	7
1.1 Ionic Liquids (ILs) and Deep Eutectic Solvents (DESs).....	12
1.2 Applications of Ionic Liquids (ILs) in Various Fields	14
1.3 Choline Based ILs:	17
1.4 PVT Cells	19
1.5 Post-Combustion carbon capture.....	20
2. Material and methods	22
2.1 Synthesis of [Cho][Pro]	22
2.2 Preparation of [Cho][Pro] solutions	24
2.3 Synthesis of [DMP][Pro]	24
2.4 Characterizations	26
2.4.1 ATR-IR	26
2.4.2 Density	27
2.4.3 Viscosity.....	29
2.4.4 DSC.....	30
2.4.5 TGA-IR	31
2.4.6 Carbon capture test.....	32
2.4.7 PVT test.....	34
3. Results and discussion	37
3.1 ATR-IR	37
3.2 Density	41
3.3 TGA-IR	42
3.5 DSC.....	62
3.6 Carbon capture test.....	68

3.7 PVT test.....	70
4. Conclusion	75
5. References.....	76

1. Introduction

Ionic liquids (ILs) are a class of salts that remain in a liquid state at temperatures below 100°C, existing entirely in ionic form. Their first documented synthesis dates to 1914, when Paul Walden prepared ethylammonium nitrate [1]. At the time, Walden’s research focused on the relationship between ionic conductivity and molecular structure, however, his discovery did not immediately spark widespread scientific interest.

Throughout much of the 20th century, ionic liquids remained largely unexplored by the broader scientific community. However, over the past two decades, their distinctive physicochemical properties —such as negligible volatility, exceptional thermal stability, and tunable solubility— have established them as promising alternatives to conventional solvents. [Figure 1].

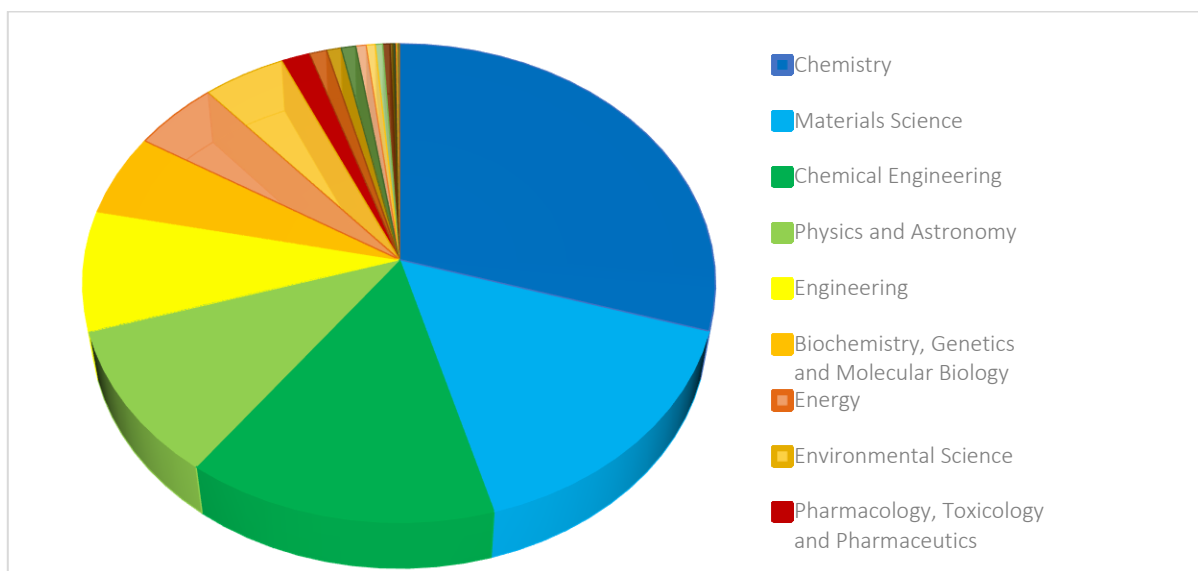


Figure 1: Percentage of Sections Dedicated to Study of ILs since 2000 [Extracted by Scopus]

Ionic liquids (ILs) consist of a cation—such as pyridinium, imidazolium, or ammonium— and an anion, forming highly versatile and tunable systems. Figure 2 shows a few common cation and anions used in ILs. Their unique physicochemical properties include low volatility, high thermal stability, and the ability to dissolve a broad range of organic and inorganic compounds [see Figure 3][5].

Unlike conventional solvents, which readily evaporate and contribute to atmospheric pollution, ILs exhibit exceptionally low vapor pressure. This characteristic arises from strong electrostatic interactions between their bulky cations and anions, which inhibit their transition into the gas phase. As a result, ILs are considered safer to handle, offering a lower environmental

impact and reduced risks in applications where solvent evaporation could pose hazards, such as high-temperature reactions or open-process systems [6].

Another key advantage of ILs' low volatility is their enhanced stability, which not only reduces solvent loss during use but also minimizes harmful emissions. These properties position ILs as promising alternatives to traditional solvents in both industrial and laboratory-scale applications, where sustainability and efficiency are critical considerations [7].

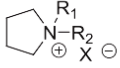
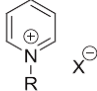
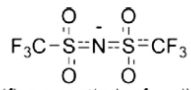
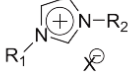
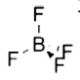
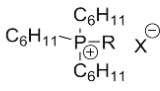
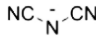
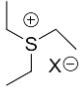
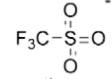

Cations	Anions
Ammonium 	Halides (chloride, bromide, iodide) F ⁻ , Cl ⁻ , Br ⁻
Pyridinium 	 bis(trifluoromethylsulfonyl)imide [NTf ₂] ⁻
Imidazolium 	 tetrafluoroborate [BF ₄] ⁻
Phosphonium 	 dicyanamide [N(CN) ₂] ⁻
Sulfonium 	 trifluoromethanesulfonate triflate, [OTf] ⁻
	 hexafluorophosphate [PF ₆] ⁻

Figure 2: Some common cations and anions used in ILs [4]

The physicochemical characteristics of ionic liquids (ILs) are inherently linked to the specific combination of cations and anions, resulting in a wide range of solvation behaviors. These behaviors are further influenced by temperature-dependent dynamics and the presence of co-solvents, which collectively determine the nature and strength of intermolecular interactions, most notably hydrogen bonding, leading to significant variations in solubility profiles [8, 9]. Among the factors influencing solubility, the nature of the anion plays a crucial role. For instance, CO₂ solubility is significantly higher in ILs containing the bis(trifluoromethylsulfonyl)-imide anion compared to those with a nitrate anion. Fluorination of the anion, as in [Tf₂N] and [methide], enhances CO₂ absorption, while modifications to the cation, such as elongation of alkyl chains, contribute to a lesser extent [10, 11]. Additionally, Aki and co-workers demonstrated that, across various ILs, CO₂ solubility increases with pressure and decreases with rising temperature [10]. Another critical consideration is water solubility. Due to their intrinsic hygroscopic nature, ILs readily absorb atmospheric moisture, particularly in flue gas

environments, which can significantly diminish their CO₂ capture efficiency [12]. However, hydrophobic ILs offer an alternative, functioning as water-immiscible polar phases, thereby mitigating this issue [13]. Furthermore, the strategic use of co-solvents can enhance IL performance in targeted applications, including catalysis, extraction, and biocatalysis, by fine-tuning solubility and reaction kinetics [14].

The tunable solubility of ionic liquids (ILs) makes them highly adaptable for a wide range of applications in green chemistry, including gas capture, liquid-liquid extraction, and their use as solvents in enzymatic and organic reactions. Their capacity to dissolve both polar and non-polar compounds underscore their versatility, making them valuable solvents in both industrial processes and scientific research [15].

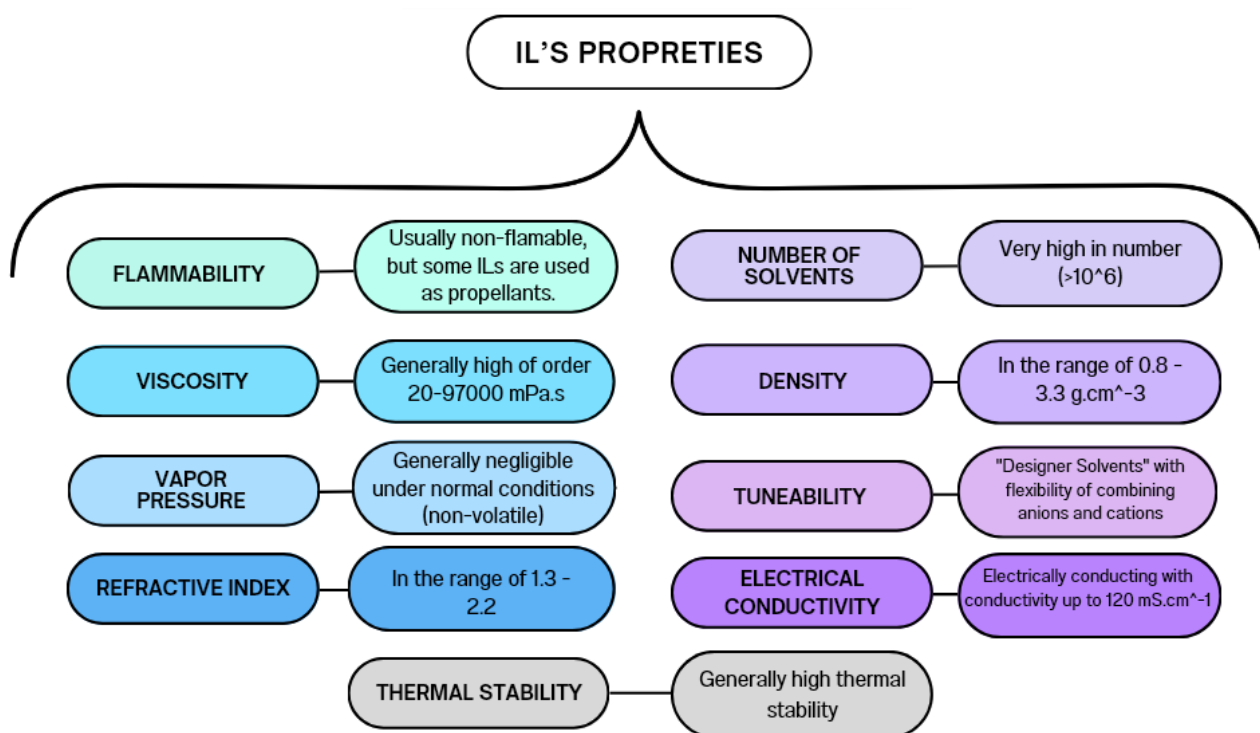


Figure 3: General Properties of Ionic Liquids [1]

Ionic liquids (ILs) are synthesized by selecting suitable cation-anion pairs and combining them through various methods, including neutralization, ion exchange, direct combination, and quaternization [2, 6].

Neutralization: This process involves the reaction between a strong acid and a weak base (a Brønsted acid and a Brønsted base), resulting in the elimination of a neutral molecule and the formation of an ionic liquid (IL). It can also lead to the production of a protic IL when specific acid-base pairs are used [16] [Figure 4]. This approach is particularly effective when employing tertiary amines with halide acids or certain organic acids [17].

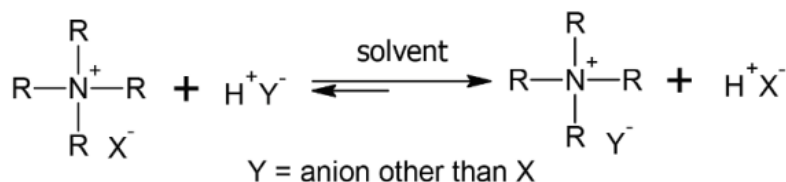


Figure 4: Synthesis of ILs by neutralization

Ion exchange or Metathesis: In this method, a metal salt—typically containing silver or a Group I metal—reacts with a primary IL to synthesize halide-free ILs [16] [see Figure 5]. While straightforward and easy to implement, this process has some limitations, including potential contamination with residual halide ions, the presence of water, or silver byproducts, which may interfere with the solute’s reactivity [17].

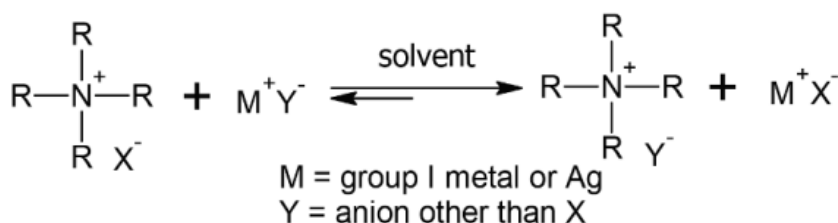


Figure 5: Synthesis of ILs by metathesis

Direct combination: ILs can also be synthesized by directly combining cations and anions under controlled conditions. For example, choline-based ILs are commonly produced by reacting choline hydroxide with an acid or amino acid, facilitating the development of biodegradable ILs [4] [see Figure 6].

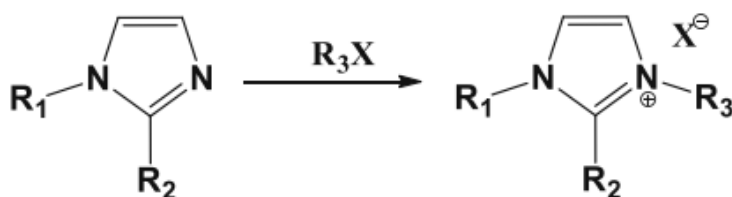


Figure 6: Synthesis of ILs by direct combination

Quaternization: This process involves the alkylation of a nitrogen-containing compound to generate a quaternary ammonium cation, which is then paired with an anion through anion exchange to form the desired IL [18] [see Figure 7]. When alkylammonium halides are absent, quaternization is required, typically through the reaction of a base with a haloalkane to produce an organic halide salt [17].

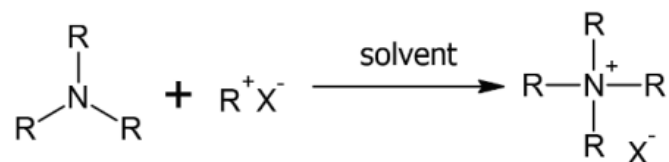


Figure 7: Synthesis of ILs by quaternization

Ionic liquids (ILs) are broadly classified based on their composition and function, with specific terms assigned to different categories. An IL can exhibit one or more of these characteristics. Below is a brief discussion of key IL types:

A. Room-temperature ionic liquids (RTILs)

RTILs are ionic liquids that remain in a liquid state at or near room temperature, making them one of the most widely studied IL categories. They are typically derived from imidazolium, pyridinium, or quaternary ammonium cations and are valued for their stability, low melting points, and ability to dissolve a broad range of substances. Common RTILs include 1-butyl-3-methyl-imidazolium hexafluorophosphate ([bmim][PF₆]) and choline-based ILs [19].

B. Protic ionic liquid (PIL)

PILs are formed through a proton transfer reaction between a Brønsted acid and a Brønsted base. These ILs are distinguished by their extensive hydrogen-bonding networks, which enhance properties such as ionic conductivity and facilitate applications in electrochemical systems [20].

C. Task-specific ionic liquids (TSILs)

TSILs are functionalized ionic salts in which a specific functional group is covalently attached to the cation and/or anion, tailoring their properties for targeted applications such as catalysis, separation, and electrochemistry [21]. These ILs have been explored for selective CO₂ capture from gas streams using amine-functionalized imidazolium salts and for catalyzing esterification reactions via sulfonic acid-modified ILs [22].

D. Bio-based ionic liquids

BBILs are derived from renewable resources, biocompatible molecules, or naturally occurring components. These ILs typically feature biodegradable anions, such as deprotonated amino acids, and cations like choline, making them environmentally friendly alternatives to conventional ILs. A prominent subclass within BBILs is **amino acid-based ionic liquids (AAILs)**, which incorporate amino acid-derived anions. These ILs are designed to minimize

toxicity while maintaining high functionality. However, De Jesus and Maciel Filho (2022) critically examined their synthesis, recovery, recycling, toxicity, and biodegradability, raising concerns about their classification as truly green solvents despite their perceived environmental benefits [23].

1.1 Ionic Liquids (ILs) and Deep Eutectic Solvents (DESs)

As mentioned earlier, the first reported IL, ethylammonium nitrate, was introduced by Paul Walden over a century ago. More recently, at the beginning of the 21st century, Abbott et al. introduced Deep Eutectic Solvents (DESs) as a new class of solvents. While some chemists consider DESs a subclass of ILs, they are fundamentally distinct, sharing certain overlapping properties while also exhibiting unique characteristics. DESs are relatively new and remain an active area of research; however, their physical properties closely resemble those of ILs [2]. Both ILs and DESs possess low vapor pressure, making them non-volatile and significantly safer to handle compared to conventional solvents. Their wide liquid-phase range allows them to function at temperatures both above and below room temperature. Moreover, these solvents are tunable, meaning that properties such as viscosity, polarity, and solubility can be adjusted to enhance their ability to dissolve a broad spectrum of organic and inorganic compounds. *Figure 8* illustrates key similarities and differences among DESs and bio-based ILs [2, 24].

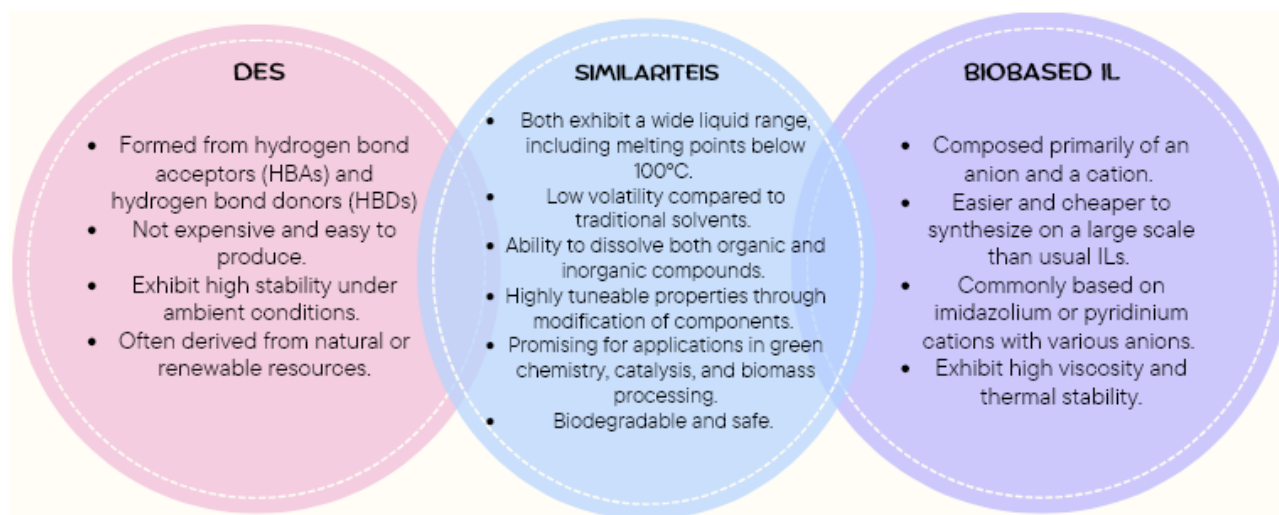


Figure 8: Similarities and differences of ILs and DESs [2]

Due to their unique properties, ILs and DESs play an important role in green chemistry and sustainable technologies, serving as both solvents and catalysts in eco-friendly chemical processes. Their applications include [2, 13, 24, 25]:

- **Green Catalysis:** Both ILs and DESs facilitate reactions such as esterification, oxidation, and organic synthesis, improving efficiency and sustainability.
- **Energy Applications:** ILs, in particular, are widely studied as electrolytes for batteries and supercapacitors due to their high thermal stability and negligible volatility.
- **Carbon Capture:** ILs exhibit strong interactions with CO₂, making them effective for carbon capture technologies, although their high viscosity can be a limiting factor. DESs are also gaining attention in this field due to their biodegradability and lower cost.
- **Biomass Processing:** DESs show remarkable efficiency in dissolving lignin and cellulose, enabling biofuel production and the extraction of valuable bio-derived chemicals.
- **Metal Processing:** DESs serve as a greener and more cost-effective alternative in applications such as electrodeposition, electropolishing, and metal oxide extraction.
- **Pharmaceutical Applications:** DESs are being explored for drug delivery, protein stabilization, and the extraction of active pharmaceutical ingredients (APIs).

Despite their similar applications, ILs and DESs differ significantly in their synthesis and raw material requirements. ILs are salts composed of organic heterocyclic cations paired with organic or inorganic anions, exhibiting melting points below 100°C. DESs, in contrast, are simple mixtures of hydrogen bond acceptors and hydrogen bond donors, where strong intermolecular interactions significantly depress the melting point of the mixture. Figure 9 compares their synthesis methods [2, 24].

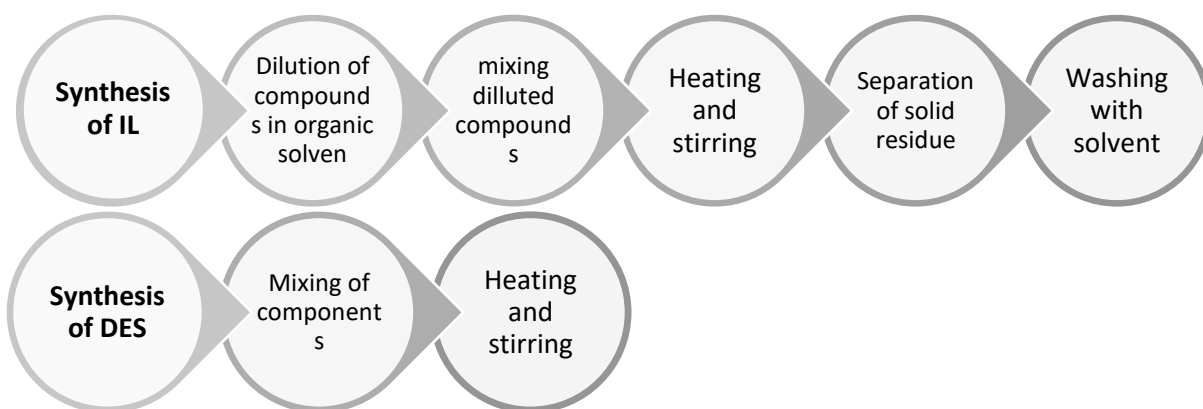


Figure 9: A comparison of the synthesis processes of ILs and DESs [2]

The synthesis of ILs typically requires multistep procedures, volatile organic solvents, and high temperatures, often generating waste and by-products. In contrast, DESs are prepared via simple methods such as heating, grinding, or freeze-drying, usually achieving near-perfect atom economy with minimal waste.

Initially, ILs were regarded as "green solvents" due to their low volatility, but later studies revealed that many ILs are toxic, non-biodegradable, and environmentally persistent. DESs, on the other hand, tend to be more environmentally friendly, as they are generally biodegradable, composed of natural raw materials, and exhibit low toxicity.

From an economic perspective, large-scale production of ILs is costly, whereas DESs are significantly cheaper and more accessible due to the renewable and inexpensive raw materials used in their synthesis. However, high viscosity remains a challenge for both ILs and DESs, though this can be mitigated by adding water or other co-solvents. Care must be taken, as excessive water content can reduce solvent performance [2, 24, 26].

1.2 Applications of Ionic Liquids (ILs) in Various Fields

After reviewing the classification of ILs, it is now essential to discuss their main applications in different fields:

1.2.1 General Studies and Reviews on Ionic Liquids

Gu and Jérôme (2013) examined the background and classification of bio-based solvents, highlighting recent advances in their applications for organic synthesis, catalysis, biotransformation, and separation processes [27]. Syahir et al. (2017) reviewed bio-based lubricants, emphasizing their superior lubricating properties compared to conventional mineral lubricants, as well as their renewability and biodegradability [28]. Noorani et al. (2022) specifically investigated cholinium-amino acid ionic liquids as biocompatible agents for CO₂ absorption, demonstrating their potential as greener alternatives in carbon capture technologies [29].

1.2.2 ILs in Chemical Synthesis and Extraction

ILs play a crucial role in dissolving both organic and inorganic compounds, making them highly effective as solvents in catalytic processes such as hydrogenation, alkylation, and hydroformylation [13]. They have also proven effective in extraction techniques, such as recovering precious metals and removing sulfur compounds from fuels, contributing to cleaner energy production and resource recovery.

For example, ILs can be employed to extract gold from electronic waste and metal alloys. Common anions used in such extractions include PF_6^- and BF_4^- , while frequently utilized cations include 1-alkyl-3-methylimidazolium ($[\text{CnMIM}]^+$) and N-alkyl pyridinium ($[\text{Cnpy}]^+$) [30].

1.2.3 ILs in Energy and Electrochemistry

ILs serve as non-volatile, thermally stable electrolytes in batteries and supercapacitors, enhancing performance and durability [1]. They are also used in dye-sensitized solar cells, where their ionic conductivity and thermal stability improve efficiency and longevity. For instance, Zaccagnini and co-workers [31], developed a novel supercapacitor using the ionic liquid $[\text{PYR}_{14}][\text{TFSI}]$ with laser-induced graphene (LIG) electrodes. This IL was chosen over BF_4^- or PF_6^- anion-based ILs due to the superior electrochemical and thermal stability of the TFSI anion, making it a strong candidate for advanced energy storage applications.

1.2.4 ILs in Metal Plating and Deposition

ILs provide an environmentally friendly alternative to conventional metal plating and deposition processes [1]. They facilitate coating applications with reduced environmental impact, lowering toxicity and minimizing industrial waste. For example, Maniam and Paul [32], reviewed the electrodeposition of zinc and zinc-nickel alloys in IL-based systems, discussing the associated benefits and challenges. Additionally, Rahali et al. [33] utilized butyl pyridinium dicyanamide ($\text{Pyri}_4\text{-DCA}$) for silver electrodeposition on platinum electrodes, leveraging its low dynamic viscosity and strong ionic conductivity.

1.2.5 ILs in Advanced Materials and Specialized Applications

ILs play a crucial role in gas chromatography, where they serve as high-selectivity, thermally stable stationary phases, enabling the efficient separation of complex mixtures [1]. They are also widely explored as industrial lubricants and heat transfer fluids, reducing wear and maintaining performance across a broad temperature range. Qu et al. [34] demonstrated that ILs function effectively as base lubricants or additives in diesel engine applications. Their study found that, compared to conventional 15W40 engine oil, pure ILs significantly reduced wear and friction. Moreover, even at low concentrations, ILs enhanced the lubricity of mineral oil, highlighting their potential in improving engine performance.

Additionally, cholinium-based ILs are particularly effective at dissolving lignin, making them valuable for biomass conversion into biofuels [35].

1.2.6. ILs in Environmental Technologies

ILs have been explored extensively for their applications in CO₂ capture [7] and water treatment [36], playing a vital role in sustainability efforts. For instance, they have been tested in flue gas treatment [37] and direct air capture technologies [38]. Their tunable properties make them highly effective for gas separation processes, often surpassing conventional solvents.

Dai et al. [39] demonstrated that combining ILs with membranes resulted in superior performance compared to commercially available alternatives. The vast range of cations and anions available allows ILs to be designed with tailored characteristics, making them particularly promising for gas separation membranes used in flue gas treatment. As the push toward a net-zero future intensifies, optimizing such technologies will become increasingly important.

1.2.7 ILs for CO₂ Capture and Carbon Reduction

This thesis explores amino acid-based IL solutions as an alternative to traditional CO₂ capture methods, demonstrating their ability to chemically bind CO₂ effectively. The current industrial standard relies on aqueous amine solutions [40], with solubility in water being a key determinant of an amine's efficiency in CO₂ absorption. Extensive research has been conducted to identify novel amines with high CO₂ absorption capacities under specific operational conditions [41].

Among the most promising candidates, Ma'mun et al. identified AEEA (a diamine with one primary and one secondary amine) and MMEA (a secondary amine) as effective options for CO₂ capture due to their reaction rates and absorption efficiency in aqueous solutions [42].

However, despite their potential, IL-based CO₂ capture technologies still face several challenges, including cost, environmental impact, and large-scale implementation hurdles. Continued research and development are essential to enhance the efficiency and economic viability of these materials, ensuring their role in global carbon reduction efforts [43].

1.3 Choline Based ILs:

Choline, also known as 1-Hydroxy-N,N,N-trimethylethan-2-ammonium chloride, is an essential nutrient vital for human health and metabolism. Recognized by the US Institute of Medicine (IoM) as a dietary requirement, choline plays a fundamental role in several physiological functions, including lipid metabolism, cell membrane signaling, and neurotransmitter synthesis—particularly in the formation of acetylcholine. Chemically, choline chloride is classified as a quaternary ammonium salt with the molecular formula $(\text{CH}_3)_3\text{N}^+\text{CH}_2\text{CH}_2\text{OHCl}^-$ [Figure 10]. Its structure consists of a positively charged nitrogen atom surrounded by three methyl groups and a hydroxyethyl group, balanced by a chloride anion. This composition makes choline highly hydrophilic, contributing to its role in cellular signaling and membrane function.

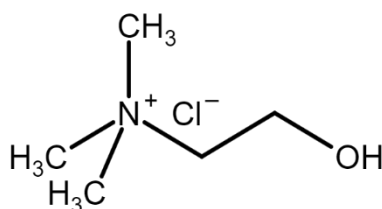


Figure 10: Chemical Structure of Choline Chloride

One of the most biologically significant derivatives of choline is phosphatidylcholine, a major phospholipid found in cell membranes. Choline is also involved in methyl group metabolism, which supports key biochemical processes such as detoxification and DNA methylation.

Dietary sources of choline are diverse, including eggs, meats, soy, and other plant- and animal-based foods. Although the human body can synthesize choline through the methylation of phosphatidylethanolamine, endogenous production is insufficient to meet daily physiological demands, necessitating dietary intake [44].

Choline-based ionic liquids (ChILs) represent an emerging class of green, biodegradable solvents that are both toxicologically and economically favorable. In these systems, choline serves as the cation, functioning as a quaternary ammonium compound. Choline is typically derived from renewable sources through a highly efficient synthesis process that generates minimal waste, aligning with sustainability objectives. [4]

ChILs are usually combinable with organic acids, like succinic or oxalic acids, to yield salts that are liquids at room temperature or slightly above. Physicochemical properties of ChILs, like their solubility in water or organic solvents, viscosity and thermal stability- can be tweaked by modifying the side-chains present on choline cation or by modifying the anion. These properties

make ChILs an eligible choice for wide variety applications, such as biomass pretreatment, gas absorption and green catalysis.

Amino acids of particular interest are those naturally occurring as constituents of peptides and proteins. These molecules are α -amino acids, meaning they possess both an $-\text{NH}_2$ (amino) group and a $-\text{COOH}$ (carboxyl) group attached to the same carbon atom. All α -amino acids are white, crystalline solids, highly soluble in water but insoluble in alcohol. With the exception of the simplest member (glycine), all are optically active due to their chiral nature [45].

Biodegradable biocatalytic ionic liquids derived from amino acids offer a highly versatile and sustainable alternative to conventional solvents, given their natural abundance and renewability. The functional groups in amino acids allow for modifications to adjust acidity, chirality, and reactivity, making them ideal for catalytic applications. These amino acid-based ionic liquids (AAILs) serve as greener substitutes for volatile organic solvents in a variety of catalyzed reactions, including the Diels-Alder reaction [46]. In the pharmaceutical sector, AAILs enhance protein solubility, crystallization, and stability, further demonstrating their suitability as green solvents. Additionally, AAILs show great potential for CO_2 capture, as their amino-functionalized anions chemically react with CO_2 via an efficient 1:1 mechanism (*Figure 11*). Note that viscosity gives a challenge. Areas explored to improve performance include addition of water or modifying hydrogen bonding network. The use includes biomass processing, especially for the specific extraction of lignin, which shows their versatility [47].

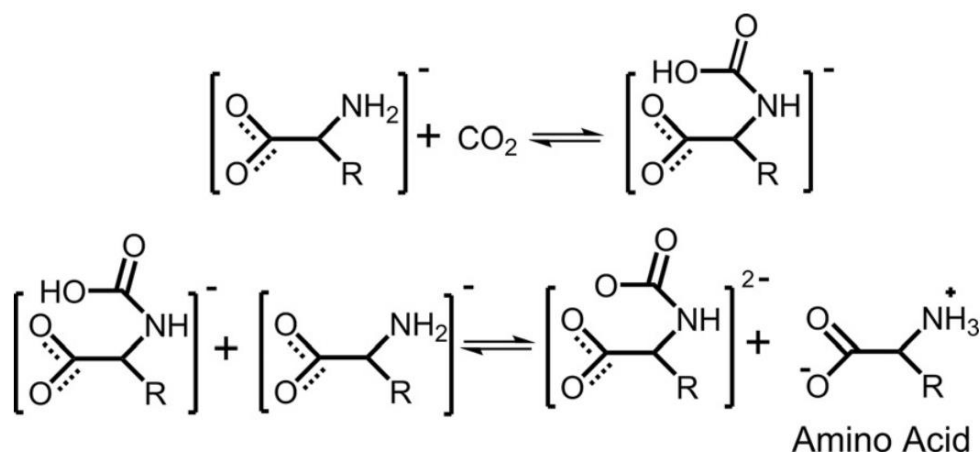


Figure 11: Universal reaction of CO_2 with the amine group in amino-acid ILs (the cations are hidden) [48]

The chemical interaction between structural functional groups of choline and AAs with CO_2 plays a key role in their efficiency for carbon capture. Choline-based amino acid ionic liquids (ChoAAILs) represent an innovative approach to overcoming viscosity limitations while

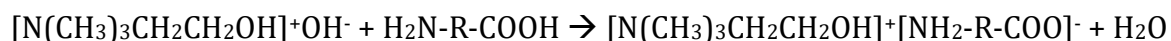
enhancing CO₂ absorption. By combining choline and amino acids, ChoAAILs create biocompatible, highly efficient CO₂ capture systems.

This efficiency arises from the amine groups in the anion, which readily react with CO₂, forming stable carbamate species. Additionally, incorporating water as a co-solvent can significantly reduce viscosity and enhance CO₂ diffusion by weakening hydrogen bonding networks. Water also acts as a catalyst, promoting a proton transfer (PT) mechanism, which further optimizes CO₂ absorption [49]. However, despite these advantages, high viscosity and economic viability remain challenges. Nonetheless, ongoing research continues to drive ChoILs and AAILs as sustainable alternatives for CO₂ capture, green chemistry, and pharmaceutical applications [47].

1.3.1 Synthesis of Cholinium-Based Amino Acid Ionic Liquids ([Cho][AA])

Cholinium-based amino acid ionic liquids ([Cho][AA]) can be synthesized through the following reaction:

Choline hydroxide (aq) + Amino acid → [Cho][AA] + H₂O



Synthesis Steps:

1. Mixing stoichiometric amounts of the amino acid with aqueous choline hydroxide.
2. Stirring at room temperature for approximately 48 hours.
3. Extracting under vacuum to obtain the viscous IL product.

1.4 PVT Cells

The behavior of fluids under varying pressures and temperatures is studied using a PVT (Pressure-Volume-Temperature) cell. These instruments are vital in the studies of petroleum engineering, fluid mechanics, and chemical processing. Their purpose focuses on better understanding a substance's physical and thermodynamic phenomena-gases, liquids, or mixtures of them. The behavior of fluids in different system environments is explained through such types of data as gathered using PVT cells to make a better decision for industrial systems design and understanding fluid behavior through various environments [50, 51].

PVT cells serve an important role in oil and gas. Their purpose is to analyze produced fluids from reservoirs for phase behavior analysis, including gas-oil ratios, oil shrinkage, and drive mechanism evaluation for the given reservoir. Furthermore, the data acquired reflect critical

pressures and temperatures for those fluids and fluid compositions. This is vital when designing efficient recovery strategies due to improved production processes.

In this experiment, PVT cell is used to study the ionic liquids. Analyzing the ILs in different pressure and temperature conditions is necessary because it demonstrates how solubility of CO₂ in ILs would change at different pressures and temperatures. High atmospheric concentration of carbon dioxide (CO₂) nowadays is a major factor influencing the climate of the Earth, intensifying the greenhouse effect and global warming. Weather conditions such as drought and floods-accelerated by global warming-are becoming increasingly severe and not conducive for agriculture and water quality, which in turn heightens the risk of wildfires. To reduce these adverse effects, CO₂ emissions must be restricted. Reaching net zero emissions could cut down by two-thirds the area of global land undergoing aridification, with a regional decrease in the intensity of hydrometeorological occurrences [52]. Reducing greenhouse gas emissions through policy can also have a large beneficial impact on public health regarding air pollution, heart disease, cancer, and obesity [53]. Thus, reducing CO₂ emissions will protect public health and stabilize the environment. One way to reduce carbon emissions is post-combustion CO₂ capture. Therefore, having the ILs examined through the PVT cell aids to understand their performance in post-combustion carbon capture. This idea will be examined further in the next chapters.

1.5 Post-Combustion carbon capture

Post-combustion CO₂ capture technology is one of the mature and well-established methods applied in a power plant for mitigation of greenhouse gases. This process involves the separation of CO₂ from flue gases after fuel combustion. It can be retrofitted easily in already existing infrastructures without interfering with energy generation. Among the available techniques, including adsorption, membrane separation, and calcium looping, chemical absorption is the most applied technique, especially with amines as the most common solvent, such as monoethanolamine [54]. MEA and ILs are the two major absorbents that have been given attention owing to their respective advantages and limitations.

MEA is an established amine-based solvent, generally recognized for its high efficiency in CO₂ capture by chemical absorption in the temperature range of 40-70 °C and atmospheric pressure, forming carbamate bonds with CO₂. It is cost-effective, highly water-soluble, and achieves as high as 99% CO₂ recovery rates. However, critical downsides to MEA include high energy requirements for its regeneration, which results in about a 20% efficiency loss in power plant

operations. Besides, MEA degrades with time, releasing toxic byproducts such as nitrosamines, which are environmental and health hazards. Other difficulties include the loss of the solvent by evaporation, corrosion problems, and intensive operation costs. In spite of all these disadvantages, MEA remains the most widely used choice for CO₂ capture because it is mature, inexpensive, and its use can be easily adapted in existing systems [54].

On the other hand, ILs are under development as potential alternatives for CO₂ absorption. As discussed earlier, these low-melting-point salts consist of organic cations paired with organic or inorganic anions. ILs are well-known for their low vapor pressure, high thermal stability, and tunable physicochemical properties, such as solubility and viscosity. Additionally, ILs can chemically bind CO₂, reducing solvent loss risks while allowing for structural modifications to enhance performance. However, ILs still face significant challenges that hinder their large-scale adoption. High viscosity limits mass transfer rates, while high production costs remain a major barrier to industrial implementation [4]. Energy-intensive regeneration is another common drawback shared by MEA and ILs, impacting both efficiency and cost. Although ILs require less energy for regeneration than MEA, they still present challenges due to their high costs, limited large-scale applicability, and viscosity-related constraints. Despite being environmentally safer and highly customizable for specific applications, these limitations currently make MEA the more practical choice in the immediate term [55].

While MEA dominates the current technology in CO₂ capture due to its practicality and reasonable cost, ILs are very promising for the future. Research is targeted at reducing IL viscosity, enhancing their CO₂ absorption efficiency, and reducing production costs so that they will be more viable. The tunable properties and smaller environmental impact of ILs perhaps one day may outcompete MEA as production and application continue to improve. For the time being, MEA remains the most common option in post-combustion capture of CO₂ and hence keeps ILs an unobstructed way to more sustainable and greener options within carbon capture technologies.

In this study, a ChoAAIL, a non-toxic and green solvent is used for carbon capture. The diluted version with some amount of DMSO showed to moderate its high viscosity while improving the absorption of CO₂. This system gets to its maximum performance when the concentration reaches an ideal balance between physical mass transfer properties and chemical reactivity [56].

2. Material and methods

The synthesis of ILs based on choline and amino acids represents a significant step toward sustainable and biodegradable solvent alternatives. Among these, choline proline ([Cho][Pro]) has gained attention due to its biocompatibility, non-toxicity, and tunable physicochemical properties. These features make it highly suitable for applications in biomass processing, CO₂ capture, catalysis, and pharmaceutical formulations.

The preparation of [Cho][Pro] follows a straightforward and efficient synthetic route, involving the reaction between choline chloride and proline, mediated by potassium hydroxide (KOH) in ethanol. This method ensures high yield and purity, with minimal environmental impact. The process involves neutralization, solvent-assisted purification, and rotary evaporation, yielding a highly viscous ionic liquid with unique solvation properties.

Additionally, other amino acid-based ILs, such as 1,1-dimethylpyrrolidinium proline ([DMP][Pro]), have been synthesized using microwave-assisted techniques. These ILs share similar functional properties but exhibit different thermal stability, solubility, and viscosity profiles, which influence their potential applications.

The following sections provide a detailed methodology for the synthesis of [Cho][Pro] and [DMP][Pro], along with characterization techniques to assess their structural, thermal, and rheological properties. These investigations help to optimize IL performance for various industrial and research applications in green chemistry, electrochemistry, and biotechnology.

2.1 Synthesis of [Cho][Pro]

0.2 mol of potassium hydroxide (KOH in pellets supplied by Sigma-Aldrich, purity 99%) was added to 100 ml of ethanol (supplied by Sigma-Aldrich, purity 99.8%) in a round-bottom flask (the scale has an instrumental error of $\pm 0,001$). Once the KOH is fully dissolved, Proline (0.2 mol (*Figure 13*), supplied by Biosynth) is gradually added. After complete dissolution, the mixture is left overnight at room temperature under stirring. The next day, 0.2 mol of Choline Chloride (ChoCl (*Figure 12*), supplied by Biosynth, purity 99%) is added, and the mixture is left to mix for a few hours. A solid precipitate of potassium chloride is formed. This precipitation is separated by centrifugation (4200 rpm for 5 min). [Cho][Pro] was produced by rotary evaporation to remove the ethanol. A solution of acetonitrile (supplied by Carlo Erba) and ethanol (9:1 v/v) was added to purify the produced [Cho][Pro] from residual inorganic salts,

which are removed by centrifugation (4200 rpm, 5 min) The solvent is evaporated by rotary evaporation, producing a transparent solution of [Cho][Pro]. (see *Figure 14* and **Figure 15**).

Proline + Potassium Hydroxide → + Ethanol → Potassium Salt of Proline + Water

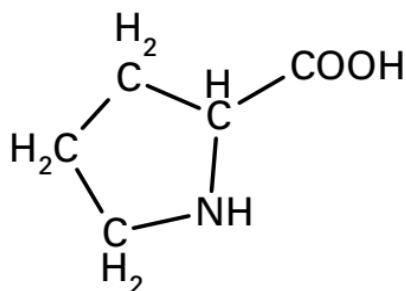


Figure 13: Chemical Structure of Proline

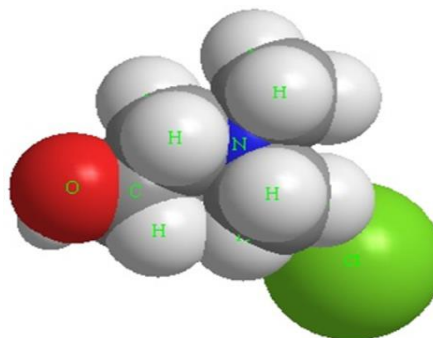


Figure 12: 3D representation of Choline Chloride

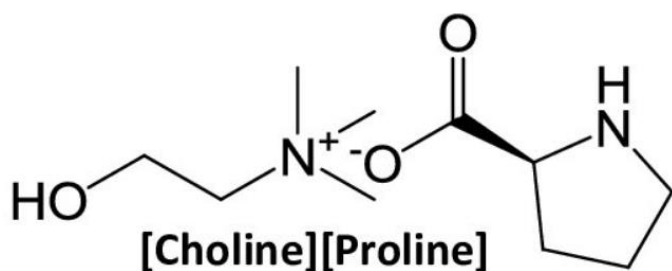


Figure 14: Chemical Structure of [Cho][Pro] [4]

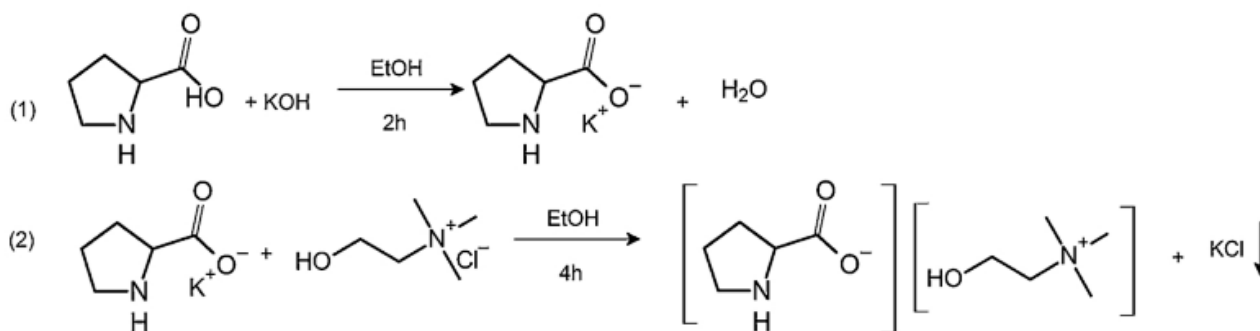


Figure 15: Synthesis of [Cho][Pro] [3]

Table 1: Amount of components to synthesize [Cho][Pro]

		Supplier	MW (g/mol)	Mole	Quantity
Anion	Proline	—	115.13	0.2	20 g
Cation	Choline Chloride	— Biosynth	139.62	0.2	24.25 g
	Potassium Hydroxide	— Sigma-Aldrich	56.105	0.2	10.72 g
Solvent	Ethanol	—	46.068	0.2	100 ml

2.2 Preparation of [Cho][Pro] solutions

Dimethyl sulfoxide (DMSO, supplied by Merck, purity 99%) was used as a solvent to reduce the challenges associated with the high viscosity of the ionic liquid. Three different solutions of [Cho][Pro] in DMSO were prepared at concentrations of 12.5%, 33%, and 50% by mixing the ionic liquid with DMSO (see *Figure 16*).



Figure 16: 3 ml different solutions of [Cho][Pro] in DMSO

2.3 Synthesis of [DMP][Pro]

In a microwave reactor, N-methyl pyrrolidine (supplied by Sigma-Aldrich) and dimethylcarbonate (DMC, supplied by Sigma-Aldrich) (1:3) are mixed together in the presence of anhydrous methanol (by Sigma-Aldrich, purity 99.8%). The resulting solution undergoes microwave irradiation at 140°C for 40 minutes at 20 bar [*Figure 17 and Figure 18*]. At the end of the reaction, the ionic liquid 1,1-dimethylpyrrolidinium methyl carbonate or [DMP][CH₃OCOO] is obtained and the solution is transferred to a round-bottom flask [*Figure 19*]. In *Table 2* the amount of each component for this synthesis is shown.



Figure 17: The reactor inside the microwave

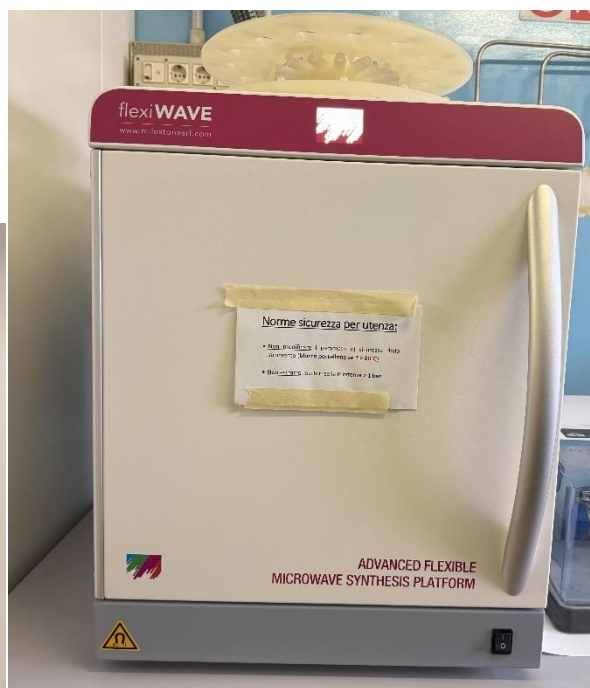


Figure 18: The microwave used for the synthesis of DMP



Figure 19: $[DMP][CH_3OCOO]$

Table 2: Synthesis of $[DMP][CH_3OCOO]$

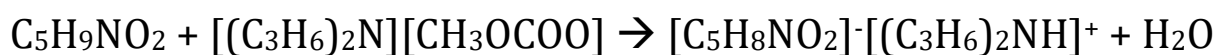
	mol	MW (g/mol)	m (g)	V (ml)
Dimethyl Carbonate	0.202	90.08	18.19	17.02
n-Methylpyrrolidine	0.067	85.15	5.73	7
Methanol		32.04	13.5	17.02
$[DMP][CH_3OCOO]$	0.067	175.12	11.79	

7.75 g of Proline are weighed using a precise scale with an instrumental error of ± 0.001 and slowly added to the solution under stirring. A minimal amount of methanol is added to the flask to dissolve proline, ensuring that the reaction medium is homogeneous. The reaction is kept stirred smoothly overnight at room temperature, as it enables the optimum single-phase mixing of the reactants, allowing the reaction to go to completion. If there is some residual unreacted amino acid, it can be removed as a solid precipitate by washing the IL with an acetonitrile/ethanol solution (9:1 v/v). Water, produced as a by-product during the neutralization reaction, is removed along with the solvent using rotatory evaporation. As a result, the IL 1,1-dimethylpyrrolidinium proline [DMP][PRO], was obtained [Table 3].

Table 3: Synthesis of [DMP][Pro]

	mol	MW (g/mol)	m (g)	V (ml)
[DMP][CH ₃ OCOO]		175.12	11.79	82.08
Proline	0.081	115.13	7.75	-
[DMP][Pro]		214	28.81	

The ionic liquid produced has been characterized using different analytical methods such as ATR-IR spectroscopy, DSC and TGA.



2.4 Characterizations

2.4.1 ATR-IR

Attenuated Total Reflectance (ATR) is a qualitative spectroscopic method for finding out the molecular structure because it is commonly applied in Fourier Transform Infrared (FTIR) spectroscopy. Specially it is used to examine solids, liquids, and semi-solids without requiring much sample preparation [57]. Below is a comprehensive description of ATR characterization explaining the concepts, applications, advantages, and references that were verified.

Total internal reflection is a phenomenon that is essential to ATR. Using infrared (IR) light from a source, this light will impose onto the surface of a very high refractive index crystal, such as diamond, germanium, or zinc selenide, through which the sample is placed, thus preventing the IR light from penetrating the sample only a small distance (in this case, about 0.5-2 μm).

The sample absorbs specific wavelengths in the infrared region, corresponding to its molecular vibrations, generating an absorption spectrum.

In ATR the waves that the instrument sends inside the sample make the bonds vibrate, stretch, or bend. So, each peak in the output is related to a specific vibration, thus a specific compound.

The ATR-IR spectra were obtained using a Bruker Tensor II Fourier transform spectrophotometer with a platinum ATR diamond accessory. The IR spectra were measured at a resolution of 4 cm^{-1} , spanning the spectral range from 4000 to 400 cm^{-1} . During the analysis, 10 background scans and sample scans were conducted. The spectra were then processed with OPUS 8.1® software.

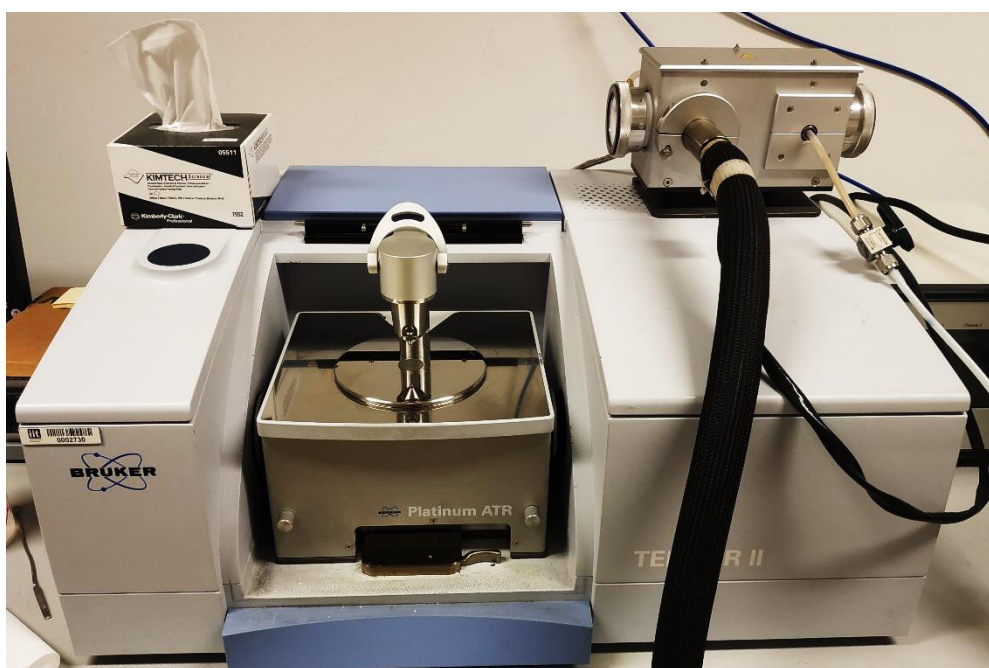


Figure 20: ATR-IR instrument

2.4.2 Density

In the domains of chemistry, food science, and industry, where liquids may be weighed per unit volume, density measurement is essential. With contemporary densimeters, such as Anton Paar's DMA series, this becomes most effective. Measuring density is necessary for ILs since knowing their characteristics and behavior are essential for studying them.

Adjustment of the dampener's external and internal components is essential to operate precisely. Turning it on and verifying the calibration would be necessary for this. The majority of densimeters, such as Anton Paar's DMA instrument series, need to be calibrated using a few

approved reference materials, such as distilled water, or standards, such as known density solutions. Maintaining the calibration is crucial since it gives the upcoming measurements more assurance.

It is required to prepare the liquid sample uniformly before there are any analytically harmful circumstances during the measurement. The findings will be impacted if there are air bubbles, contaminants, or sediments present. The liquid may need to be filtered or degassed in order to obtain reliable results. This is particularly crucial for samples that create foam or are viscous liquids, as air bubbles can disrupt the oscillation frequency while measuring density.

Maintaining the solution temperature is crucial since the density value is dependent on the temperature at which it is measured. Internal temperature control allows the operator to select temperatures for studies in densimeters like the DMA 5001.

20°C is chosen as the temperature for every application that does density measurements because it is the international standard temperature for the majority of industrial and scientific applications. In this study the upper limit is 70°C with increments of 10°C, each step measured 3 times, and then an average is chosen.

The measuring cell of the probe receives the liquid sample and is typically U-shaped. The usual procedure is to fill the cell completely; if not, the liquid will rise slowly and eventually eject some air, leaving the cell partially empty, which will cause the U-tube to oscillate incorrectly.

The instrument uses a certain type of measuring procedure. For instance, the oscillating U-tube method is used as a tool for density analysis measurements for the DMA 5001 model. This type of measurement tool is also seen in a filled tube with an estimated natural oscillation frequency. Using the recorded frequency, the gadget does an extremely accurate density calculation. It will then additionally recognize the content of certain specified components and calibrate the density with the temperature.

However, the machine's balanced density is shown on the densimeter in the range of values for heating only. Courts are often granted tolerances a few decimal places over the permitted range (e.g., ± 0.000005 g/cm³ for the DMA 5001). Many of the newest gadgets can save, export, or integrate with software to send data to platforms for further in-depth research.

Cleaning the chamber after measurement is critical as well. It is possible for any remaining liquid to contaminate subsequent samples or even harm the densimeter itself. For long-term use, the cell must be cleaned using the proper cleaning solvent and dried with air.

2.4.3 Viscosity

One of the key elements influencing the use of ILs is their viscosity, particularly when it comes to their use as solvents for extraction and catalysis, among other processes. Consequently, a lot of work has gone into creating and designing low-viscosity ILs [58]. Because of its polar aprotic character and comparatively low toxicity as compared to other solvents, DMSO improves the compatibility and performance of [Cho][Pro] by decreasing its viscosity [59].

The viscosity analysis can be done using Rheometer MCR 702e Anton Paar (*Figure 21*). This device is appropriate for advanced rheological measurement. Two parallel plates were inserted in the device because this geometry is more suitable for high viscous fluids. The zero gap is then set after alignment. The temperature was set and stabilize on 25°C to reach the maximum during the test which is 70°C. The humidity was set on 30% and the N₂ pressure is set on 6 bar. A few drops of the sample are put on the device, enough to cover the plates surface.

Through the software, the test is initiated. The rheometer applies precise shear stress and shear rate to the sample and measures the resulting deformation or flow behavior. The viscosity is calculated from *Equation 1*:

Equation 1: Calculation of viscosity by rheometer

$$\eta = \frac{\tau}{\dot{\gamma}}$$

where η is the viscosity (Pa·s), τ is the shear stress (Pa), and $\dot{\gamma}$ is the shear rate (s⁻¹).

After about an hour the software obtains the plot of viscosity vs. temperature. The viscosity should decrease with increasing temperature, so the resulting curves must be descending.

This test can be performed in future to give a more comprehensible understanding of ILs behavior.



Figure 21: Viscosity Meter instrument

2.4.4 DSC

Differential Scanning Calorimetry (DSC) is to understand the intrinsic behavior of materials. There is a furnace inside the instrument (Netzsch DSC 204 F1) (*Figure 22*), coped with a precise balance. The sample IL is weighed in tiny aluminum cups called crucibles. The difference of this method with TGA is that here there is a closed crucible which is being compared to a reference empty crucible.

A hole is made in the crucible's lid to allow possible exhalent gas from the sample, IL. In case of [Cho][Pro]solutions in DMSO the hole is not needed. Then, the pressing machine is used to close the lid before it is placed inside the instrument.

The machine is operated in three cycles. The temperature is increased from 20 °C to 150 °C to remove impurities and weak-bonded ligands, and it is held at this temperature for 10 minutes to stabilize. Then, it is dropped to -70 °C to crystallize the system. The heat rate is set to 10 K/min. After the first round, the real analysis is started. This process is repeated for three cycles, taking almost 3 hours. The protective purge is kept at 50 $\frac{ml}{min}$. A flux of 20 ml of N₂ is chosen since the changes are made more evident by using this flux.



Figure 22: DSC characterization instrument

2.4.5 TGA-IR

Thermogravimetric analysis (TGA) is used to characterize the thermal behavior of materials over time. With this measurement, much information about the sample can be obtained. For this device (Netzsch TG 209 F1 [Figure 23]), O₂ and N₂ are used. If different gases are used, the behavior would change.

The crucibles are made of ceramic with a standard weight of 160 mg. Using gloves and ethanol, the instrument is cleaned before the crucible is placed inside without any lid. By pushing the two closing buttons simultaneously, the crucible is isolated and closed. The first step is for the empty crucible to be weighed, and the super-sensitive balance inside the instrument is tared. Then, the cap is opened, and the crucible is filled with the sample, [Cho][Pro]. One drop of IL is enough for the machine to respond. The preferable amount of sample for a TG analysis is considered to be between 10 and 40 mg. After a few minutes of oscillation, the weight is more stable and the measurement is started, which takes about 48 minutes. The sample is subject to a wide range of temperature changes at a constant rate of 20 K, starting from 30 °C, and its mass is meticulously measured over time.



Figure 23: TGA-IR characterization instrument

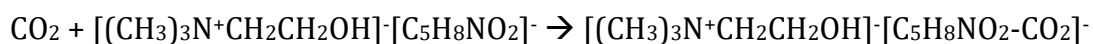
2.4.6 Carbon capture test

Gravimetric analysis is a quantitative procedure in analytical chemistry used for determining the mass of a substance for calculating its concentration. In this application, however, the quantity of CO₂ consumed is measured by using an appropriate absorbent to collect the gas from a gas stream before weighing it post-collection to determine mass change.

Because of particular characteristics of ionic liquids (ILs), for instance, their ability to absorb CO₂ at very high levels, tunable chemistries, and low volatilities, CO₂ absorption with ILs, such as choline proline ([Cho][Pro]), has emerged as a promising carbon capture theme. Since [Cho][Pro] is highly viscous, diluted solutions of [Cho][Pro] in DMSO were tested.

As [Cho][Pro] contains the proline anion, which combines with CO₂ to generate carbamate or bicarbonate species, it absorbs CO₂ through a chemical process.

The following is a summary of the reaction:



Method: A small vial of 5 ml volume was prepared as the sample holder of the reactor. Its volume was confirmed by measuring it with distilled water. Then the empty dried vial and the whole reactor plus a tiny magnetic stirrer were weighted. 2.5 ml of solution was poured into the reactor using a pipette, and then weighted again. In this way the initial mass of the solution is obtained under inactive condition to establish a baseline. The reactor is connected to the instrument, ready for the test (Figure 24).

The procedure to purify the system which is done to study CO₂ uptake in the presence of an ionic liquid requires certain steps to be followed. One such step is to introduce a nitrogen flow. Using the software, the sample gets exposed to a controlled flows of CO₂ and N₂. The temperature is set at 25 °C at 0.9 bar and the flux at 10 ml/min. It is crucial to begin with N₂ flow to ensure that the residual gases such as CO₂, O₂ and humidity are minimized. These adjustments help maintain stable temperature and pressure conditions of the system through the flow of nitrogen, and thus prevent distortion in results related to subsequent CO₂ absorption from the environment. It is through this approach that IL is effectively analyzed. By adhering to such stringent measures, guarantee of obtaining highly accurate and repeatable results is achieved.



Figure 24: The reactor containing 2.5 ml of IL

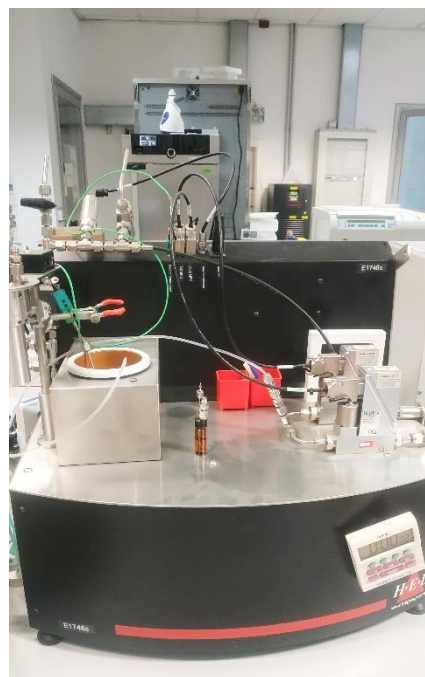


Figure 25: The gravimetric analyzer for CO₂ absorption test

After nitrogen flux, the reactor is weighted again. Then it goes through CO₂ exposure. Each ten minutes, the procedure is paused and the weight of the reactor is measured by a digital scale with a precision of 0.00001 gram. If some amount of CO₂ is dissolved into the solution, the mass of the reactor should be increased. Once this increment becomes stable or negative, the maximum absorption capacity has been reached, thus the procedure is finished. The percentage of absorbed CO₂ is then calculated and compared to other solutions.

The H.E.L E1746s gravimetric analyzer (*Figure 25*) was used for this test. It functions as a gas sorbent measuring device for different materials including ionic liquids. It allows the estimation

of absorption kinetics and capacities of samples that are immersed in certain gases like CO₂ at controlled pressure and temperature conditions.

2.4.7 PVT test

The PVT cell in this study, PVT 300/700 FV EDU by Sanchez technologies [Figure 27], is comprising a fluid mixer on a piston, a precise pressure transducer, and electric heater control for temperature. A digital camera system under sapphire windows positions on the cell's visual head to view the liquid/gas interface. To ensure safety in handling the substances, all parts coming in contact with fluids are made from Hastelloy to withstand intense pressures and temperatures. At the outlet, the liberated gas after each pressure step is cooled down by the dry-ice cooling system before entering the gasometer [60] as shown in the schematic of the experimental setup in [Figure 26].

The PVT machine is equipped with a piston mechanism that can be adjusted by the operator to reach either a constant volume or a specific pressure. From the piston position the software can calculate the cell's volume. Sensors within the cell monitor temperature and pressure, guiding the piston until reaching the desired conditions. More detailed description of the instrument is available in the study done by Tawil et. al [15].

Some of the PVT FV characteristics are as follows:

- Constant temperature control system
- Stirring by magnetic coupling
- Automatic valves
- Control cabinet
- Calibrated pressure sensor and temperature sensor
- CCD digital video camera 6M pixels
- Data acquisition and processing system
- High pressure valves, pipes and filters

Several experiments can be done by this PVT cell, including: Constant Compositional Expansion, Constant Compositional Depletion, Constant Volume Depletion, Fluid Envelop Phase, Separator Test, and Differential Vaporization.



Figure 27: Sanchez PVT Cell

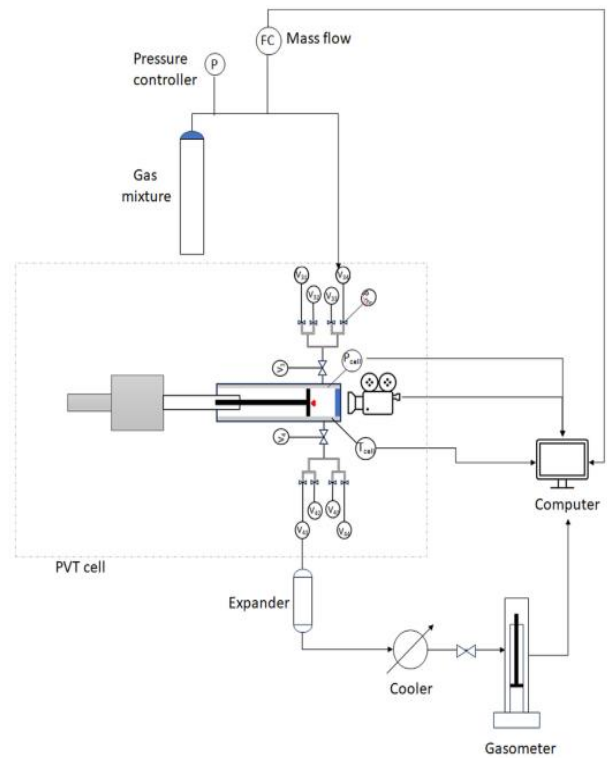


Figure 26: Schematic of experimental setup

Three solutions of [Cho][Pro] in DMSO were tested at pressures of 3, 5, 10, and 20 bar with temperature kept at 40 °C in a constant volume.

The experiment is carried out at a constant volume of 300 ml. First, the cell is loaded with 25 ml of the solution, while the remainder of its space is filled with CO₂ at 3 bar which takes about 10 minutes. Using the PVT software (Euclid), the cell's volume is calculated after the injected flow rate is monitored by the flow meter. The temperature is heated to 40 °C at 3 bar. Then again, the software calculates the new volume of gas. The cell is rotated to vertical position to create a cylindrical liquid column for estimation of the diffusivity coefficient. The system with the solution in contact with the gas is then let to equilibrate for the necessary amount of time, while the pressure sensor tracks the changes in pressure with time.

The stirring mechanism is activated to improve the absorption process. As Hu et. al [61] experiment demonstrates, increasing the velocity of gas by increasing the pressure of CO₂ and increasing the stirrer speed to accelerate the flow of liquid both can excellently diminish the mass transfer resistance in the corresponding phases, and move the transition faster towards physisorption. Thus, it indicates that CO₂ is absorbed more quickly when the solution is stirred more strongly.

Then the cell is turned back to horizontal position for the software to measure the residual volume of gas. As the first step finishes at 3 bar, the volume is reduced in order to increase the cell's pressure to 5 bar. Waiting for the pressure to reach equilibrium at a constant volume may take several hours depending on the concentration of ionic liquid and type of the test. Once the solution had taken up as much CO₂ as possible for the given pressure and temperature, this procedure will be also repeated for P at 10 and 20 bar.

At this point, the cell's pressure is brought down to 2 bar and the gas is discharged, being sent to gasometer for a more precise measurement. Although the software estimates the gas and liquid filled amounts at the interface selected manually, this approach only provides approximations of volumes. More accurate volume measurements can be provided using a gasometer, but that can only be done when the gas has vented from the cell at the end of the test. Thus, visual estimations form the basis of quantity measurements taken during the test.

Additionally, the cell was heated to 85 degrees to break the chemical bonds. At this point, the pressure was lessened further to release all the liberated gas, which was then measured using the gasometer.

3. Results and discussion

3.1 ATR-IR

In *Figure 29* the scale is maximized to ensure the curve and peaks are seen well since the Y axis is an arbitrary unit related to the absorbents of liquid. The X axis is the wavenumbers in cm^{-1} . The higher wavenumbers (left-side) are not considered very useful since many reflections from the surface occur and are not reliable. The curves are reversed by the software (OPUS) to remove this part and allow the peaks to be shown in a better way.

Positional and intensity changes between the peaks indicate variations in the strength and bending of bonds, which were shown to be influenced by molecular and ionic interactions in the samples.

The IR spectrum of pure [Cho][Pro] (see *Figure 28*) exhibits characteristic bands related to its molecular structure, primarily associated with the carboxylate ($-\text{COO}^-$) and amine ($-\text{NH}$) groups of the proline anion and the hydroxyl ($-\text{OH}$) group of the choline cation. The most significant bands observed are:

- 1590 cm^{-1} – Asymmetric stretching of the carboxylate ($-\text{COO}^-$) group.
- 1380 cm^{-1} – Symmetric stretching of the carboxylate ($-\text{COO}^-$) group.
- $3200\text{--}3400 \text{ cm}^{-1}$ – Broad band associated with hydrogen-bonded OH and NH stretching.
- $950\text{--}1050 \text{ cm}^{-1}$ – C–N stretching, characteristic of the choline cation.

These peaks define the spectral fingerprint of pure [Cho][Pro], before it interacts with CO_2 or undergoes dilution in a solvent. The broad OH/NH stretching band in the $3200\text{--}3400 \text{ cm}^{-1}$ region suggests strong intermolecular hydrogen bonding, a common feature in choline-based ionic liquids.

When [Cho][Pro] is dissolved in DMSO, notable spectral changes occur due to solvent interactions:

- The broad OH/NH stretching band ($3200\text{--}3400 \text{ cm}^{-1}$) significantly decreases in intensity, indicating that DMSO disrupts hydrogen bonding between IL molecules.
- The carboxylate ($-\text{COO}^-$) stretching bands at 1590 cm^{-1} and 1380 cm^{-1} shift slightly due to solvent-induced electronic effects, but remain prominent.

- New peaks appear in the 1000–1100 cm^{-1} range, corresponding to DMSO's characteristic S=O stretching vibrations, which overlap with C-N stretches from the IL.

These changes suggest that DMSO weakens intra-IL hydrogen bonding, leading to a different molecular environment for CO_2 interaction compared to pure [Cho][Pro].

The spectral variations follow a consistent trend across different IL concentrations, suggesting that the CO_2 interaction mechanism remains unchanged. Additionally, the relative intensity of IL-specific peaks increases as IL concentration increases, confirming the concentration-dependent spectral response.

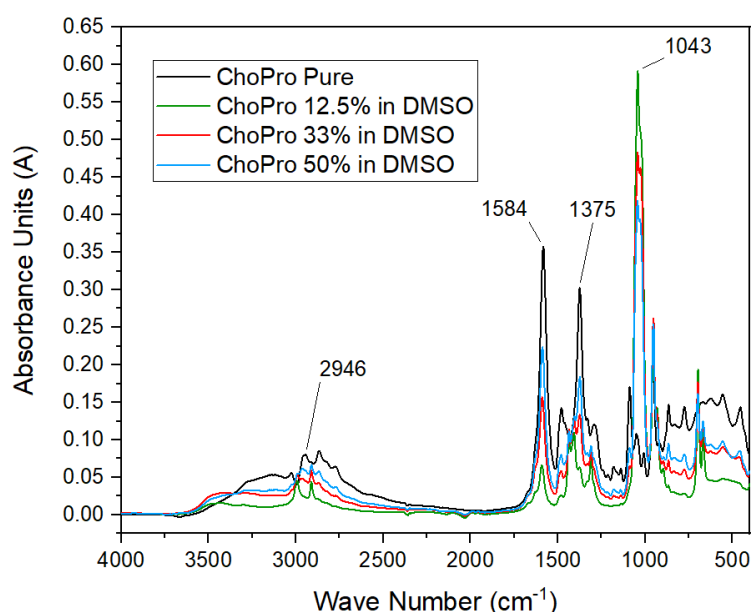


Figure 28: Comparison of [Cho][Pro] ATR-IR at various solutions

Upon CO_2 absorption, DMSO solution of [Cho][Pro] exhibit major spectral modifications, confirming the formation of carbamic acid and ammonium carbamate species. Key changes include:

- The appearance of a new band at $\sim 1683 \text{ cm}^{-1}$, corresponding to C=O stretching of carbamic acid.
- The carboxylate ($-\text{COO}^-$) asymmetric stretching mode shifting from 1590 cm^{-1} to $\sim 1628 \text{ cm}^{-1}$, indicating CO_2 binding.
- The presence of NH_2^+ species, confirmed by the appearance of bending modes at $\sim 1570 \text{ cm}^{-1}$ and $\sim 1381 \text{ cm}^{-1}$, associated with secondary amine protonation.

CO_2 reacts with the amine group of proline, forming either carbamic acid or ammonium carbamate, depending on solvent effects. The intensity of these new bands is higher in pure [Cho][Pro] compared to its DMSO solution, suggesting stronger CO_2 interactions in the absence of a solvent.

In DMSO solutions, the formation of ammonium carbamate becomes more prominent with dilution, due to the influence of solvent polarity and dilution effects [Figure 28, Figure 29, Figure 30, and Figure 31].

[Cho][Pro] 12.5% in DMSO:

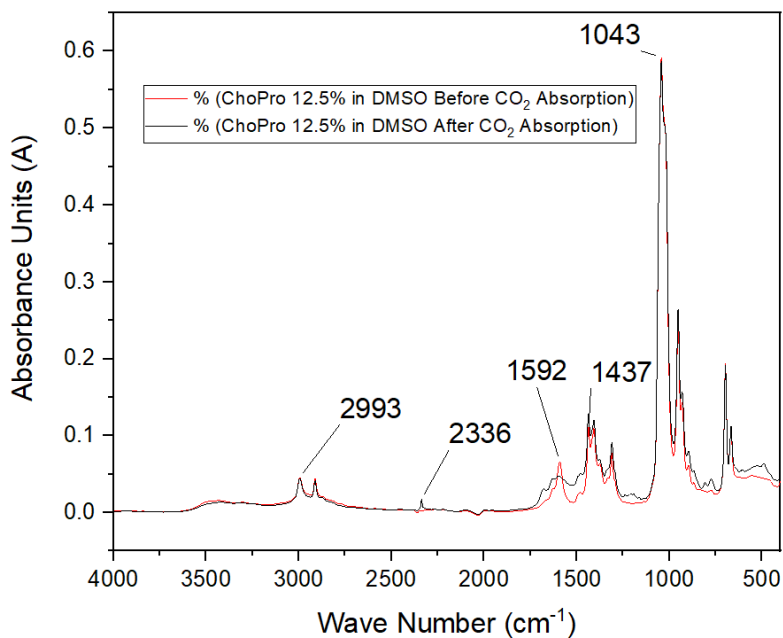


Figure 29: ATR-IR of [Cho][Pro] 12.5% in DMSO

[Cho][Pro] 33% in DMSO:

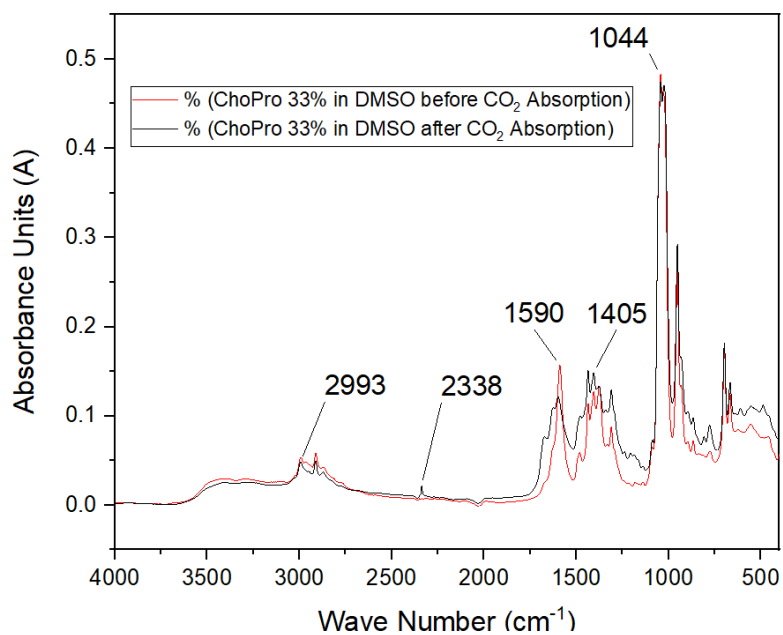


Figure 30: ATR-IR of [Cho][Pro] 33% in DMSO

[Cho][Pro] 50% in DMSO:

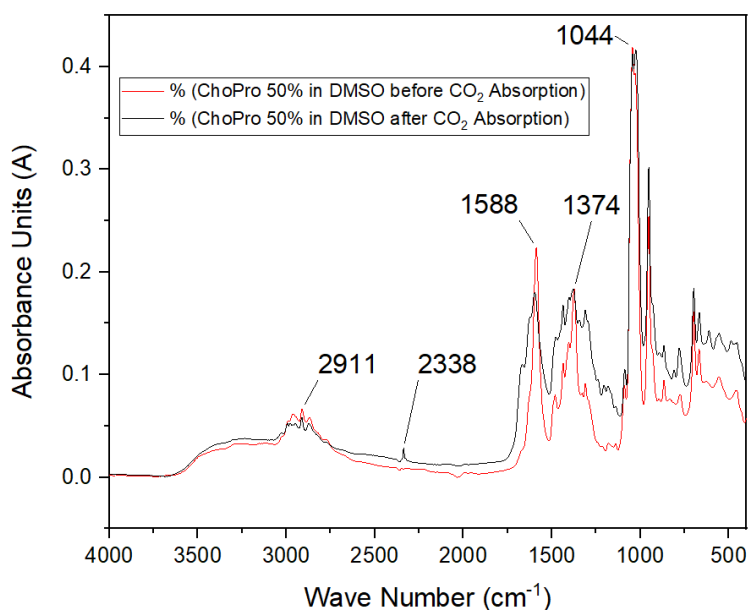


Figure 31: ATR-IR of [Cho][Pro] 50% in DMSO

[DMP][Pro]:

The IR spectrum of N,N-dimethylpyrrolidinium proline [DMP][Pro] (see Figure 32) retains the fundamental vibrational features of the proline anion while exhibiting distinct modifications in the C–H stretching and bending regions due to the presence of the pyrrolidinium cation.

1. Comparison with [Cho][Pro]

In direct comparison with [Cho][Pro], the main absorption bands associated with the carboxylate ($-\text{COO}^-$) group of proline remain nearly unchanged, specifically:

The asymmetric stretching mode at $\sim 1588\text{ cm}^{-1}$ and symmetric stretching mode at $\sim 1375\text{ cm}^{-1}$, characteristic of the proline carboxylate, are still present.

The N–H and C–N stretching bands associated with the amine group of proline also maintain similar positions, confirming that the fundamental structure of the anion is preserved.

However, significant changes occur in the spectral regions influenced by the N,N-dimethylpyrrolidinium cation, particularly in the C–H stretching and bending vibrations:

The C–H stretching region ($2800\text{--}3000\text{ cm}^{-1}$) exhibits new bands and increased intensity, due to the presence of the methyl ($-\text{CH}_3$) and methylene ($-\text{CH}_2$) groups in the pyrrolidinium ring.

The C–H bending vibrations ($1350\text{--}1450\text{ cm}^{-1}$) are slightly shifted compared to [Cho][Pro], reflecting the altered electronic environment introduced by the pyrrolidinium cation.

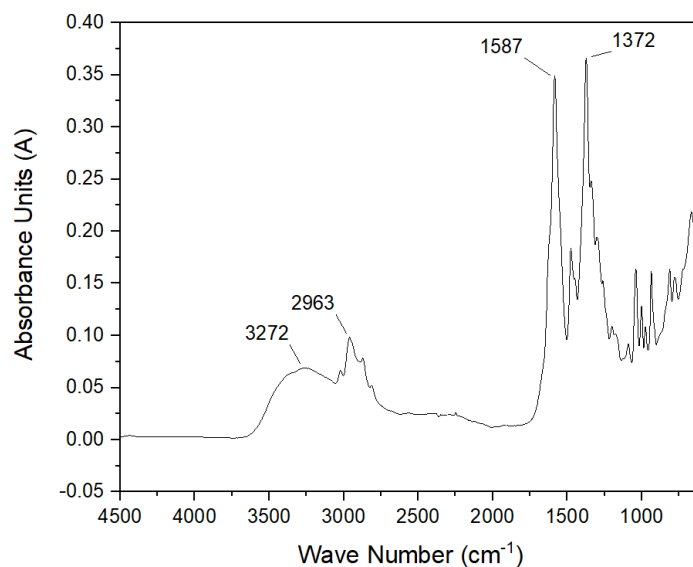


Figure 32: ATR-IR Spectra of [DMP][Pro]

3.2 Density

As discussed before in section 2.4.2 Density, using Anton Paar DMA 5001, the density of ILs was measured. *Table 4* shows the results of these measurements. Expectedly, pure [Cho][Pro] has the highest density at 20°C . As the temperature increases, the density decreases with a linear trend, leading to the lowest density for the most diluted [Cho][Pro]-DMSO solution at the highest measured temperature [*Figure 33: Density trends measured for ILs*].

This trend is consistent with expectations since pure ionic liquids generally exhibit higher densities due to the strong electrostatic interactions between ions and the intrinsic molecular packing. When diluted with DMSO, the overall density decreases because DMSO, having a lower intrinsic density, disrupts the structured ion network, leading to an overall reduction in density. Additionally, as temperature rises, thermal expansion further reduces density across all compositions, with a more pronounced effect in diluted solutions due to the greater presence of solvent molecules, which are more thermally responsive.

The observed density variations confirm that the strength of intermolecular interactions in the IL solution is directly influenced by both temperature and concentration, aligning with previously reported trends for IL-solvent systems

Table 4: Density Comparison of ILs at different Temperatures

Temp (°C)	Density (g/ml)			
	12.50%	33.00%	50.00%	Pure [Cho][Pro]
20	1.095	1.099	1.109	1.119
30	1.085	1.091	1.101	1.113
40	1.076	1.083	1.093	1.107
50	1.066	1.075	1.086	1.101
60	1.057	1.066	1.078	1.095
70	1.047	1.057	1.070	1.089

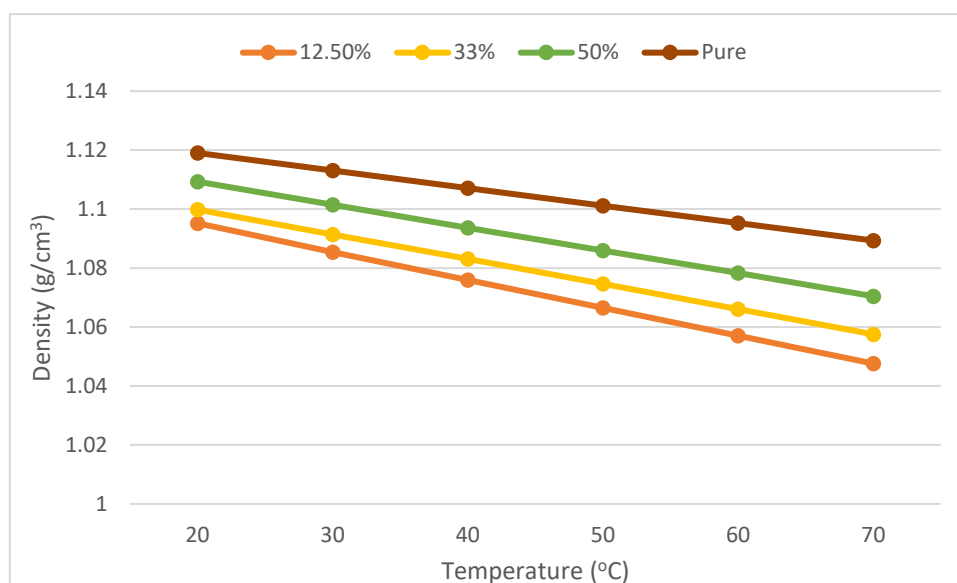


Figure 33: Density trends measured for ILs

3.3 TGA-IR

[Cho][Pro] 12.5%:

Figure 34 belongs to the TGA of [Cho][Pro] 12.5% in DMSO. As seen on the graph, the first degradation must belong to the DMSO since it is 87.5% w/w of the solution, and its mass change is showing the same amount of loss. Its onset temperature is about 128.6 °C and the minimum peak of 1st derivative is at 167.1 °C. The second step belongs to degradation of [Cho][Pro]. Its onset temperature is at 199.2 °C and minimum peak of 1st derivative is at 222.7°C.

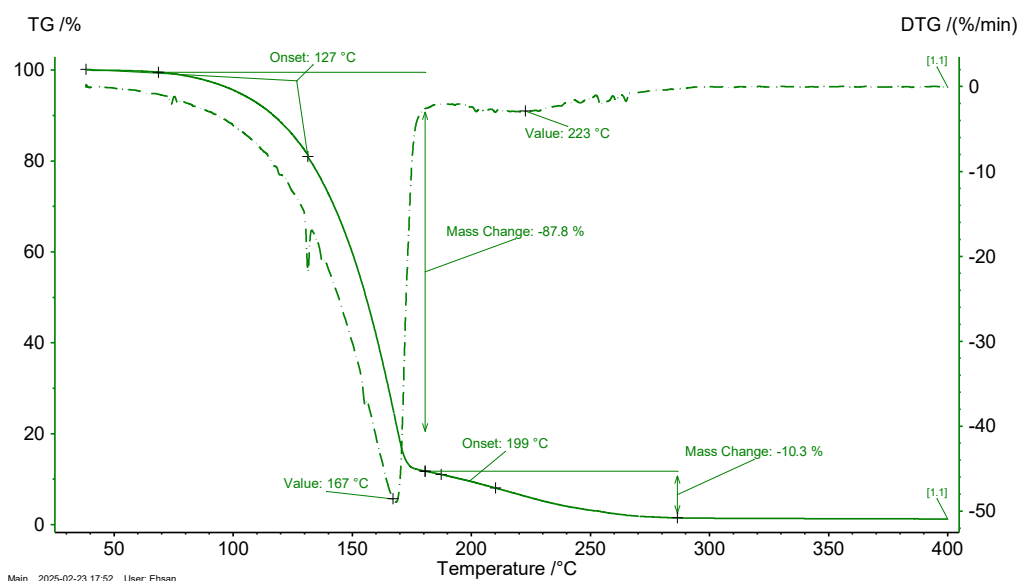


Figure 34: TGA and its 1st derivative curve for [Cho][Pro] 12.5% in DMSO

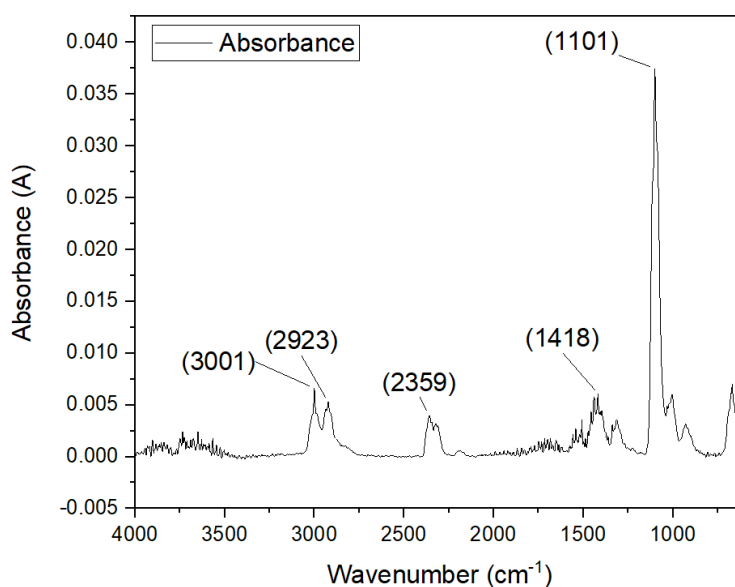


Figure 35: Gas-phase IR spectrum of [Cho][Pro] 12.5% in DMSO at 106.5 °C

The peak at 3001 cm^{-1} corresponds to the stretching vibrations of C-H within sp^2 hybrid carbons, which usually exist for unsaturated or aromatic systems. Most probably, it originates from the methyl or methylene parts from the proline or choline molecule in this case.

As for the peak concerning alkyl groups because it is associated with C-H stretching vibrations of sp^3 hybridized carbons, namely at 2923 cm^{-1} , has been acquired from the choline cation (-CH₂ and -CH₃ groups) and perhaps DMSO, which has contributed to the same.

In fact, the peak at 2359 cm^{-1} corresponds to or indicates the evolution of the gas CO₂ at that temperature, which is presumably caused by the decarboxylation of the proline anion. The result is the incipient thermal degradation of the ionic liquid.

1418 cm^{-1} : This peak is due to the scissoring or bending vibrations of the C-H bonds of methyl and methylene groups. This is more likely resultant from interacting with DMSO or choline cations in vapor phase.

1101 cm^{-1} is a highly favored peak that indicates the S=O stretching vibrations of DMSO. The intensity shows that during heating, DMSO is either being evaporated or incorporated to the evolved gases.

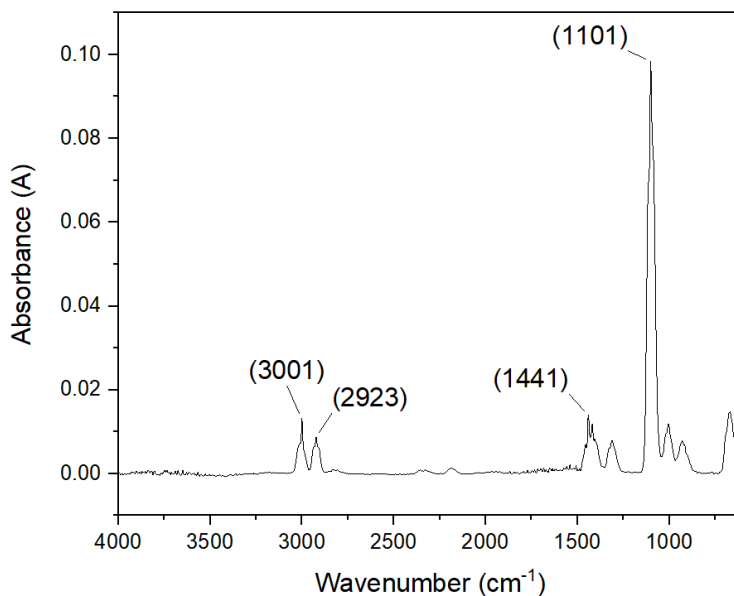


Figure 36: Gas-phase IR spectrum of [Cho][Pro] 12.5% in DMSO at 193.5 °C

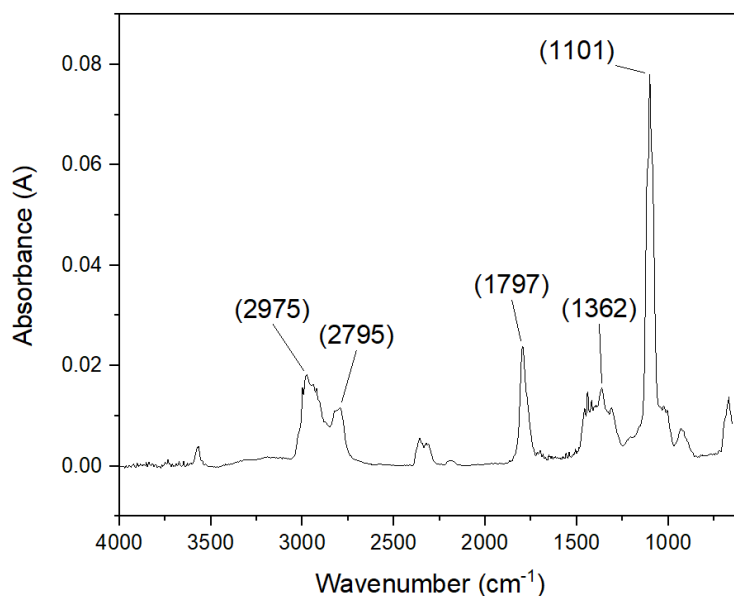


Figure 37: Gas-phase IR spectrum of [Cho][Pro] 12.5% in DMSO at 221 °C

Stretching frequencies involving C-H bonding for sp^3 hybridized carbons found in methyl and methylene moieties are characterized by peaks at 2975 cm^{-1} and 2795 cm^{-1} . This type of

vibration is caused by the methyl (-CH₃) and methylene (-CH₂-) groups of choline or those added by DMSO.

The C=O stretching vibrations indicated by this peak, which is located at 1797 cm⁻¹, are most likely caused by disintegrating products containing carbonyl functional groups (acids such as proline or choline, as well as likely some intermediates created during their thermal breakdown). This signal through carbonyl species, or CO₂, is most likely caused by the decarboxylation of the proline anion.

1362 cm⁻¹: This peak represents the methyl and methylene groups' C-H bending vibrations, often known as asymmetric bending or scissoring. The alkyl groups in choline or the intermolecular interactions in DMSO are most likely the cause.

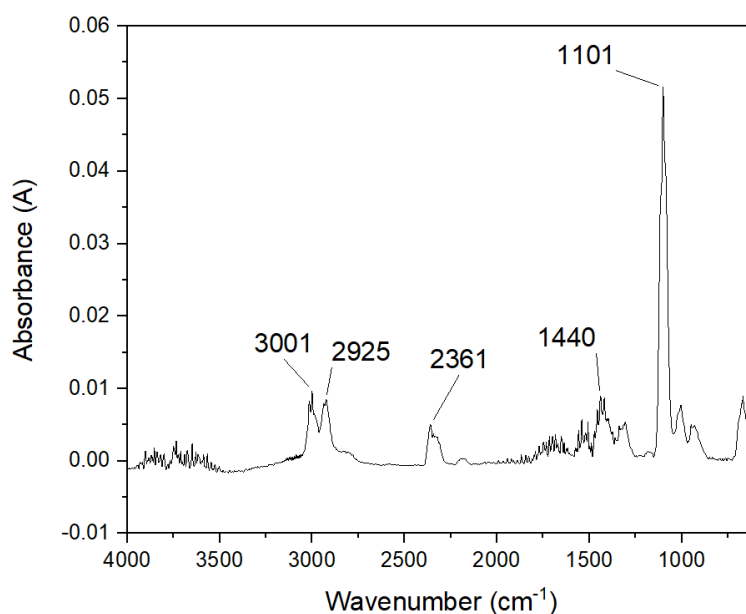


Figure 38: Gas-phase IR spectrum of [Cho][Pro] 12.5% in DMSO at 602 °C

[Cho][Pro] 33% in DMSO:

Figure below belongs to the TGA of [Cho][Pro] 33% in DMSO. As seen on the graph, the first degradation must belong to the DMSO since it makes 66% w/w of the solution, and its mass change is showing almost the same amount of loss. Its onset temperature is about 127.6 °C and the minimum peak of 1st derivative is at 159.2 °C. The second step belongs to degradation of [Cho][Pro]. Its onset temperature is at 290.9 °C and minimum peak of 1st derivative is at 222.1 °C. The noisy look of the graph is most probably an indication of water presence in the solution.

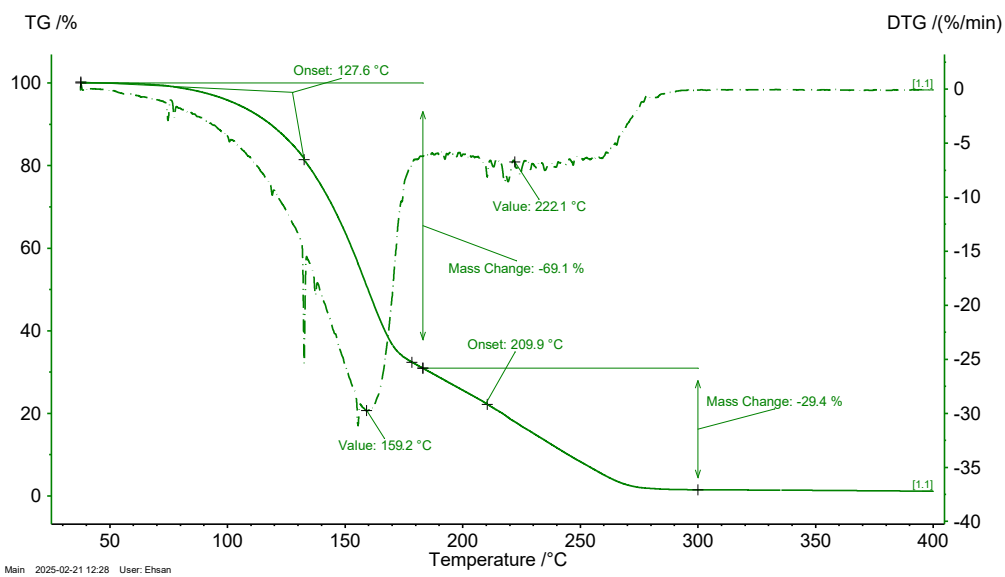


Figure 39: TGA and its 1st derivative curve for [Cho][Pro] 33% in DMSO

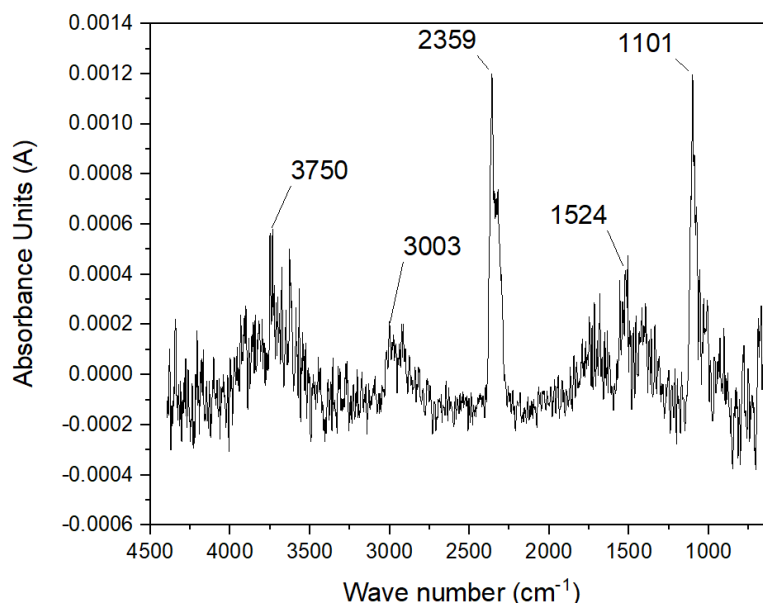


Figure 40: Gas-phase IR spectrum of [Cho][Pro] 33% in DMSO at 125 °C

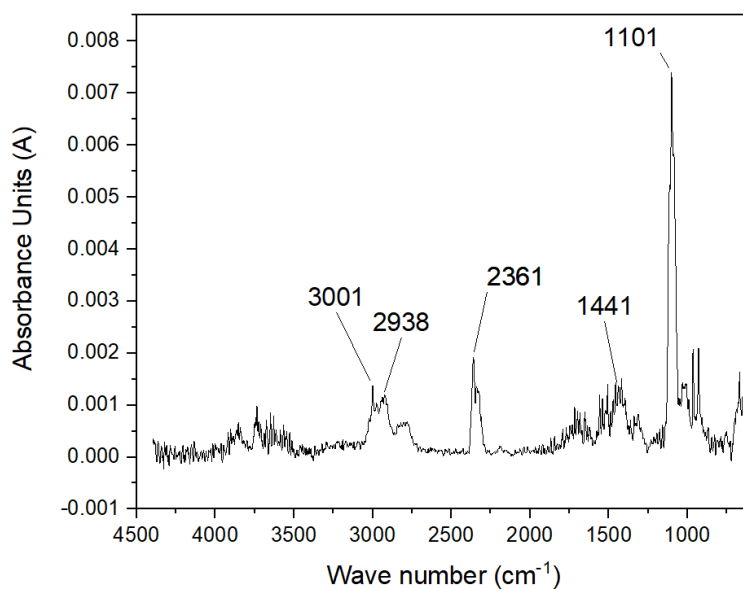


Figure 41: Gas-phase IR spectrum of [Cho][Pro] 33% in DMSO at 158 °C

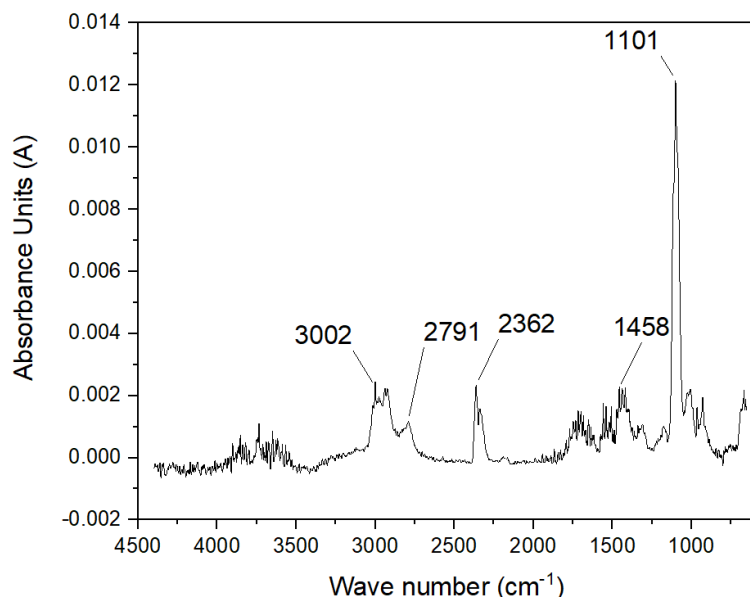


Figure 42: Gas-phase IR spectrum of [Cho][Pro] 33% in DMSO at 221 °C

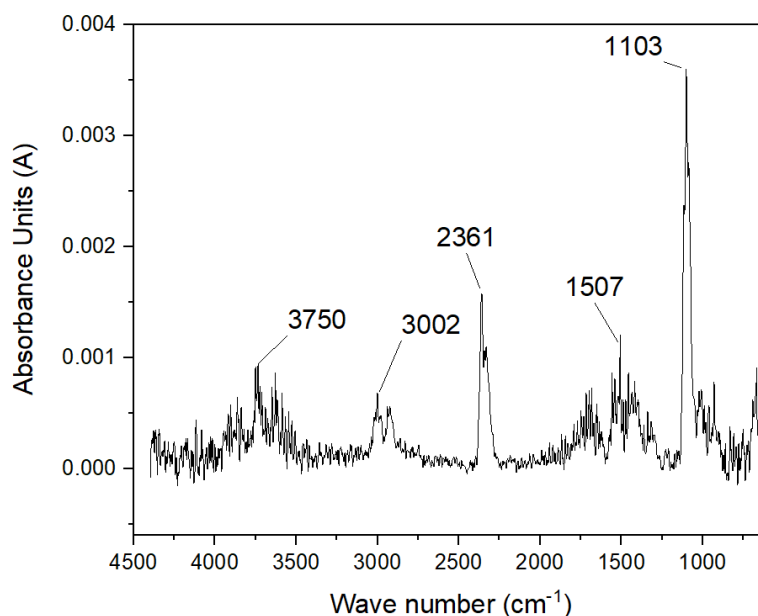


Figure 43: Gas-phase IR spectrum of [Cho][Pro] 33% in DMSO at 602 °C

[Cho][Pro] 50% in DMSO:

Figure 44 belongs to the TGA of [Cho][Pro] 50% in DMSO. As seen on the graph, the first degradation must belong to the DMSO since it is 50% w/w of the solution, and the its mass change is showing the same amount of loss. Its onset temperature is about 114 °C and the minimum peak of 1st derivative is at 153 °C. The second step belongs to degradation of [Cho][Pro]. Its onset temperature is at 189 °C and minimum peak of 1st derivative is at 256 °C. The noisy look of the graph is most probably an indication of water presence in the solution.

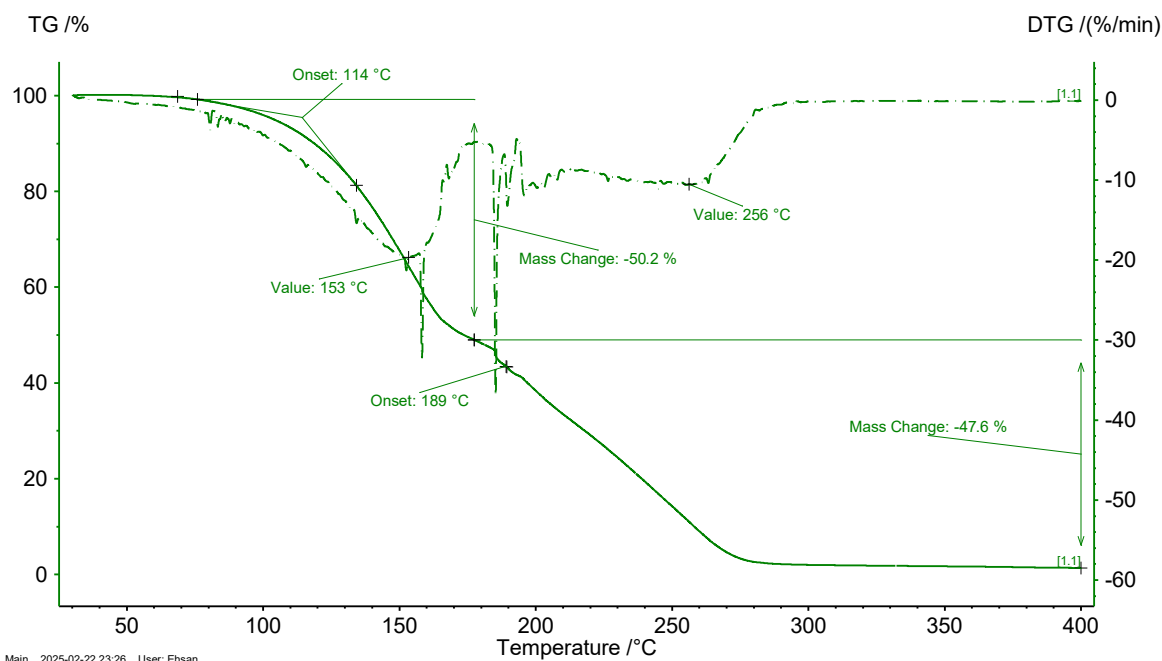


Figure 44: TGA and its 1st derivative curve for [Cho][Pro] 50% in DMSO

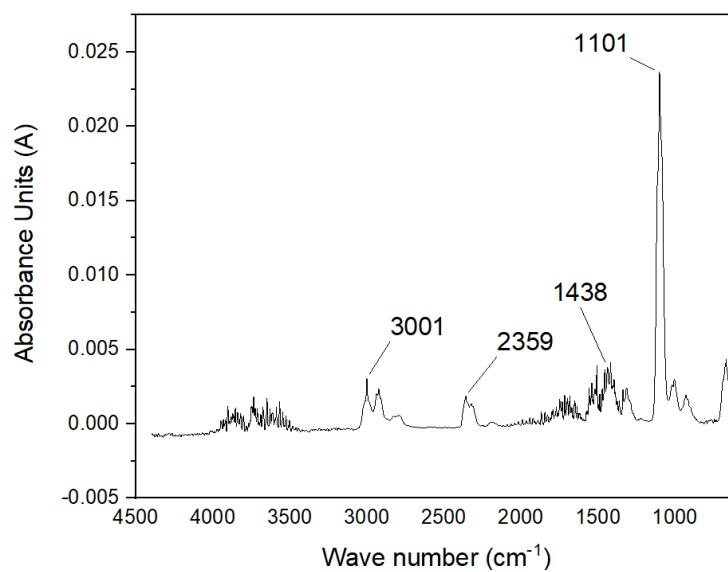


Figure 45 Gas-phase IR spectrum of [Cho][Pro] 50% in DMSO at 112 °C

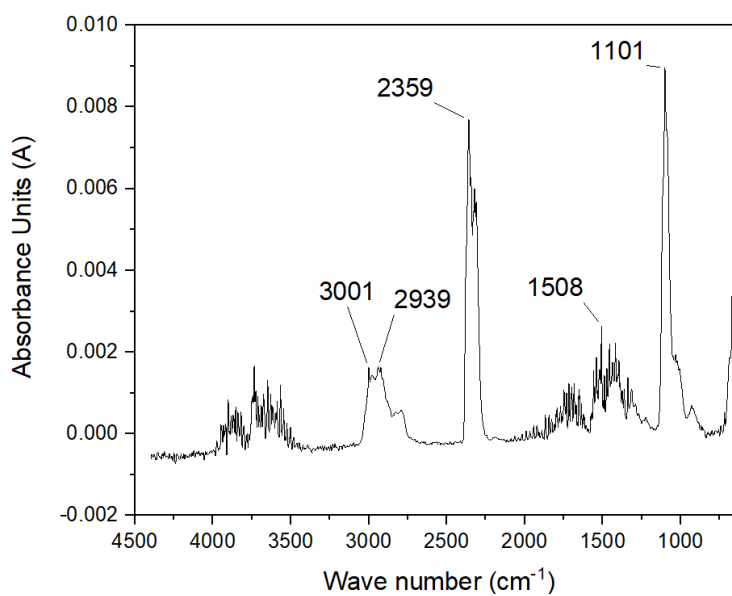


Figure 46: Gas-phase IR spectrum of [Cho][Pro] 50% in DMSO at 150 °C

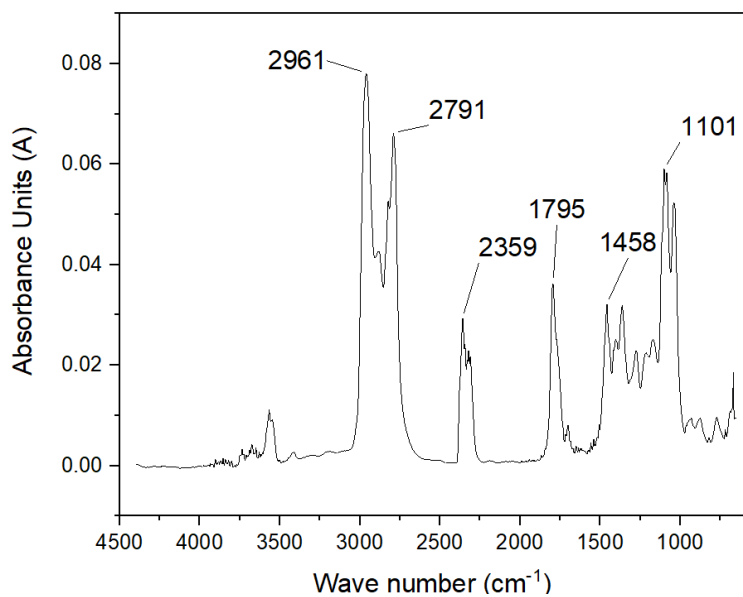


Figure 47: Gas-phase IR spectrum of [Cho][Pro] 50% in DMSO at 251 °C

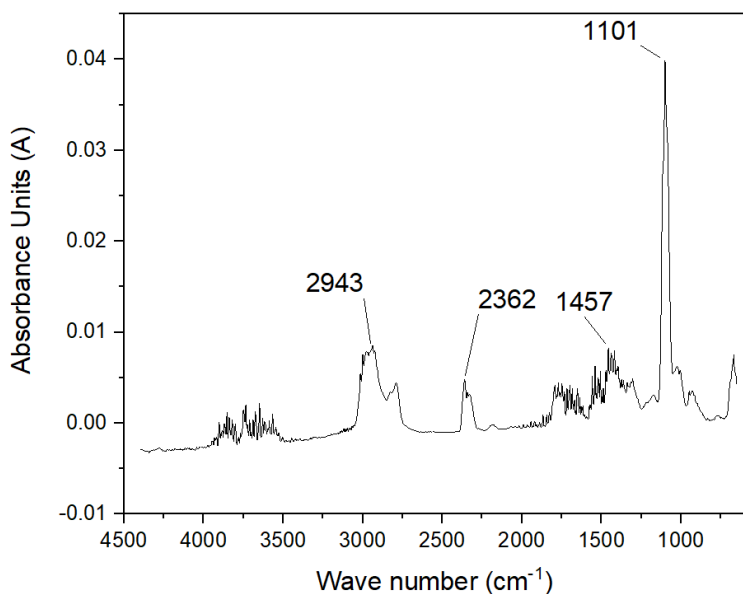


Figure 48 Gas-phase IR spectrum of [Cho][Pro] 50% in DMSO at 600 °C

[Cho][Pro] Pure:

Figure 49 belongs to the TGA of [Cho][Pro] pure. As seen on the graph, the first degradation could belong to the impurities, and its mass change is showing the same amount of loss, almost 6%. Its onset temperature is about 90 °C. The second step belongs to degradation of [Cho][Pro]. Its onset temperature is at 183.4 °C the minimum peak of 1st derivative is at 264.1 °C.

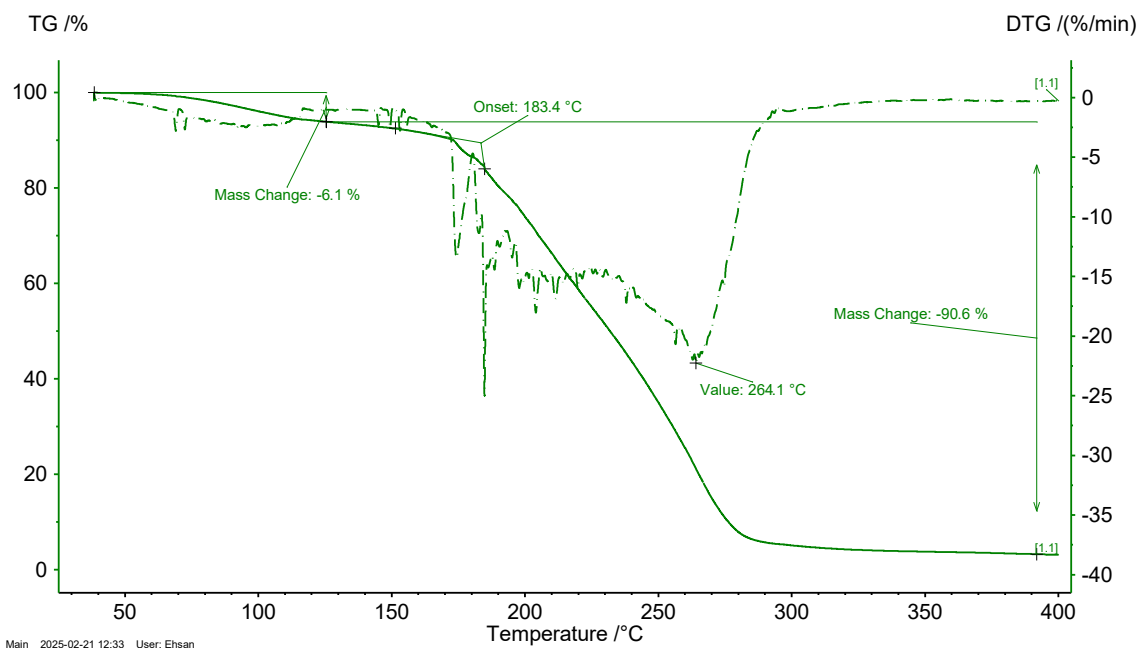


Figure 49: TGA and its 1st derivative curve for [Cho][Pro] Pure

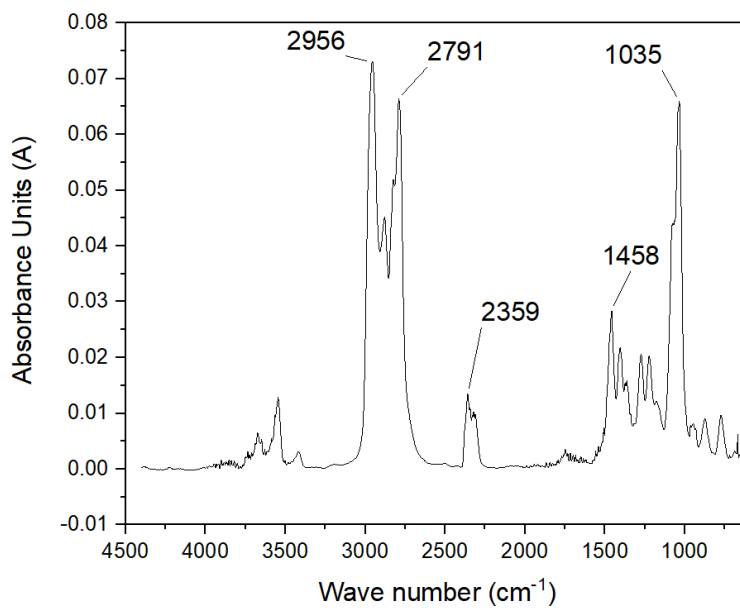


Figure 50: Gas-phase IR spectrum of [Cho][Pro] Pure at 182 °C

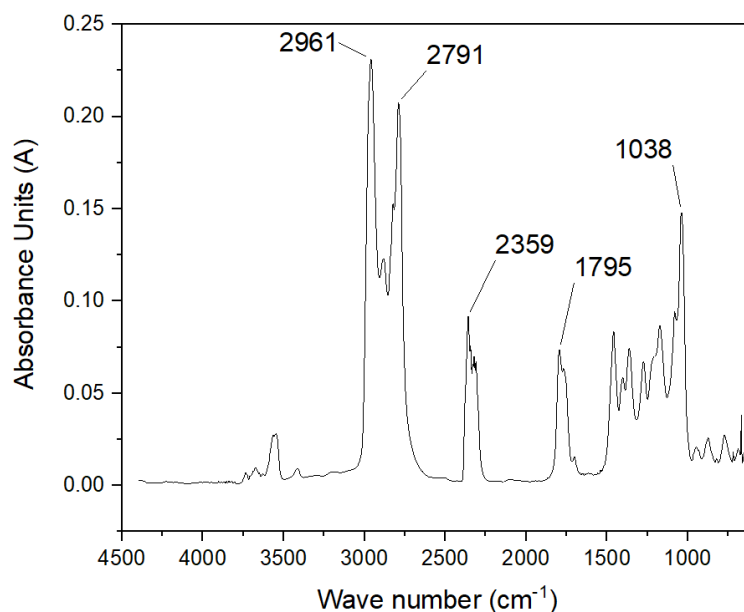


Figure 51: Gas-phase IR spectrum of [Cho][Pro] Pure at 259 °C

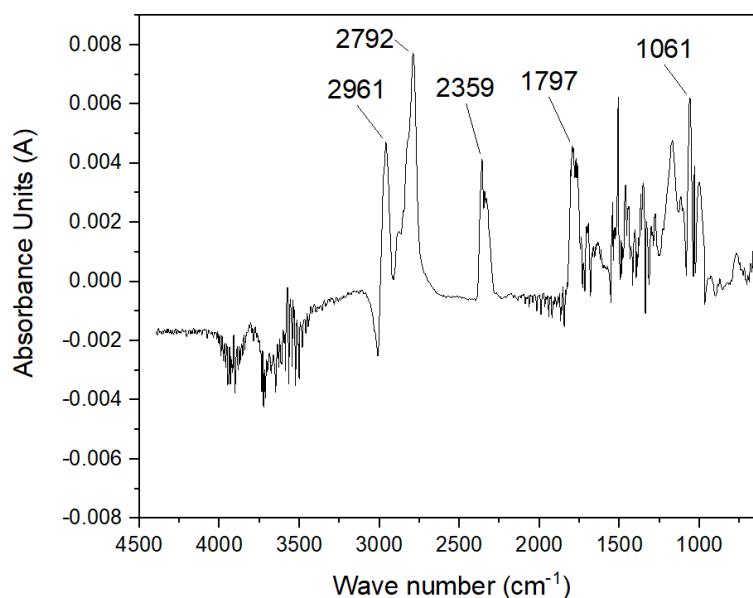


Figure 52: Gas-phase IR spectrum of [Cho][Pro] Pure at 600 °C

[Cho][Pro] 12.5% in DMSO Post CO₂ Capture:

Figure 53 belongs to the TGA of [Cho][Pro] 12.5% in DMSO after gravimetric analysis. As seen on the graph, the first degradation must belong to the DMSO since it is 87.5% w/w of the solution, and its mass change is showing almost the same amount of loss. Its onset temperature is about 131 °C and the minimum peak of 1st derivative is at 164 °C. The second step belongs to degradation of [Cho][Pro]. Its onset temperature is at 193 °C and minimum peak of 1st derivative is at 220 °C.

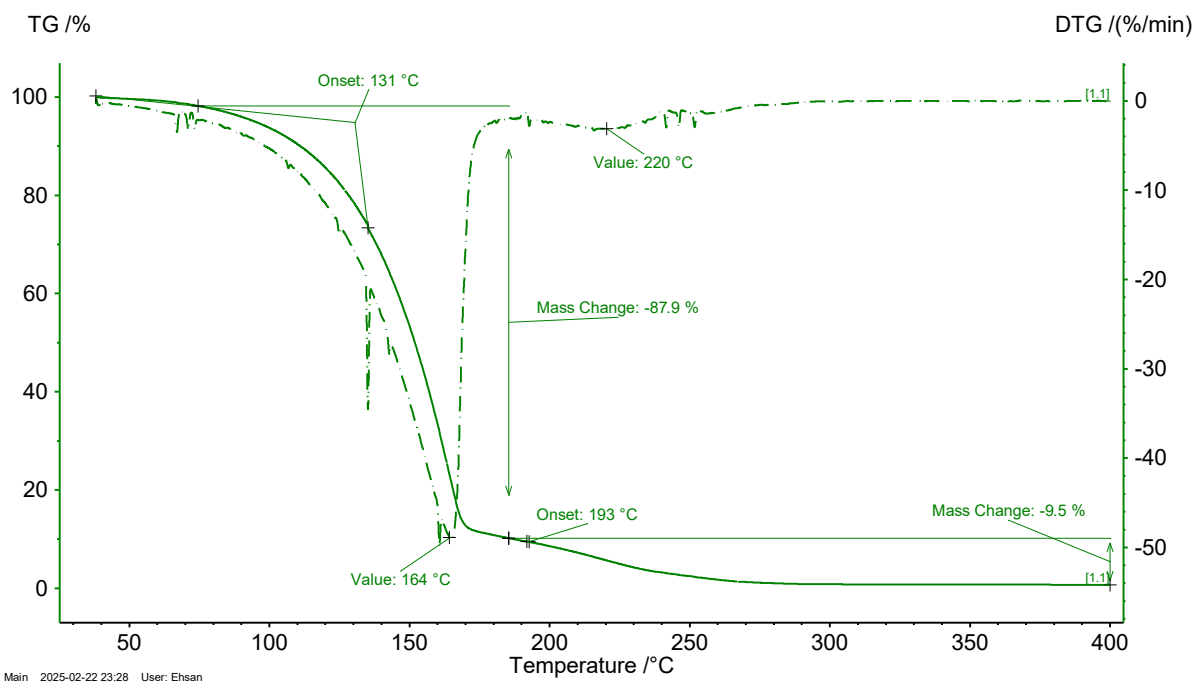


Figure 53: TGA-IR curve for [Cho][Pro] 12.5% in DMSO after Gravimetric test

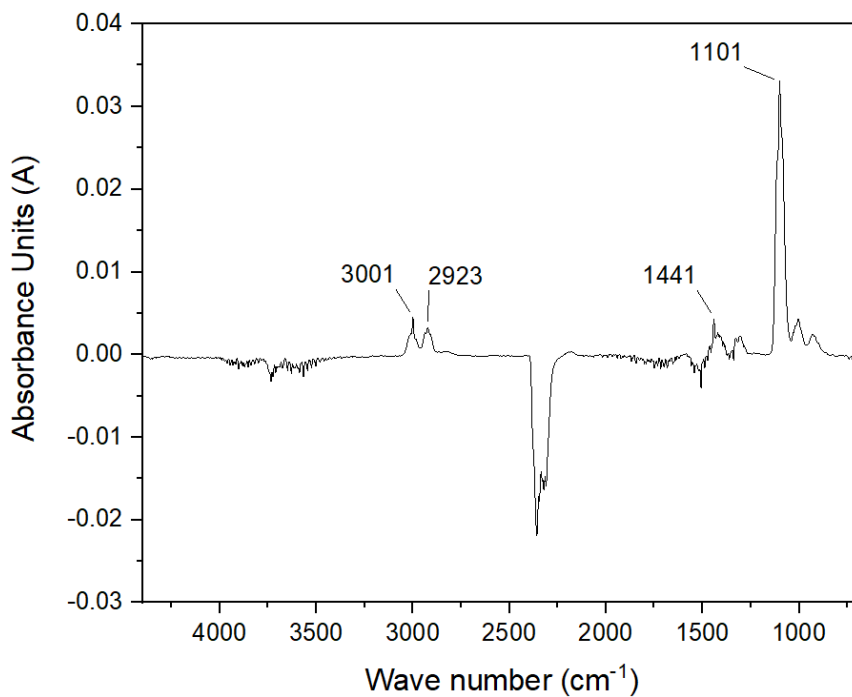


Figure 54: Gas-phase IR spectrum of [Cho][Pro] 12.5% in DMSO after Gravimetric test at 121 °C

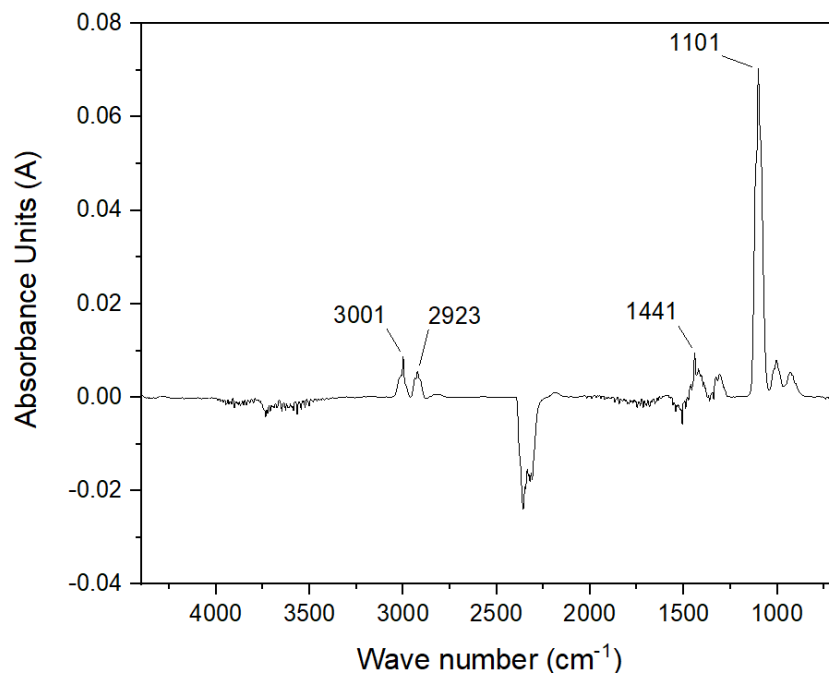


Figure 55: Gas-phase IR spectrum of [Cho][Pro] 12.5% in DMSO after Gravimetric test at 159 °C

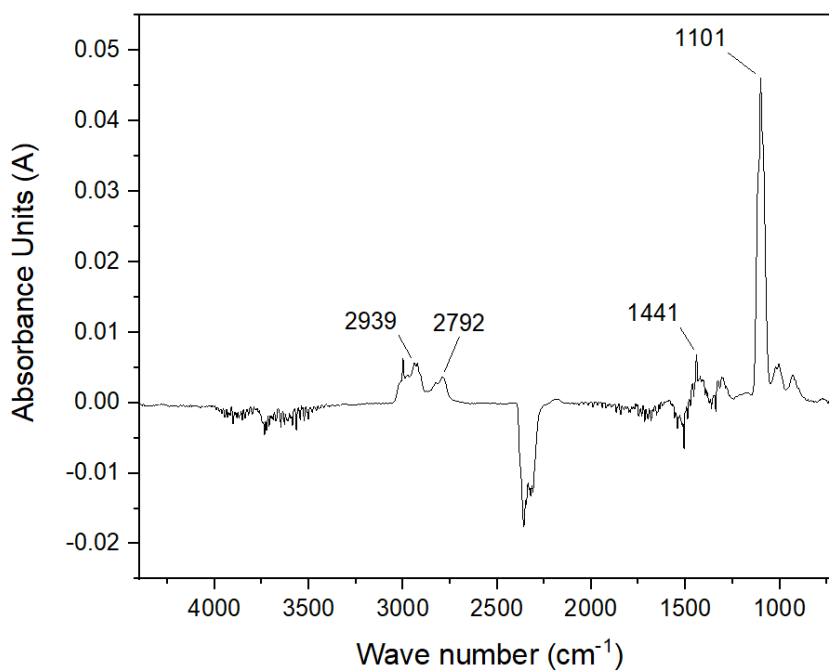


Figure 56: Gas-phase IR spectrum of [Cho][Pro] 12.5% in DMSO after Gravimetric test at 217 °C

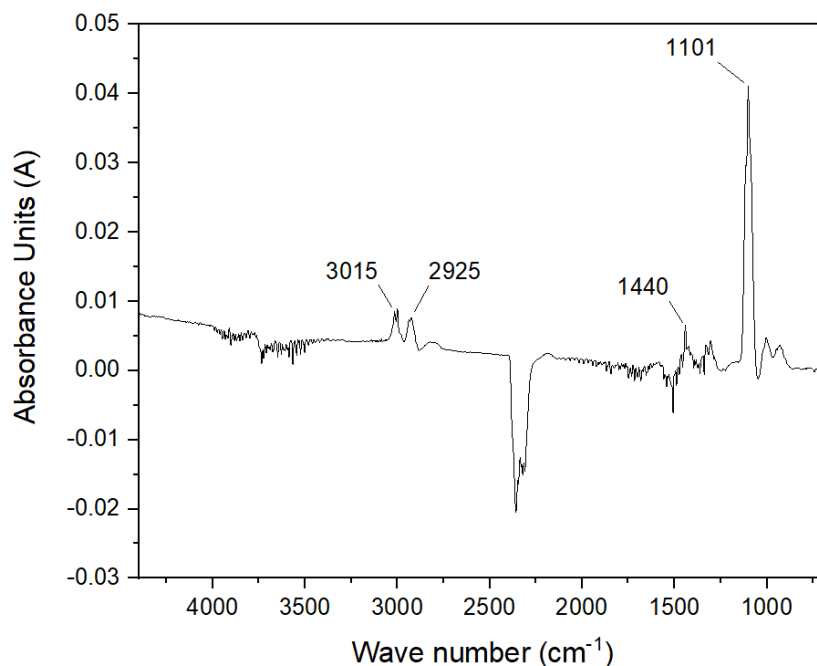
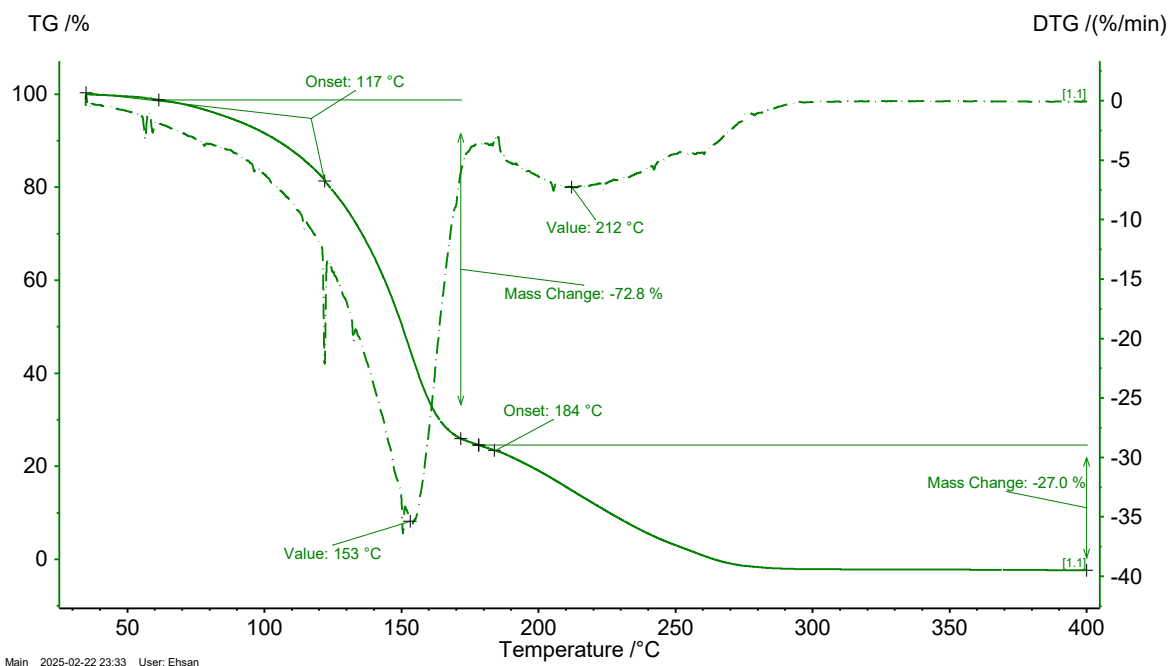


Figure 57 Gas-phase IR spectrum of [Cho][Pro] 12.5% in DMSO after Gravimetric test at 600 °C

[Cho][Pro] 33% in DMSO Post CO₂ Capture:

Figure 58 belongs to the TGA of [Cho][Pro] 33% in DMSO. As seen on the graph, the first degradation must belong to the DMSO since it makes 66% w/w of the solution, and its mass change is showing more or less the same amount of loss. Its onset temperature is about 117 °C and the minimum peak of 1st derivative is at 153 °C. The second step belongs to degradation of [Cho][Pro]. Its onset temperature is at 184 °C and minimum peak of 1st derivative is at 212 °C.



Main 2025-02-22 23:33 User: Ehsan

Figure 58: TGA-IR curve for [Cho][Pro] 33% in DMSO after Gravimetric test

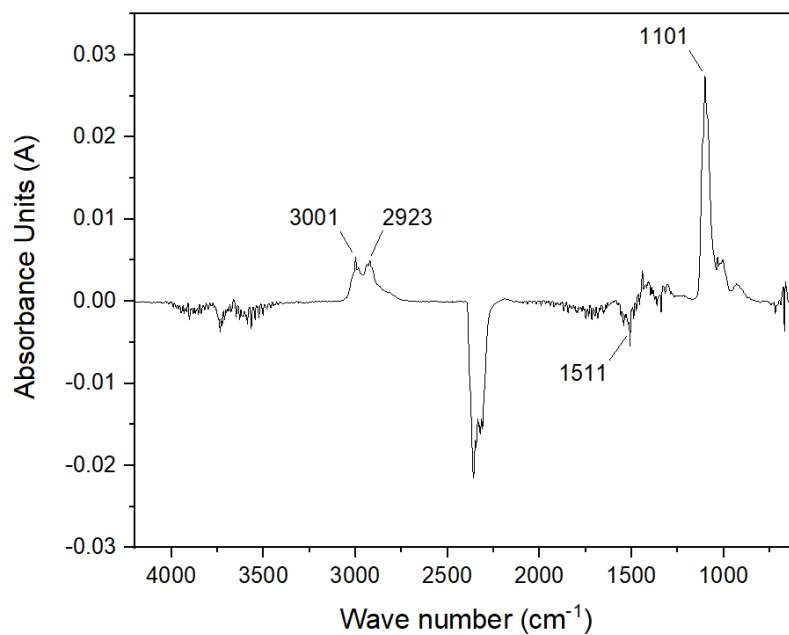


Figure 59: Gas-phase IR spectrum of [Cho][Pro] 33% in DMSO after Gravimetric test at 116 °C

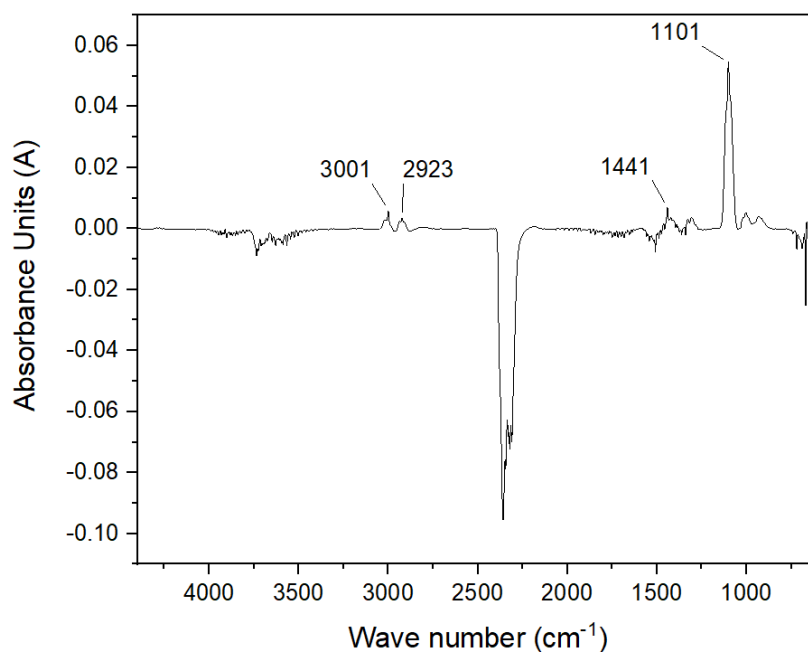


Figure 60: Gas-phase IR spectrum of [Cho][Pro] 33% in DMSO after Gravimetric test at 149 °C

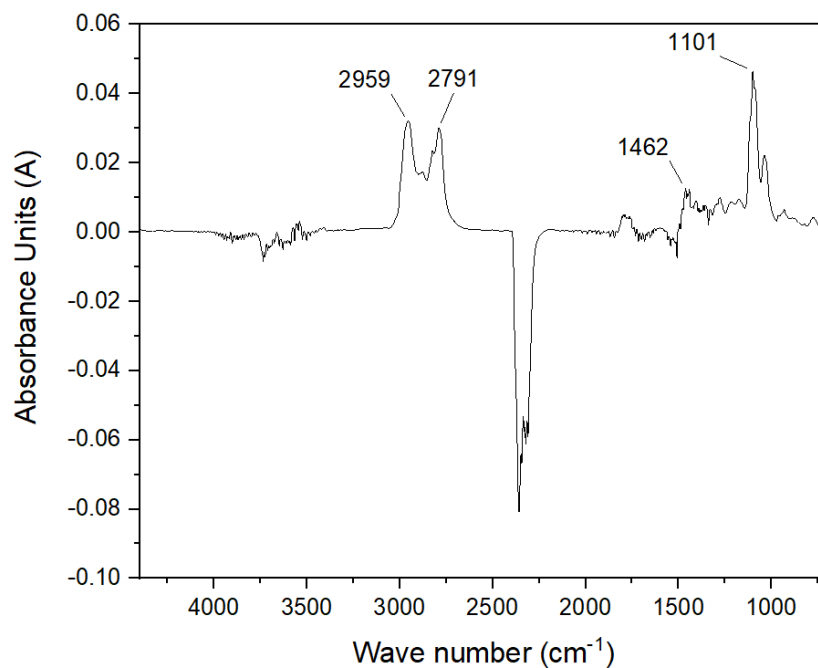


Figure 61: Gas-phase IR spectrum of [Cho][Pro] 33% in DMSO after Gravimetric test at 216 °C

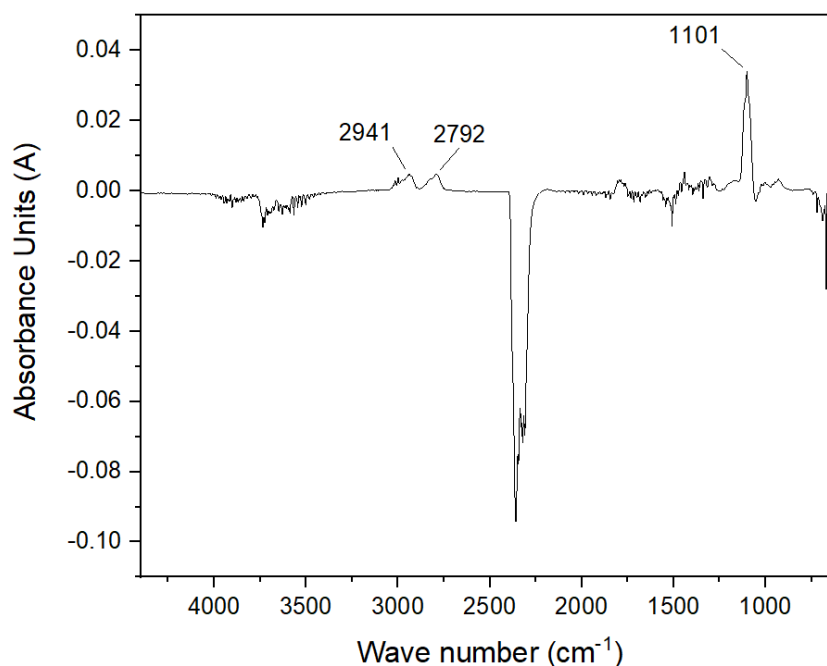


Figure 62: Gas-phase IR spectrum of [Cho][Pro] 33% in DMSO after Gravimetric test at 600 °C

[Cho][Pro] 50% in DMSO Post CO₂ Capture:

Figure 63 belongs to the TGA of [Cho][Pro] 50% in DMSO. As seen on the graph, the first degradation must belong to the DMSO since it is 50% w/w of the solution, and its mass change is showing almost the same amount of loss. Its onset temperature is about 97 °C and the minimum peak of 1st derivative is at 157 °C. The second step belongs to degradation of [Cho][Pro]. Its onset temperature is at 191 °C and minimum peak of 1st derivative is at 198 °C.

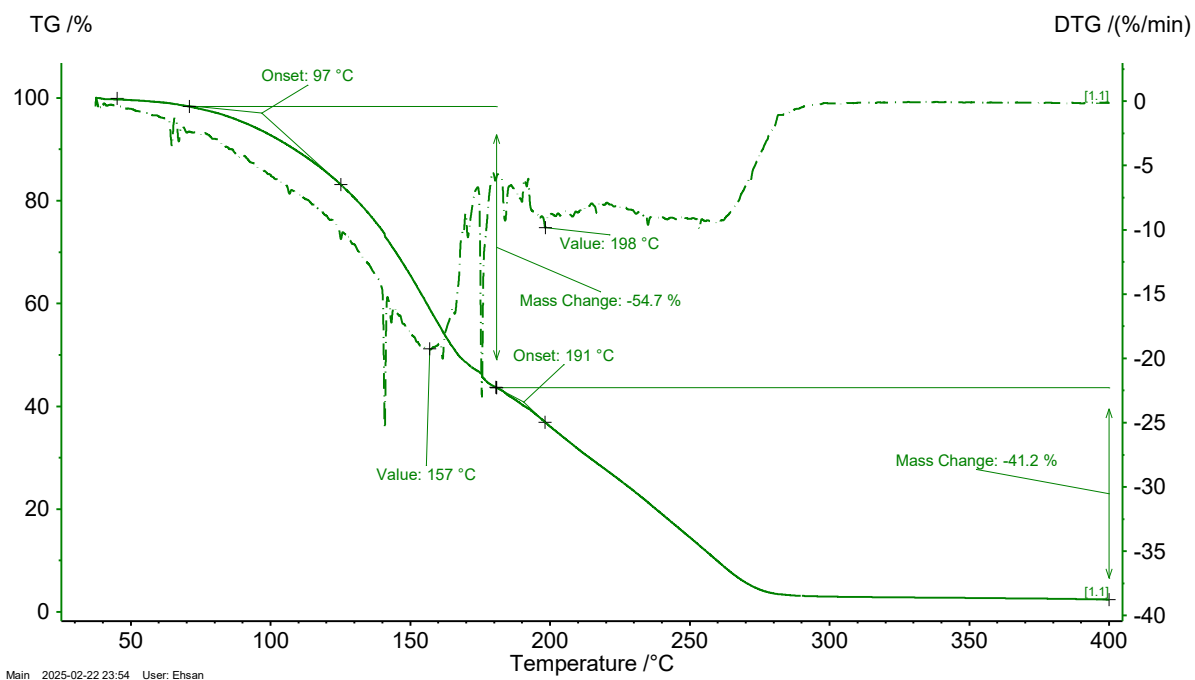


Figure 63: TGA-IR curve for [Cho][Pro] 50% in DMSO after Gravimetric test

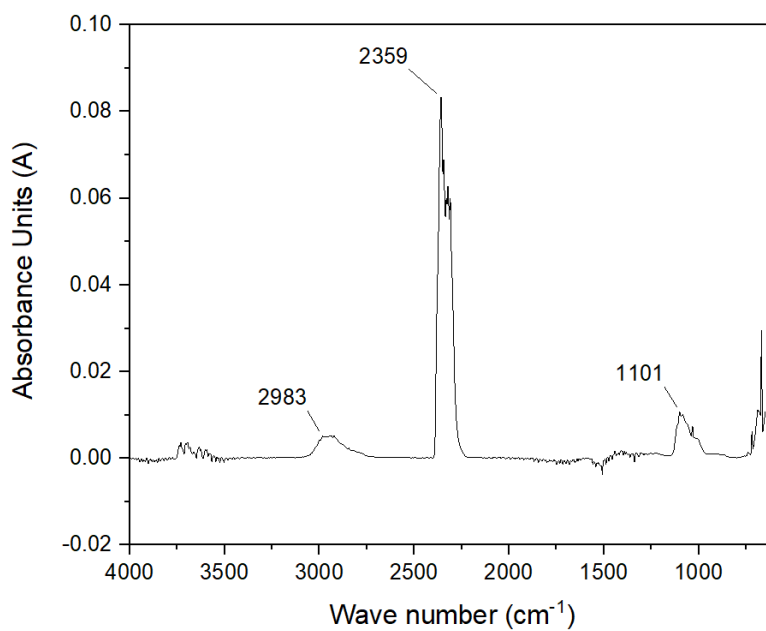


Figure 64: Gas-phase IR spectrum of [Cho][Pro] 50% in DMSO after Gravimetric test at 92 °C

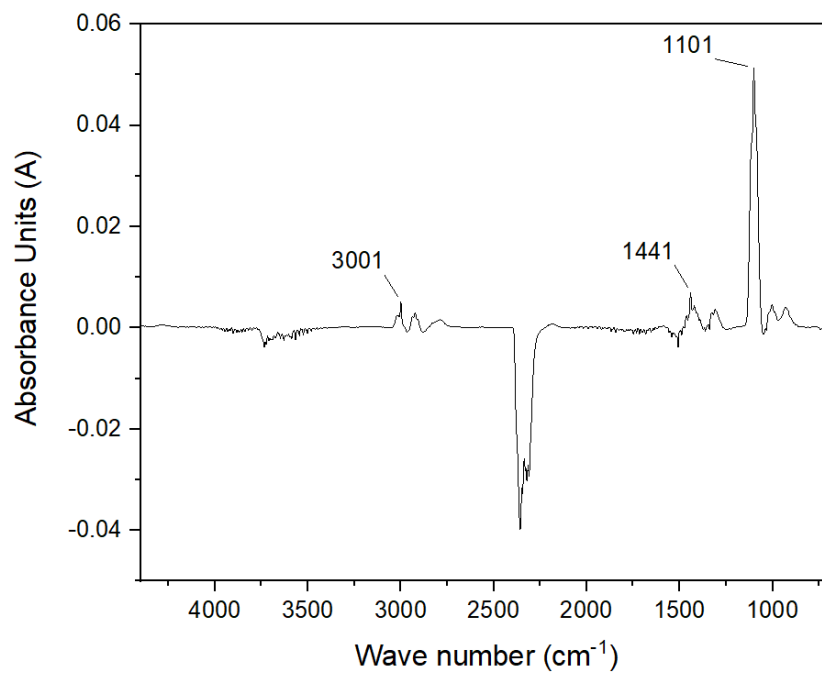


Figure 65: Gas-phase IR spectrum of [Cho][Pro] 50% in DMSO after Gravimetric test at 155 °C

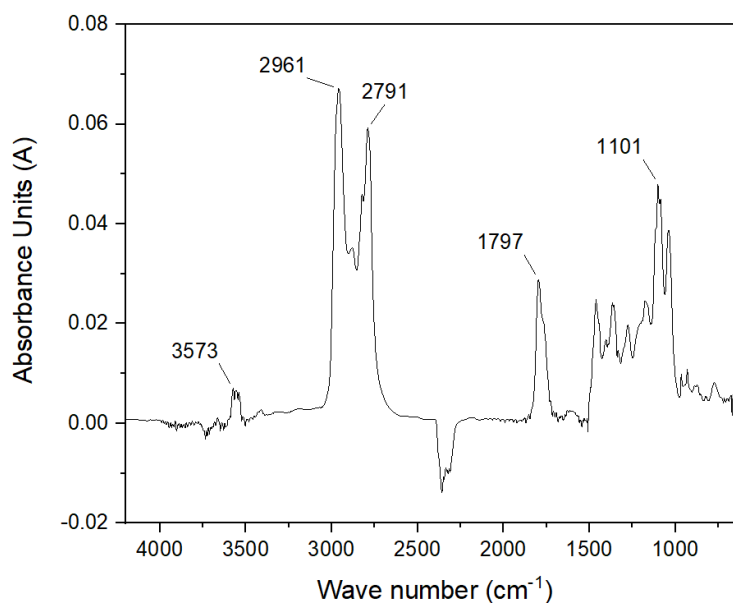


Figure 66: Gas-phase IR spectrum of [Cho][Pro] 50% in DMSO after Gravimetric test at 255 °C

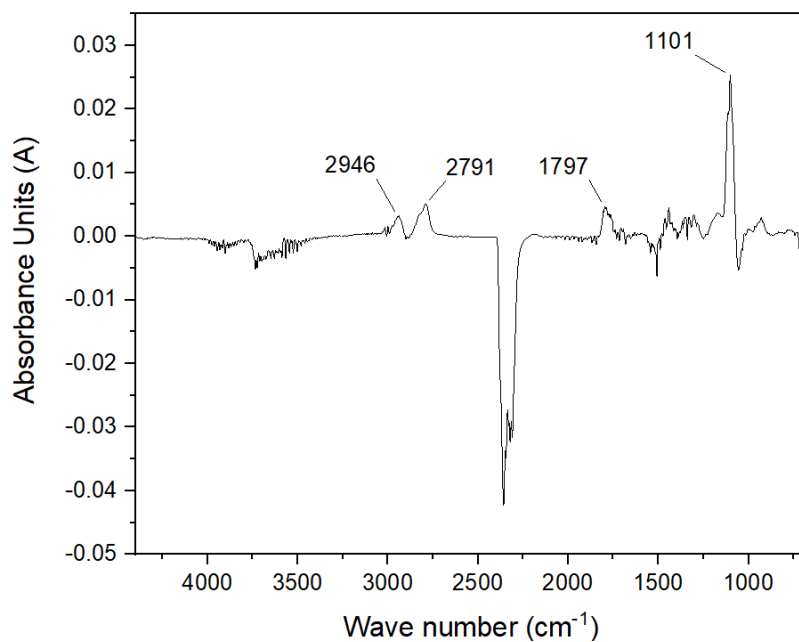
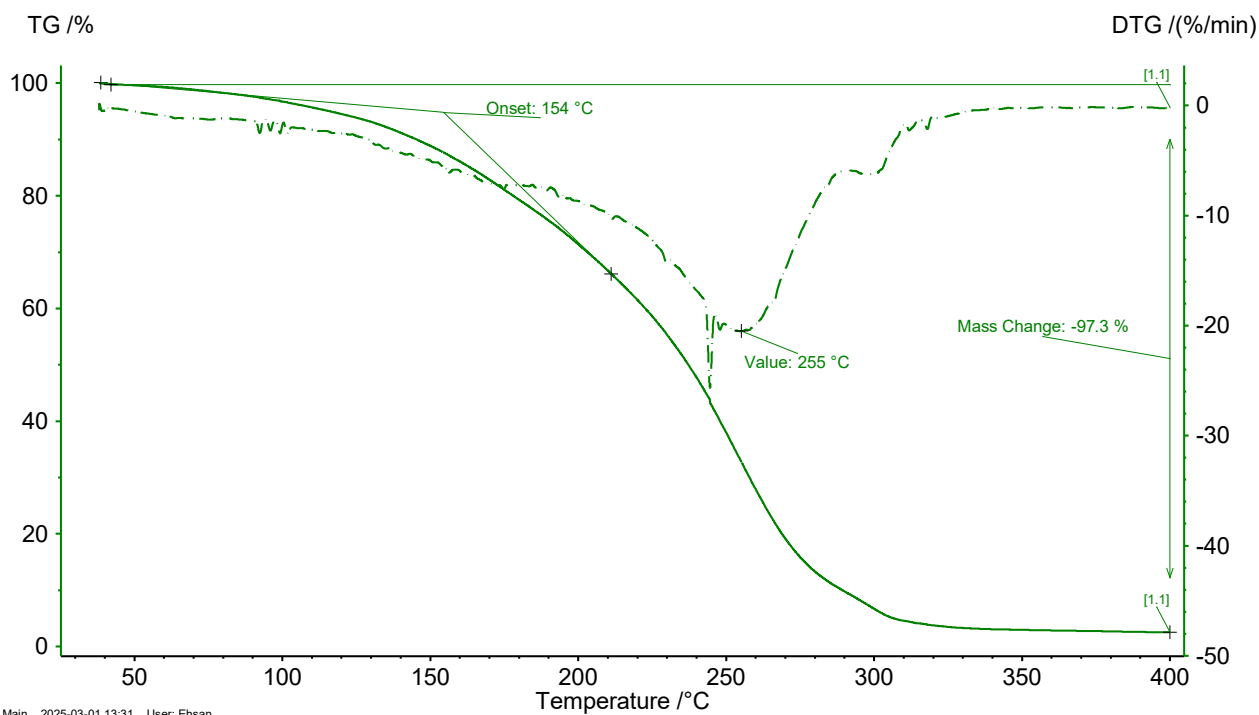


Figure 67: Gas-phase IR spectrum of [Cho][Pro] 50% in DMSO after Gravimetric test at 600 °C

[DPM][Pro]:



Main 2025-03-01 13:31 User: Ehsan

Figure 68: TGA-IR curve for [DMP][Pro]

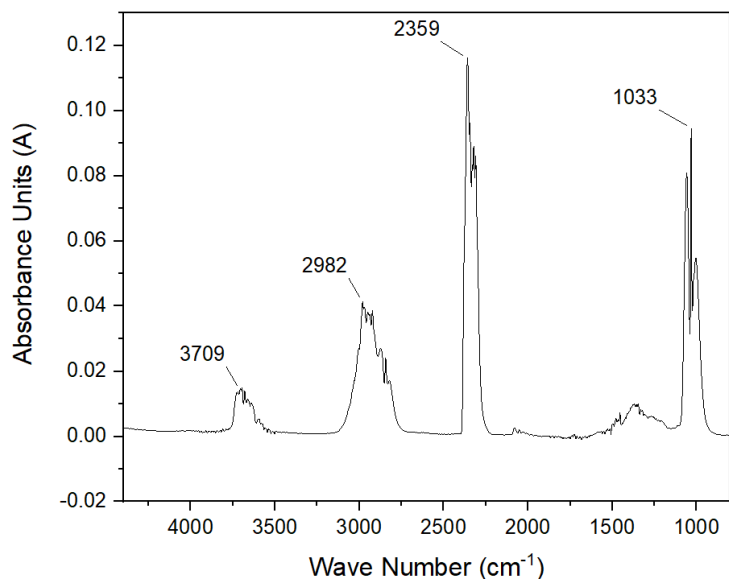


Figure 69: Gas-phase IR spectrum of [DMP][Pro] at 154 °C

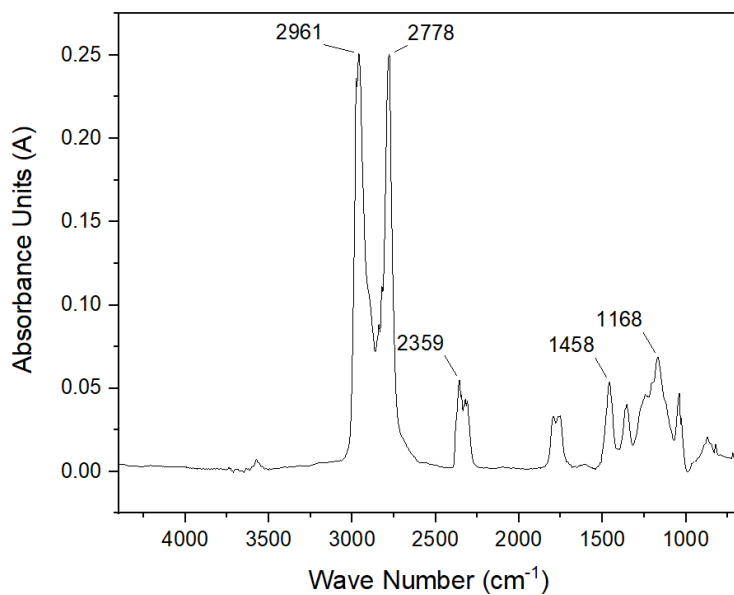


Figure 70: Gas-phase IR spectrum of [DMP][Pro] at 254 °C

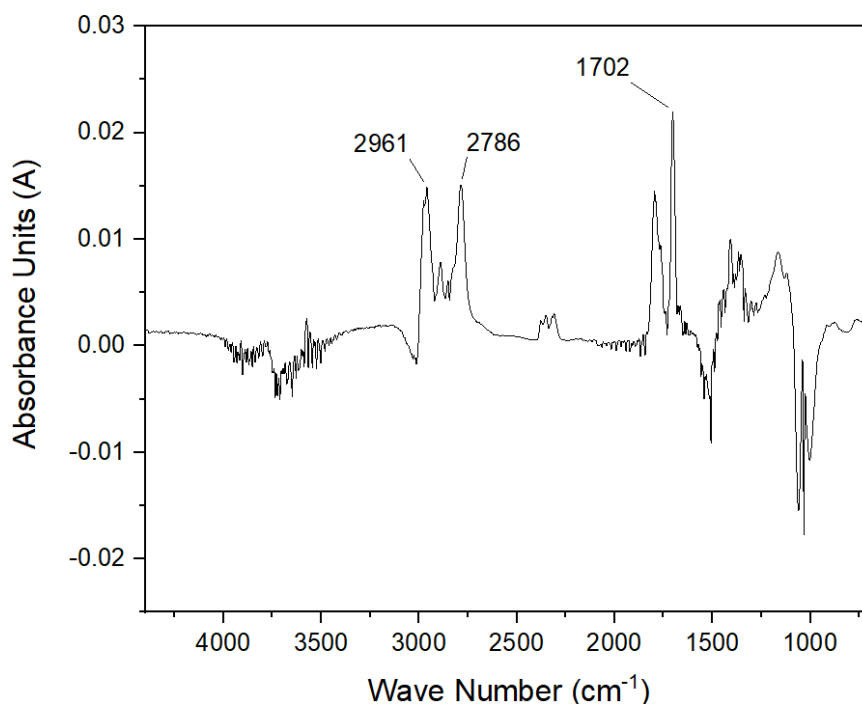


Figure 71: Gas-phase IR spectrum of [DMP][Pro] at 400 °C

Table 5: TGA Onset and 1st Derivative Minimum temperature for tested ILs

Ionic Liquid	Before CO ₂ capture		After CO ₂ Capture	
	Onset Temp. (°C)	Min. of 1st Derivative Peak (°C)	Onset Temp. (°C)	Min. of 1st Derivative Peak (°C)
[Cho][Pro] 12.50%	127	167	131	164
[Cho][Pro] 33%	127.6	159.2	117	153
[Cho][Pro] 50%	114	153	97	157
[Cho][Pro] Pure	184	264	-	-
[DMP][Pro]	154	255	-	-

3.5 DSC

[Cho][Pro] 12.5%:

The DSC diagram shows heat flow as a function of temperature in mW, with results expressed in degrees Celsius. It can be deduced that the blue curve represents cooling, whereas the red curve represents the heat phase. Endothermic (upward peaks) or exothermic (downward peaks) changes are examples of significant thermal events, such as phase transitions (including but not limited to melting, crystallization, and glass transitions).

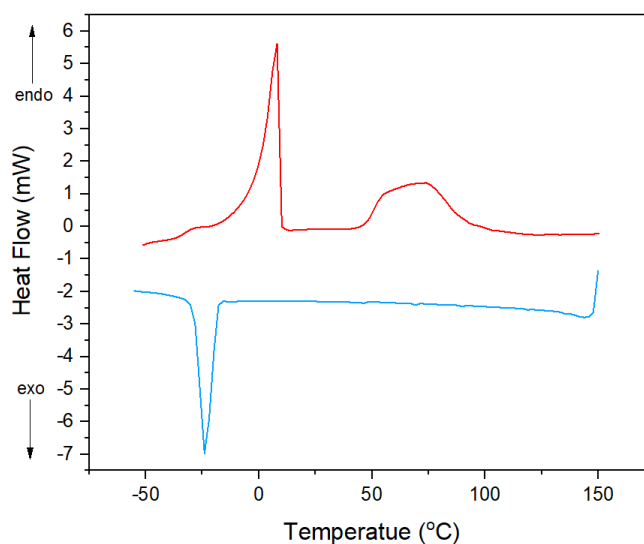


Figure 72: DSC curves for [Cho][Pro] 12.5% in DMSO, 2nd phase, -70 to 150 and to -70 °C

The glass transition temperature (T_g) for a material that is changing from a hard glassy state to an amorphous, rubbery state is around $-40\text{ }^\circ\text{C}$, as seen by the blue curve, which also exhibits cooling. This was demonstrated for common ionic liquids and DMSO combinations, which demonstrated outstanding thermal behavior and verified a wide disorder in the sample's molecular architecture.

Melting Temperature (about $0\text{ }^\circ\text{C}$): The red curve's abrupt endothermic peak in the heating phase, which is close to $0\text{ }^\circ\text{C}$, easily matches the melting temperature of pure DMSO and serves as a marker for the transition from solid to liquid phase. At these temperatures, pure DMSO dissolves.

Broad Endotherm Event ($\sim 50\text{-}100\text{ }^\circ\text{C}$): The extremely wide endothermic zone in the heating trend between 50 and $100\text{ }^\circ\text{C}$ indicates that the ionic liquid may still be undergoing some structural rearrangements or that some water may still be evaporating. It appears that complicated thermal behavior might result from these interactions between choline proline and DMSO.

Crystallization ($\sim -20\text{ }^\circ\text{C}$): The liquid crystallizes into a semi-ordered or crystalline phase, as indicated by the abrupt exothermic peak in the cooling phase (blue curve). The components of the DMSO or the ionic liquid combination may be to blame for this.

Thermal stability ($\sim 150\text{ }^\circ\text{C}$): The ionic liquid was confirmed to be thermally stable at this temperature and under these experimental circumstances as no notable endothermic or exothermic peaks were detected above $150\text{ }^\circ\text{C}$.

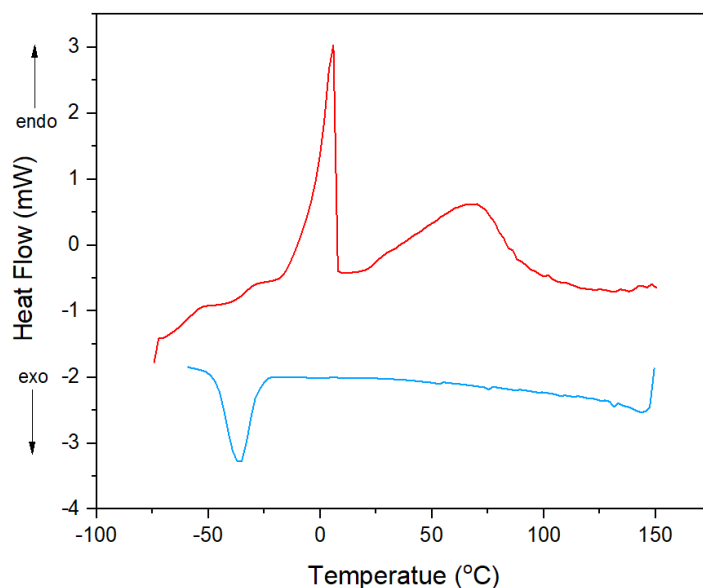


Figure 73: DSC curves for [Cho][Pro] 12.5% in DMSO, 3rd phase, -70 to 150 and to -70 °C

1. Glass Transition (~ -75 °C): The glass transition temperature (T_g), which is located at -75 °C, is associated with a subtle step shift in the cooling phase (blue curve). A change from a glassy (rigid) state to an amorphous (rubbery) state is thus indicated. When an ionic liquid and DMSO combination have a disordered molecular structure, this is what they usually exhibit.

2. Melting Point (~ 0 °C): To indicate the transition of DMSO from solid to liquid, the red curve's (heating phase) abrupt endothermic peak around 0 °C correlates to that melting point. The pure melting temperature of DMSO is exactly in line with this.

3. Broad Endothermic Event ($\sim 30-80$ °C): The heating phase between 30 and 80 °C shows a broad endothermic peak, which might indicate internal rearrangements in the choline proline-DMSO combination or the evaporation of the remaining water. Because of hydrogen bonds and ionic interactions, the thermal behavior most likely results from interactions between choline proline and DMSO.

4. Crystallization (~ -50 °C): Crystallization is shown by the strong down exotherm in the cooling phase (blue curve) close to -50 °C. This is the change from a liquid to a semi-organized or crystalline phase, which might be the case for an ionic liquid or DMSO component.

For the purpose of simplicity and conciseness, the analysis of DSC curves is done only for one solution, and for the rest the same approach can be applied.

[Cho][Pro] 33% in DMSO:

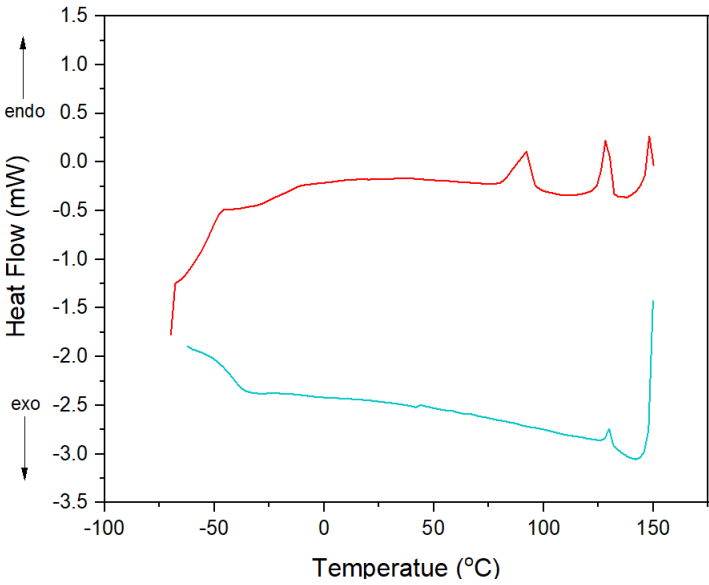


Figure 74: DSC curves for [Cho][Pro] 33% in DMSO, 2nd phase, -70 to 150 and to -70 °C

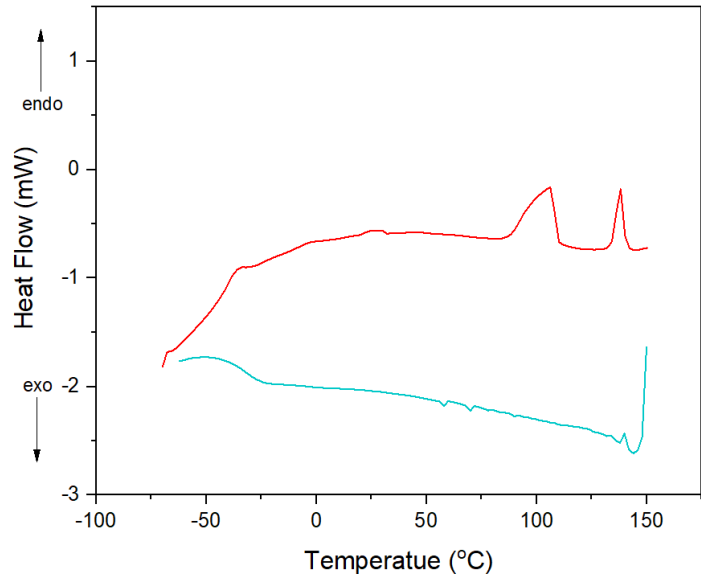


Figure 75: DSC curves for [Cho][Pro] 33% in DMSO, 3rd phase, -70 to 150 and to -70 °C

[Cho][Pro] 50% in DMSO:

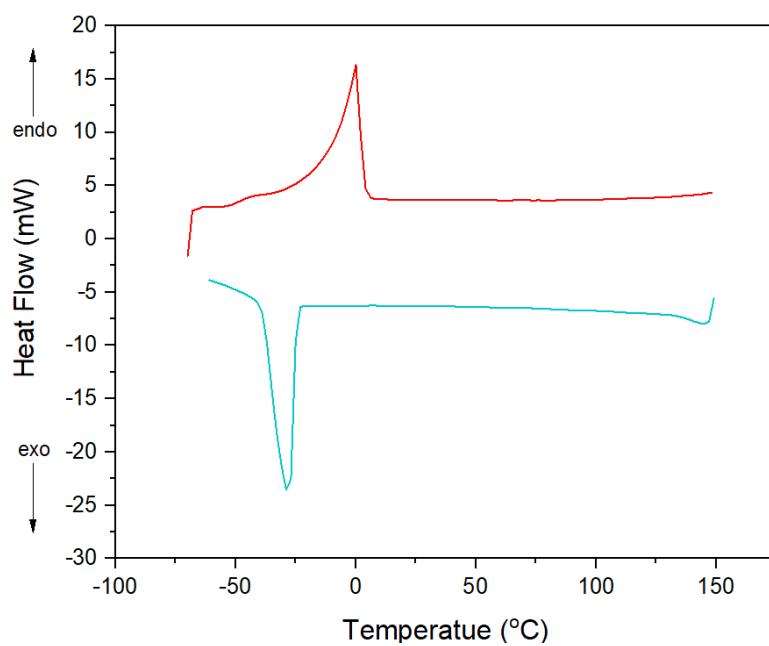


Figure 76: DSC curves for [Cho][Pro] 50% in DMSO, 2nd phase, -70 to 150 and to -70 °C

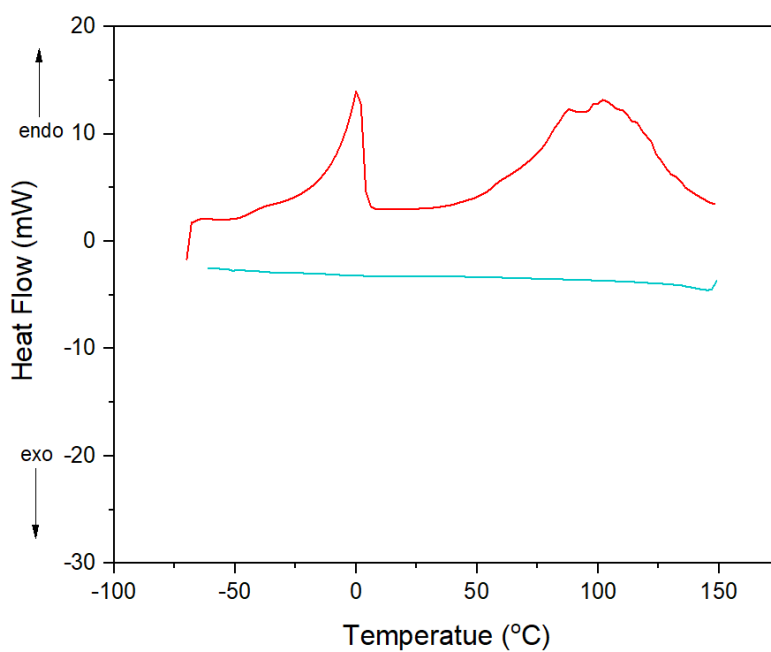


Figure 77: DSC curves for [Cho][Pro] 50% in DMSO, 3rd phase, -70 to 150 and to -70 °C

[Cho][Pro] Pure:

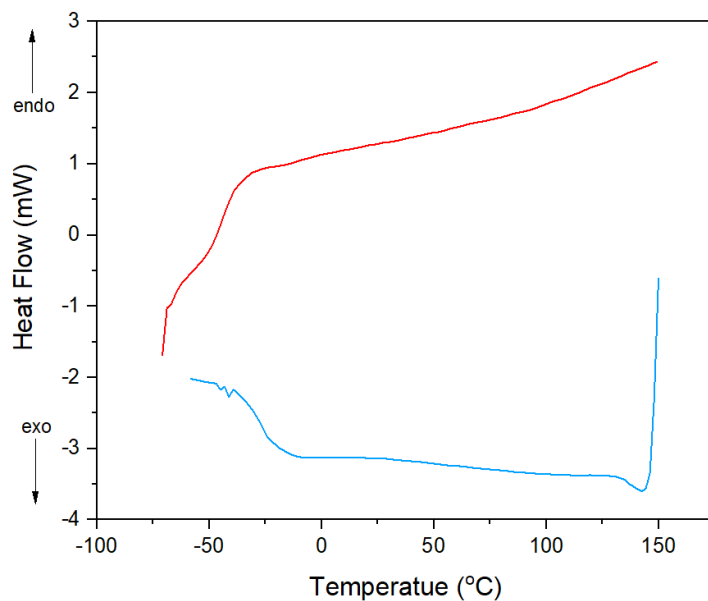


Figure 78: DSC curves for Pure [Cho][Pro], 2nd phase, -70 to 150 and to -70 °C

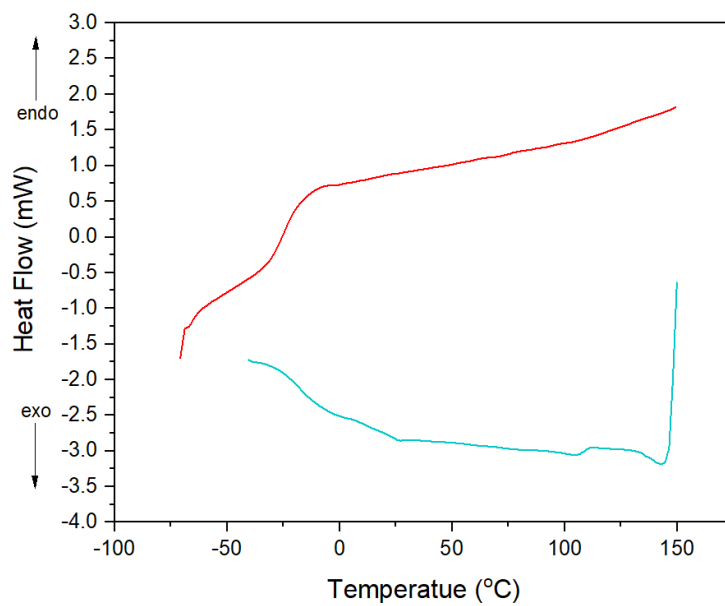


Figure 79: DSC curves for Pure [Cho][Pro], 3rd phase, -70 to 150 and to -70 °C

[DMP][Pro]:

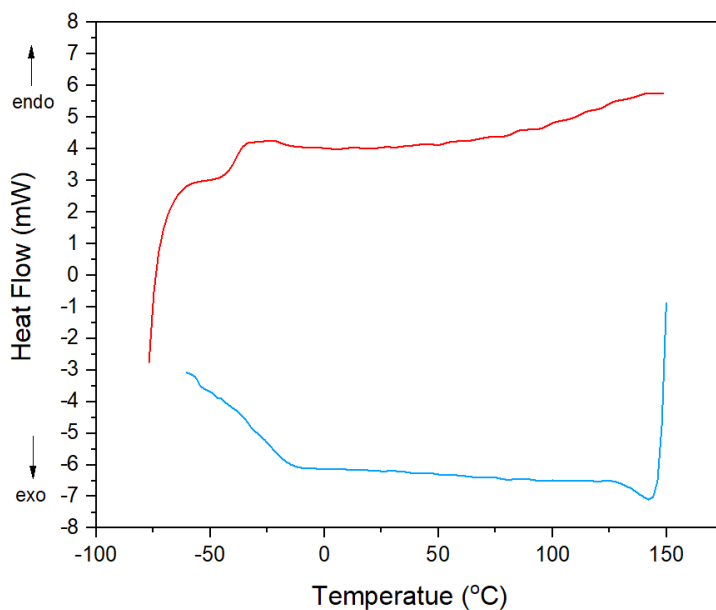


Figure 80: DSC curves for [DMP][Pro], 2nd phase, -70 to 150 and to -70 °C

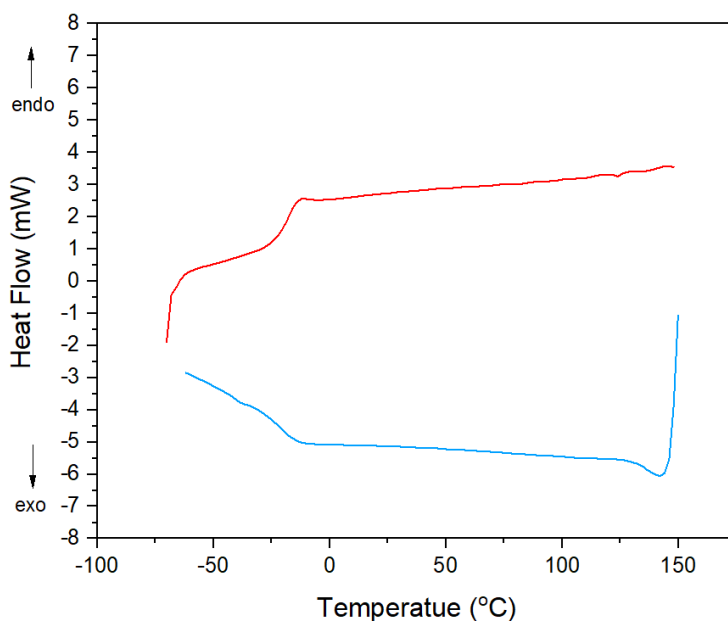


Figure 81: DSC curves for [DMP][Pro], 3rd phase, -70 to 150 and to -70 °C

3.6 Carbon capture test

The CO₂ absorption was not evaluated for pure [Cho][Pro] and [DMP][Pro] due to their high viscosity, which made it impossible to obtain clear and reproducible measurements. Preliminary tests showed that excessive viscosity led to bubble formation and material loss, preventing a reliable assessment of CO₂ absorption capacity. Furthermore, the extreme viscosity of these ILs would make them unsuitable as absorbent liquids in gas-liquid contact

columns, where efficient mass transfer and proper fluidity are essential for process effectiveness.

To overcome this limitation, [Cho][Pro] and [DMP][Pro] solutions in DMSO were tested, with DMSO acting as a co-solvent to reduce viscosity and improve the handling of the absorption process. The following sections present the results obtained for different concentrations in DMSO, evaluating the impact of dilution on absorption performance and system stability.

The gravimetric analysis results in *Table 6* confirm that the absolute amount of CO₂ absorbed increases with higher IL concentration, as expected. This trend aligns with the findings discussed in section 2.4.6 Carbon capture test, where the higher presence of [Cho][Pro] in the solution leads to a greater overall CO₂ uptake due to the increased availability of reactive amine sites.

Figure 82: Gravimetric Analysis trends further illustrates this trend, demonstrating that solutions with higher IL content exhibit higher w/w absorption efficiency.

However, when analyzing the molar efficiency (mol CO₂ per mol [Cho][Pro]), a reverse trend is observed:

- The most diluted solution (12.5% [Cho][Pro]) exhibits the highest molar efficiency (0.71), meaning each mole of IL captures more CO₂.
- As the IL concentration increases (33% and 50% solutions), the molar efficiency decreases to 0.59 and 0.56, respectively.

This behavior is consistent with previous studies on [Cho][Pro]-DMSO systems, as discussed in the article. The reduction in molar efficiency at higher IL concentrations can be attributed to:

1. Increased viscosity in more concentrated solutions, which hinders gas diffusion and reduces the accessibility of CO₂ to all reactive sites.
2. Stronger ionic interactions in pure or highly concentrated ILs, which may limit the reactivity of the amine group towards CO₂.
3. Possible formation of carbamic acid and ammonium carbamate species, which might alter the reaction equilibrium at different IL concentrations.

These results confirm that while higher IL content enhances absolute CO₂ absorption, it does not necessarily maximize molar efficiency, indicating a trade-off between absorption capacity and reaction efficiency.

Table 6: Gravimetric Analysis Results

% of [Cho][Pro] in DMSO	After CO ₂ capture	
	w/w Efficiency %	Molar Efficiency
12.50%	2.20	0.71
33%	4.84	0.59
50%	6.97	0.56

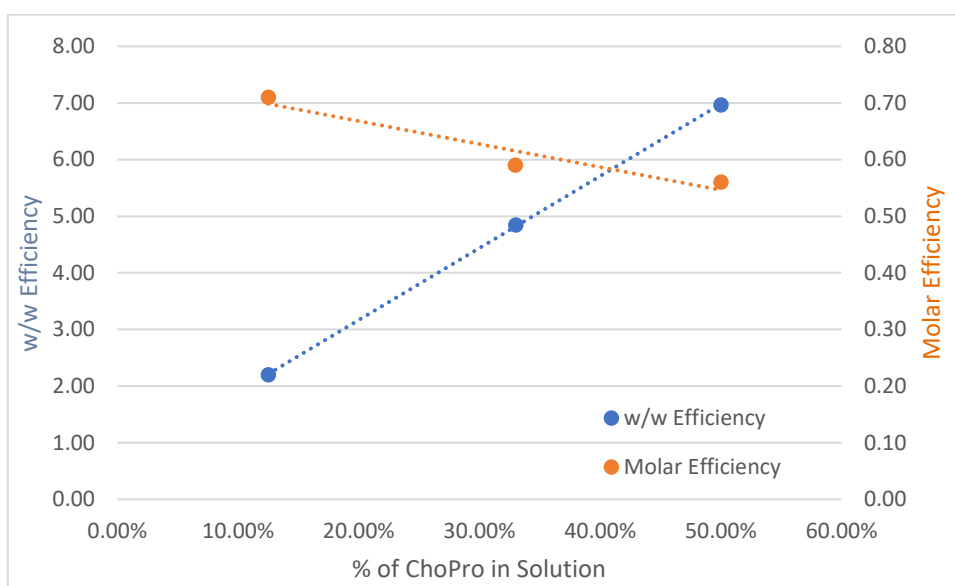


Figure 82: Gravimetric Analysis trends

3.7 PVT test

PVT tests were conducted on solutions of [Cho][Pro] at 12.5%wt, 33%wt and 50%wt in DMSO. By way of example, here are reported the results of the test for the 33%wt. Further analysis is beyond the scope of this thesis.

The presented test is composed of four pressure steps, starting from 3, 5, 10 and 20 bars respectively (see *Figure 83*). The duration of the third step is significantly longer because it didn't reach equilibrium during the working day, so the adsorption was allowed to continue during the night. The temperature, initially in ambient conditions, was increased to 40°C during the first step and maintained to 40° until the last step reached equilibrium. Afterwards, the temperature was increased to 85 degrees to break chemical bonds. For further details on the test see section 2.4.7.

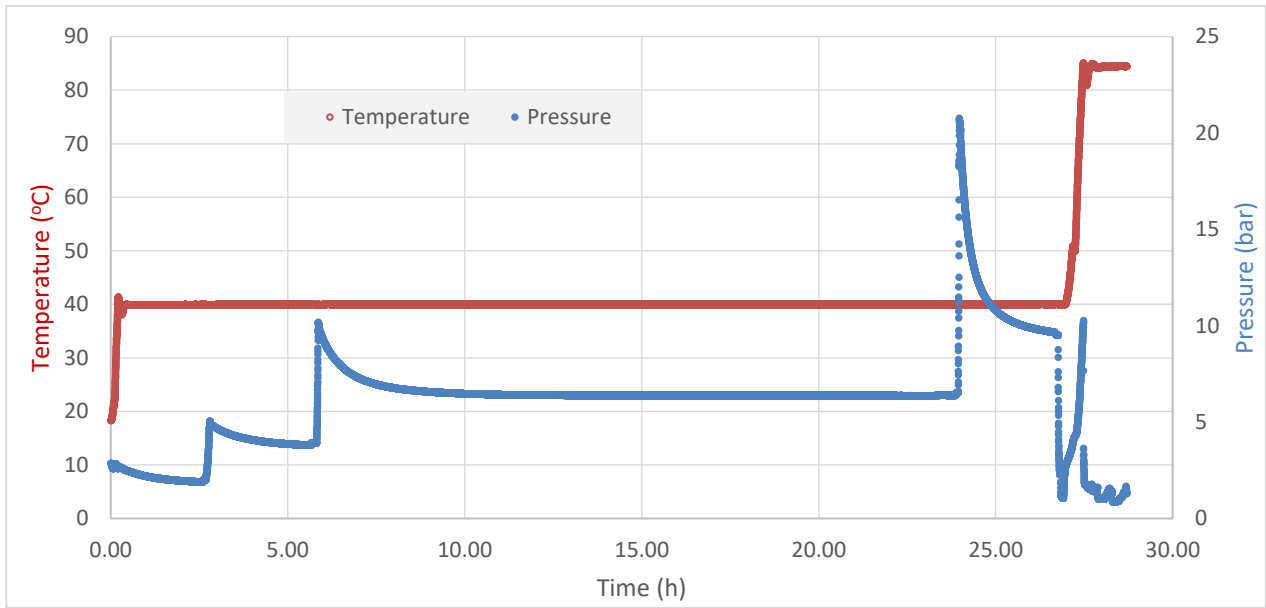


Figure 83: PVT test steps for [Cho][Pro] 33% in DMSO

It can be observed that at the beginning, during the first step at 3 bar, there is some impact from temperature because, at that moment, it was still rising from ambient temperature (around 18-20°C) to 40°C. As a result, the pressure trend is partially affected by the fact that the temperature is still increasing.

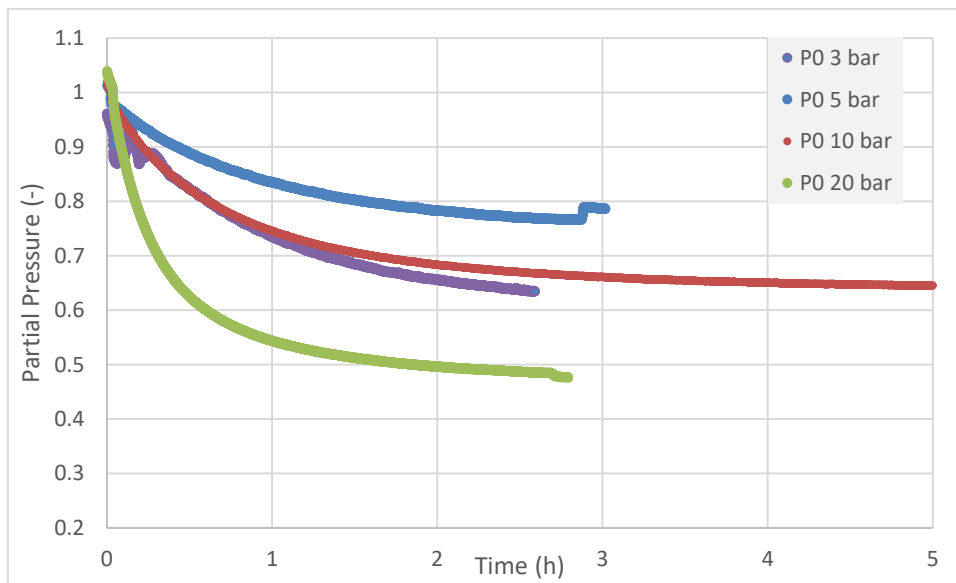


Figure 84: A comparison of the normalized pressure trends of PVT test for [Cho][Pro] 33% in DMSO

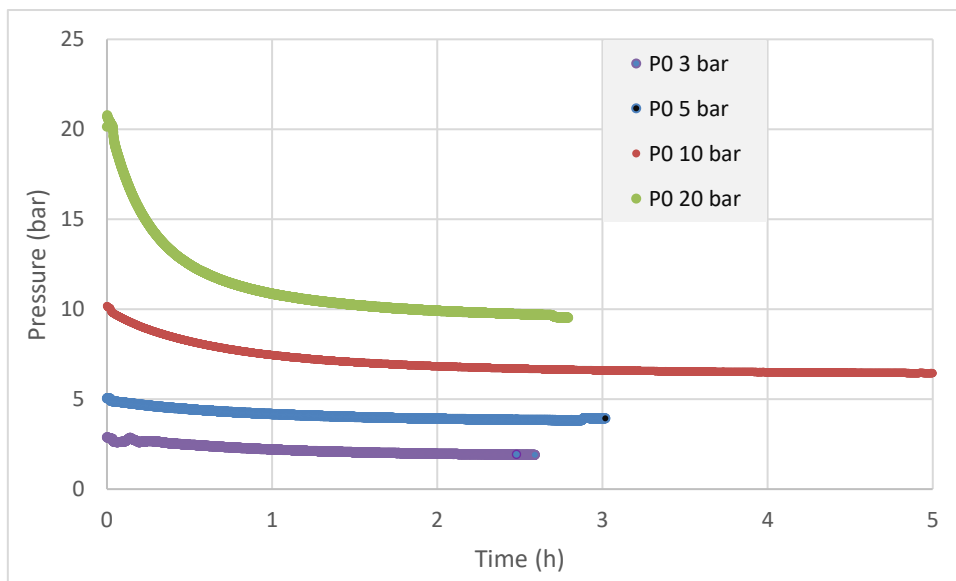


Figure 85: A comparison of the pressure trends of PVT test for [Cho][Pro] 33% in DMSO

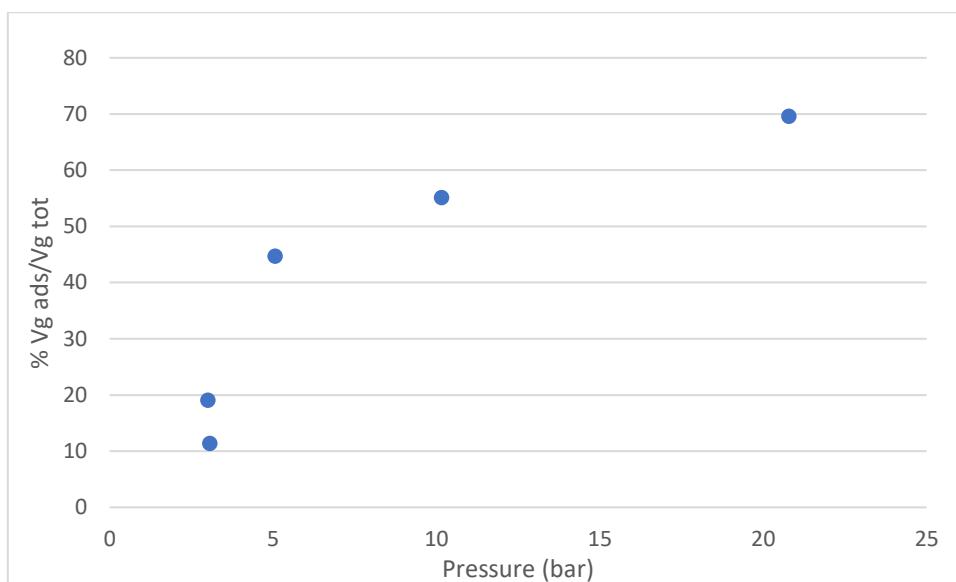


Figure 86: Percentage of volume of adsorbed gas to the total volume of gas at different pressure steps

The ratio between the absorbed gas and the liquid volume indicates that as the pressure increases, more gas is absorbed as is obvious in *Table 7* and *Figure 86*.

Table 7: Experiment data at each step

T cell (°C)	P cell (bar)	z (-)	V cell (ml)	V _{liquid} (ml)	V _{gas @ cell cond.} (ml)	V _{gas @ sc} (ml)	V _{gas adsorbed} (ml)	V _{g adsorb} / V _{g tot} (%)
						965.25		
18.5	3.06	0.991379	300	24.20	275.80	855.65	109.60	11.35
40	3	0.991379	300	24.20	275.80	781.28	183.97	19.06
40	5.06	0.982698	135	24.20	110.80	534.06	431.19	44.67
40	10.15	0.960713	68	24.20	43.80	433.15	532.10	55.12
40	20.78	0.914366	38	24.20	13.80	293.50	671.75	69.59

Table 8: Comparison of Flowmeter with Gasometer data

		P (bar)	T (°C)	V (ml sc)	V _{sc} (ml)
SC		1.014	20		
Flowmeter		1.014	0	899.4	965.2539264
Gasometer	Before heating	1.05	19.54	431.53	447.5528749
	After heating	1.008	20.23	352.54	350.1792204
		1.031	20.45	100.51	102.0384447
		0.998	20.58	58.87	57.8266742
	Total				957.5972143

After calculation of V_{sc} it can be deduced that the gas injected by the mass flow meter in the beginning is very close in quantity to the gas recovered at the end of the test [Table 8]. This means that almost all the gas injected was successfully extracted at the end of the experiment.

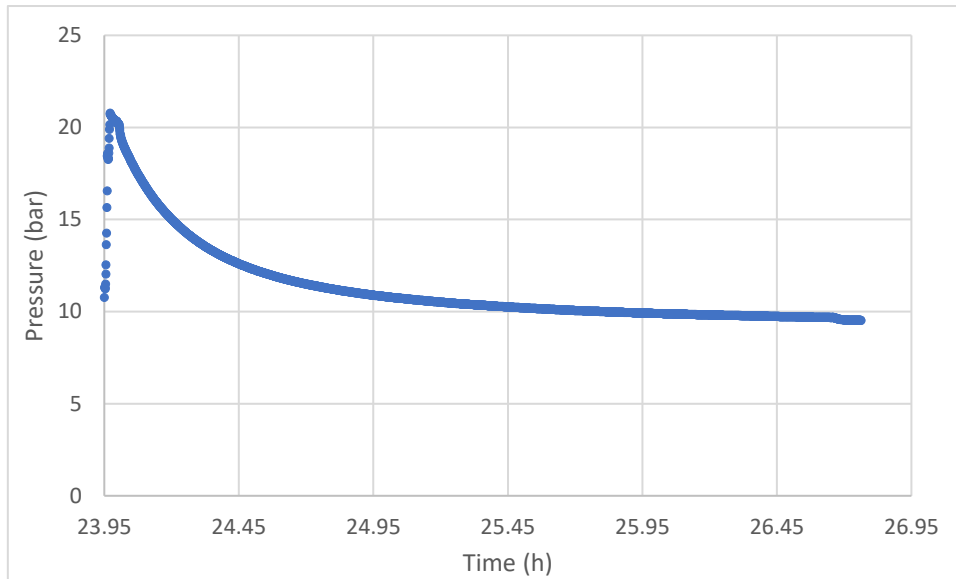


Figure 87: Starting point of Chemisorption at 20 bar

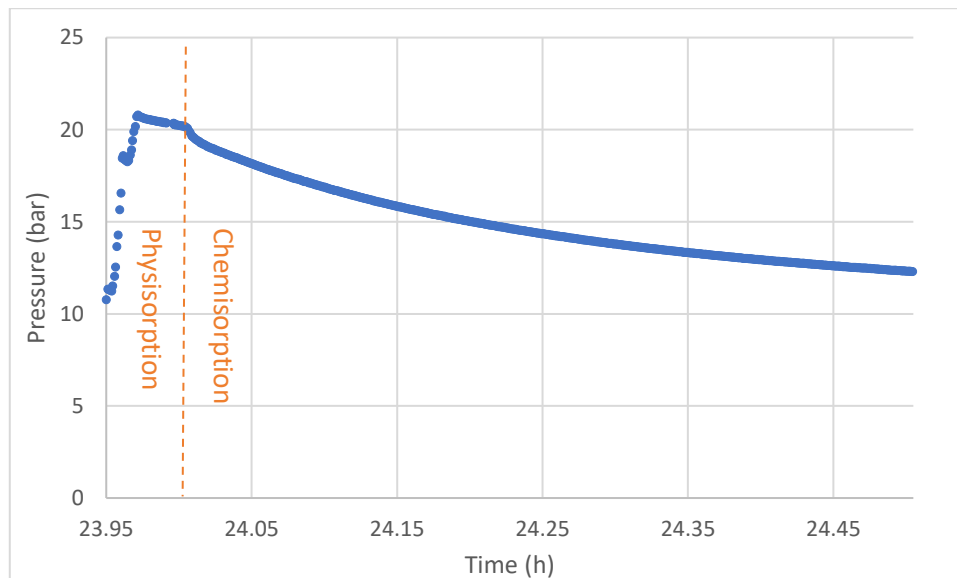


Figure 88: Visible shift from Physisorption and Chemisorption

It can be observed from the pressure trend at $P_0 = 20$ bar that it helps separate the phase where physisorption is dominant from the phase where chemisorption takes over. In the higher-pressure steps like *Figure 87*, it is pretty clear because physisorption lasts a bit longer. *Figure 88* is a zoomed-in version of *Figure 87* where the pressure-drop and shifting towards chemisorption is more evident. For the other pressures, this effect is also present, but its duration is much shorter, making it harder to detect.

4. Conclusion

This study provides a detailed analysis of CO₂ absorption in [Cho][Pro]-DMSO solutions, with a particular focus on Pressure-Volume-Temperature (PVT) measurements as a tool to improve the understanding of gas-liquid interactions in ionic liquid-based systems.

The results confirm that higher concentrations of [Cho][Pro] lead to greater absolute CO₂ absorption, while more diluted solutions exhibit higher molar efficiency in CO₂ uptake. This suggests a trade-off between total absorption capacity and the efficiency of IL utilization. Gravimetric analysis showed that while the IL concentration enhances CO₂ absorption, the diffusion and reaction kinetics are significantly influenced by the solvent environment and viscosity of the system.

The PVT measurements provide key insights into the CO₂ absorption process under controlled temperature and pressure conditions, offering a more comprehensive understanding of the physical diffusion constant and equilibrium CO₂ concentration at high pressures. These data are essential for developing more accurate models for gas absorption and improving process simulations for an eventual scale-up of IL-based CO₂ capture technologies.

Future research should further explore the high-pressure behavior of ILs, focusing on quantifying diffusion coefficients and equilibrium solubility at varying pressures, to refine the thermodynamic and kinetic models needed for industrial applications. The ability to integrate PVT analysis into CO₂ capture studies represents a significant advancement in the precision and applicability of IL-based separation processes

5. References

1. Kaur, G., H. Kumar, and M. Singla, *Diverse applications of ionic liquids: A comprehensive review*. Journal of Molecular Liquids, 2022. **351**: p. 118556.
2. Płotka-Wasyłka, J., et al., *Deep eutectic solvents vs ionic liquids: Similarities and differences*. Microchemical Journal, 2020. **159**: p. 105539.
3. Latini, G., et al., *Unraveling the CO₂ reaction mechanism in bio-based amino-acid ionic liquids by operando ATR-IR spectroscopy*. Catalysis Today, 2019. **336**: p. 148-160.
4. Gadilohar, B.L. and G.S. Shankarling, *Choline based ionic liquids and their applications in organic transformation*. Journal of Molecular Liquids, 2017. **227**: p. 234-261.
5. H. Davis, J., Jr., *Task-Specific Ionic Liquids*. Chemistry Letters, 2004. **33**(9): p. 1072-1077.
6. Wasserscheid, P. and W. Keim, *Ionic Liquids—New “Solutions” for Transition Metal Catalysis*. Angewandte Chemie International Edition, 2000. **39**(21): p. 3772-3789.
7. Rashid, T.U., *Ionic liquids: Innovative fluids for sustainable gas separation from industrial waste stream*. Journal of Molecular Liquids, 2021. **321**: p. 114916.
8. Rogers, R.D. and K.R. Seddon, *Ionic Liquids--Solvents of the Future?* Science, 2003. **302**(5646): p. 792-793.
9. Hallett, J.P. and T. Welton, *Room-Temperature Ionic Liquids: Solvents for Synthesis and Catalysis*. 2. Chemical Reviews, 2011. **111**(5): p. 3508-3576.
10. Aki, S.N.V.K., et al., *High-Pressure Phase Behavior of Carbon Dioxide with Imidazolium-Based Ionic Liquids*. The Journal of Physical Chemistry B, 2004. **108**(52): p. 20355-20365.
11. Brennecke, J.F. and B.E. Gurkan, *Ionic Liquids for CO₂ Capture and Emission Reduction*. The Journal of Physical Chemistry Letters, 2010. **1**(24): p. 3459-3464.
12. Anthony, J.L., E.J. Maginn, and J.F. Brennecke, *Solution Thermodynamics of Imidazolium-Based Ionic Liquids and Water*. The Journal of Physical Chemistry B, 2001. **105**(44): p. 10942-10949.
13. Vekariya, R.L., *A review of ionic liquids: Applications towards catalytic organic transformations*. Journal of Molecular Liquids, 2017. **227**: p. 44-60.
14. Zhao, H., S. Xia, and P. Ma, *Use of ionic liquids as ‘green’ solvents for extractions*. Journal of Chemical Technology & Biotechnology, 2005. **80**(10): p. 1089-1096.
15. Hayes, R., G.G. Warr, and R. Atkin, *Structure and Nanostructure in Ionic Liquids*. Chemical Reviews, 2015. **115**(13): p. 6357-6426.
16. Ebrahimi, M., et al. *A Review on Ionic Liquids-Based Membranes for Middle and High Temperature Polymer Electrolyte Membrane Fuel Cells (PEM FCs)*. International Journal of Molecular Sciences, 2021. **22**, DOI: 10.3390/ijms22115430.
17. Ferraz R, P.C., Vieira M, Fernandes R, Noronha JP, et al., *Ionic Liquids Synthesis – Methodologies*. Organic Chem Curr, 2015. **4**(1).
18. Ratti, R., *Ionic Liquids: Synthesis and Applications in Catalysis*. Advances in Chemistry, 2014. **2014**(1): p. 729842.
19. Zhang, X., et al., *Carbon capture with ionic liquids: overview and progress*. Energy & Environmental Science, 2012. **5**(5): p. 6668-6681.
20. Greaves, T.L. and C.J. Drummond, *Protic Ionic Liquids: Properties and Applications*. Chemical Reviews, 2008. **108**(1): p. 206-237.
21. Lee, S.-g., *Functionalized imidazolium salts for task-specific ionic liquids and their applications*. Chemical Communications, 2006(10): p. 1049-1063.
22. Chaturvedi, D., *Recent developments on task specific ionic liquids*. Current Organic Chemistry, 2011. **15**(8): p. 1236-1248.
23. de Jesus, S.S. and R. Maciel Filho, *Are ionic liquids eco-friendly?* Renewable and Sustainable Energy Reviews, 2022. **157**: p. 112039.
24. Smith, E.L., A.P. Abbott, and K.S. Ryder, *Deep Eutectic Solvents (DESs) and Their Applications*. Chemical Reviews, 2014. **114**(21): p. 11060-11082.
25. Maneffa, A.J., et al., *Deep Eutectic Solvents Based on Natural Ascorbic Acid Analogues and Choline Chloride*. ChemistryOpen, 2020. **9**(5): p. 559-567.

26. Lim, E., J.-S. Yon Pang, and E.V. Lau, *A comparative study of thermophysical properties between choline chloride-based deep eutectic solvents and imidazolium-based ionic liquids*. *Journal of Molecular Liquids*, 2024. **395**: p. 123895.
27. Gu, Y. and F. Jérôme, *Bio-based solvents: an emerging generation of fluids for the design of eco-efficient processes in catalysis and organic chemistry*. *Chemical Society Reviews*, 2013. **42**(24): p. 9550-9570.
28. Syahir, A.Z., et al., *A review on bio-based lubricants and their applications*. *Journal of Cleaner Production*, 2017. **168**: p. 997-1016.
29. Noorani, N. and A. Mehrdad, *Cholinium-amino acid ionic liquids as biocompatible agents for carbon dioxide absorption*. *Journal of Molecular Liquids*, 2022. **357**: p. 119078.
30. Makertihartha, I.G.B.N., et al., *Solvent extraction of gold using ionic liquid based process*. *AIP Conference Proceedings*, 2017. **1805**(1): p. 030008.
31. Zaccagnini, P., et al., *Flexible and high temperature supercapacitor based on laser-induced graphene electrodes and ionic liquid electrolyte, a de-rated voltage analysis*. *Electrochimica Acta*, 2020. **357**: p. 136838.
32. Maniam, K.K. and S. Paul *Progress in Electrodeposition of Zinc and Zinc Nickel Alloys Using Ionic Liquids*. *Applied Sciences*, 2020. **10**, DOI: 10.3390/app10155321.
33. Rahali, S., et al., *Electrodeposition of silver from the ionic liquid Butylpyridinium dicyanamide*. *Journal of Electroanalytical Chemistry*, 2020. **871**: p. 114289.
34. Qu, J., et al., *Ionic Liquids as Novel Lubricants and Additives for Diesel Engine Applications*. *Tribology Letters*, 2009. **35**(3): p. 181-189.
35. Hasanov, I., S. Shanmugam, and T. Kikas, *Extraction and isolation of lignin from ash tree (Fraxinus excelsior) with protic ionic liquids (PILs)*. *Chemosphere*, 2022. **290**: p. 133297.
36. Isoaari, P., V. Srivastava, and M. Sillanpää, *Ionic liquid-based water treatment technologies for organic pollutants: Current status and future prospects of ionic liquid mediated technologies*. *Science of The Total Environment*, 2019. **690**: p. 604-619.
37. Raeissi, S., L.J. Florusse, and C.J. Peters, *Purification of flue gas by ionic liquids: Carbon monoxide capture in [bmim][Tf2N]*. *AIChE Journal*, 2013. **59**(10): p. 3886-3891.
38. Hospital-Benito, D., et al., *Direct air capture based on ionic liquids: From molecular design to process assessment*. *Chemical Engineering Journal*, 2023. **468**: p. 143630.
39. Dai, Z., et al., *Combination of ionic liquids with membrane technology: A new approach for CO₂ separation*. *Journal of Membrane Science*, 2016. **497**: p. 1-20.
40. Meng, F., et al., *Research progress of aqueous amine solution for CO₂ capture: A review*. *Renewable and Sustainable Energy Reviews*, 2022. **168**: p. 112902.
41. El Hadri, N., et al., *Aqueous amine solution characterization for post-combustion CO₂ capture process*. *Applied Energy*, 2017. **185**: p. 1433-1449.
42. Ma'mun, S., et al., *Selection of new absorbents for carbon dioxide capture*. *Energy Conversion and Management*, 2007. **48**(1): p. 251-258.
43. Greer, A.J., J. Jacquemin, and C. Hardacre, *Industrial Applications of Ionic Liquids*. *Molecules*, 2020. **25**(21): p. 5207.
44. Zeisel, S.H. and K.A. da Costa, *Choline: an essential nutrient for public health*. *Nutr Rev*, 2009. **67**(11): p. 615-23.
45. Daintith, J., *The Facts on File Dictionary of Organic Chemistry*. 2014: Facts On File, Incorporated.
46. Tao, G.-h., et al., *Preparation, characterization and application of amino acid-based green ionic liquids*. *Green Chemistry*, 2006. **8**(7): p. 639-646.
47. Le Donne, A. and E. Bodo, *Cholinium amino acid-based ionic liquids*. *Biophysical Reviews*, 2021. **13**(1): p. 147-160.
48. Yang, Q., et al., *New Insights into CO₂ Absorption Mechanisms with Amino-Acid Ionic Liquids*. *ChemSusChem*, 2016. **9**(8): p. 806-812.
49. Li, W., et al., *Mechanism and Kinetic Study of Carbon Dioxide Absorption into a Methyl-diethanolamine/1-Hydroxyethyl-3-methylimidazolium Lysine/Water System*. *Energy & Fuels*, 2018. **32**(10): p. 10813-10821.

50. Danesh, A., *PVT and Phase Behaviour Of Petroleum Reservoir Fluids*. 1998: Elsevier Science.
51. McCain, W.D., *The Properties of Petroleum Fluids*. 1990: PennWell Books.
52. Hartley, A. and S. Turnock, *What are the benefits of reducing global CO emissions to net-zero by 2050?* Weather, 2022. **77**(1): p. 27-28.
53. Roberts, I., *The health co-benefits of climate change policies: doctors have a responsibility to future generations*. Clin Med (Lond), 2009. **9**(3): p. 212-3.
54. Cuccia, L., et al., *Analytical methods for the monitoring of post-combustion CO₂ capture process using amine solvents: A review*. International Journal of Greenhouse Gas Control, 2018. **72**: p. 138-151.
55. de Riva, J., et al., *Ionic liquids for post-combustion CO₂ capture by physical absorption: Thermodynamic, kinetic and process analysis*. International Journal of Greenhouse Gas Control, 2017. **61**: p. 61-70.
56. Cannone, S.F., et al., *Biobased ionic liquid solutions for an efficient post-combustion CO₂ capture system*. Carbon Capture Science & Technology, 2024. **13**: p. 100312.
57. Gong, Y., X. Chen, and W. Wu, *Application of fourier transform infrared (FTIR) spectroscopy in sample preparation: Material characterization and mechanism investigation*. Advances in Sample Preparation, 2024. **11**: p. 100122.
58. Liu, Q.-P., et al., *Ionic liquids from renewable biomaterials: synthesis, characterization and application in the pretreatment of biomass*. Green Chemistry, 2012. **14**(2): p. 304-307.
59. Shaikh, A.R., et al., *Choline-based amino acid ionic liquids for CO₂ capture*. Journal of Molecular Liquids, 2025. **424**: p. 127084.
60. Tawil, M., et al., *Solubility of H₂-CH₄ mixtures in brine at underground hydrogen storage thermodynamic conditions*. Frontiers in Energy Research, 2024. **12**.
61. Hu, X., et al., *Elucidating the transition between CO₂ physisorption and chemisorption in 1,2,4-triazolate ionic liquids at a molecular level*. Chemical Engineering Journal, 2022. **435**: p. 134956.